Escola Tècnica Superior d'Enginyeria Química
Departament d'Enginyeria Química

UNIVERSITAT ROVIRA I VIRGILI

Development and Application of Molecular Modeling Techniques for the Characterization of Porous Materials

A dissertation to obtain the Degree of Doctor of Philosophy (Chemical Engineering) presented by:

Susana Figueroa Gerstenmaier

Supervised by Dr. Lourdes F. Vega
Tarragona, October 2002

Dedicada a la memoria
de mi padre y de Ernesto,
a las ilusiones vanas,
y al tiempo perdido...

"...Tu tiempo es ahora una mariposa,
navecita blanca, delgada, nerviosa,
Siglos atrás inundaron un segundo
debajo del cielo, encima del mundo...".
silvio rodríguez

ACKNOWLEDGEMENT

Quiero agradecer a todas las personas y organismos que colaboraron e hicieron posible la realización de este trabajo.

Al Departamento de Ingeniería Química y a la Universidad Rovira i Virgili por otorgarme la beca que he disfrutado durante estos 5 años, y al Consejo Nacional de Ciencia y Tecnología mexicano por el complemento y extensión de beca. Al Ministerio de Ciencia y Tecnología español por los proyectos: PB96-1025, PPQ2000-2888-E, y PPQ2001-0671. A la Generalitat de Catalunya por financiar parte de mi estancia en North Carolina State University, y a Keith Gubbins por financiar la otra parte y por acogerme en su grupo de investigación.

A Lourdes Vega por supervisar este trabajo, y por su entusiasmo, optimismo, y energía inagotable. A los miembros del tribunal por aceptar ser parte del mismo. A Keith Gubbins por plantear las primeras ideas de este trabajo. Al grupo del TRI/Princeton (Alexander Neimark, Peter Ravikovitch, y Aleksey Vishnyakov) por los datos que gentilmente compartieron con nosotros. A Martin Schoen por aceptar mi autoinvitación al *Workshop "phase transitions for confined fluids"* de Lyon.

A Lev Gelb por permitirme utilizar sus resultados, así como suministrarme generosamente toda la información que le pedí, contestar todas mis dudas, por tontas que fueran, y contestar todos mis *e-mails*.

A Paco Medina por resolverme dudas, por permitirme al acceso al equipo experimental para medir isotermas, y por suministrar y calcinar las alúminas usadas en este trabajo. También por la ayuda financiera para aguantar los últimos meses. A Yolanda Cesteros por enseñarme a usar el equipo y ayudarme a hacer los experimentos. A Alvaro Morato por permitir que me "pirateara" el software y enseñarme a usarlo.

A Jorge Hernández por ayudarme, allá en los albores de los primeros tiempos con mi primer código de simulación dentro de un poro cilíndrico.

A Oliver por la ayuda técnica (informática), a Josep Pamies por lo mismo, y por ayudarme en otras cosas como la edición de esta tesis y con el catalán (el idioma, que al igual que los chicos, tampoco se me da bien), ¡ah! Y también por bajarme todos los artículos de la red gracias a sus influencias extranjeras. A Carlos por ayudarme cada vez que se lo pedía, en especial cuando yo no era capaz de ver las cosas en 3D. A Allan por su ecuanimidad y buena madera.

A Angel, Roger, Rosa Marcos y todas las personas que en un momento u otro me ayudaron a disipar dudas.

A Dani por dejarme sus libros, resolver mis dudas sobre el Office, y financiar parte de los litros y litros de café que me he bebido en estos años.

A Paula por echarme una mano con el inglés, y corregir mis manuscritos cada vez que se lo pedía, y claro, por dejarme la bola sujetapapeles de la suerte.

A Coray, Jorge Pikunic y Sandra Gavaldà por la cálida acogida con la que me dispensaron en Raleigh.

A Alex, Toni, Marcos, Rafa, e Ismael por soportar con paciencia todas mis demandas de soporte informático.

A Pilar, por su buen humor y por creer que no soy tan mala en el laboratorio. A Sam, Dolors, Raquel y Merche, por resolver tantas cosas.

A Miguel Costas y a Vicente Talanquer por su apoyo incondicional y sus atinados consejos durante todos estos años. A la Dra. Arechavaleta (ésta si es doctora de verdad) por seguir y controlar mis depresiones vía *e-mail* sin cobrarme nunca nada.

A Alfonso por darme el dinero para poder adquirir a Maquinón, por invitarme a Vicenza (con gastos pagados), y pagarme el último viaje a México, todo esto para hacerme la vida más fácil con potentes antidepresivos.

Muy especialmente a mi madre, por todo su apoyo y cariño. A Sandra por sus divertidos *e-mails*. A Laura por resolverme todos los problemas prácticos en México.

A Oleguer, por compartir conmigo tiempos difíciles (y los buenos también). Por todo su apoyo. A Xauen y Titu, nuestros niños, porque si no fuera por ellos quizá hace mucho que habría claudicado.

A Isabel, por ser tan buena casera. A las novelas de narrativa "contemporánea" (al estilo de Bridged Jones) que me han hecho más llevadera sobre todo la última etapa.

Y de una forma muy especial quiero agradecer a Josep Bonet y a Felipe Jiménez por todo el apoyo y amistad que me han brindado y por todas las horas y horas de trabajo que han compartido conmigo. En particular, Josep, porque a pesar de considerarme un melón me ha ayudado muchísimo durante los últimos 3 años. Me resolvió dudas pacientemente, y me echó una mano cientos de veces. Agradezco su curiosidad inagotable, su clara inteligencia, y su generosidad. En cuanto a Felipe, hemos compartido alegrías y sinsabores desde mi llegada a Tarragona, me ayudó y explicó muchas cosas desde el principio, y desde que se marchó a Huelva ha estado ahí, tras la línea telefónica, ayudándome en todo lo que podía. Agradezco su entusiasmo, y hasta le perdono que me llame cateta.

Finalmente quiero agradecer a mis amigos en Tarragona por las alegrías y los momentos difíciles compartidos, y por cuidarme y apapacharme cuando me hacía falta. A Gabriela, Dani, Josep María, Carlos, Mónica, Isabela, Paula, Vessy…

También a mis otros amigos, compañeros de comidas, desayunos, cafés, vermuts, reivindicaciones y luchas precarias, …, Josep Pamies, Vanessa, Catalina, Roger, Orlandito, Montse, Gloria, Alvarito, Mikaela, Mariana, Mohammad, Albert, Carmelo… Y a todos los demás que no menciono porque no acabaría nunca, con los que he compartido penas, alegrías y sobretodo, muchas horas cada día durante los últimos 5 y pico años…

SUMMARY

Porous materials are widely used in many branches of modern science and technology, such as catalysis, separation of mixtures, purification of fluids and fabrication of membranes. A successful application of porous solids requires a precise characterization of their surface and structural properties, as well as a good understanding of the physical and chemical behavior of fluids inside the pores. Some materials, such as zeolites, have well defined porous structures, but others, such as porous oxides, carbons and controlled-porous glasses, are quite amorphous. Therefore, a proper characterization of this kind of materials is an important topic, and more often than not, a complicated one. For many years, gas adsorption has been used to study properties of porous solids, since it is fast, simple and informative. Many methods were developed to extract information about porosity and surface properties of materials from adsorption isotherm data. In the last two decades, with the aid of the increasingly faster computers, the use of molecular modeling techniques has been gaining relevance. In this context, the general objective of this thesis is to develop tools at the molecular level using statistical mechanics for the characterization of adsorbent materials.

After a brief introduction on the topic (chapter 1), chapter 2 is devoted to a review of the basic methodology employed in this work. In chapter 3 we have implemented the Fundamental-Measure density functional theory (FMT) due to Kierlik and Rosinberg to describe the adsorption of Lennard-Jones molecules in cylindrical pores. To our best knowledge, this is the first time that this theory is applied to a cylindrical geometry. The accuracy of the theory in predicting adsorption isotherms and density profiles is checked by comparison with Grand Canonical Monte Carlo simulations for a wide range of pore sizes, showing very good agreement in all cases. In addition, the theory has been applied to the adsorption in slit-like pores to study the influence of the pore geometry on this property. The results indicate that the confinement of the cylindrical geometry introduces significant differences in the shape of the adsorption isotherms and density profiles. These differences are relevant for the characterization of porous materials. Our results indicate that a layering behavior takes place in the smallest cylindrical pore considered, while the adsorption in a planar pore of the same size needs a much higher chemical potential to achieve a significant adsorption. As the pore size increases, the influence of the geometry becomes less important, although a certain shift in the capillary condensation transition can still be observed. Additionally, for wider pores, we obtain multilayer adsorption with capillary condensation at high chemical potentials, with the same qualitative behavior observed for both geometries. When the diameter size reaches the limit where the curvature effects are not of further relevance, the cylindrical pores reduce to the same quantitative behavior of the slit-like pores. The formation of a thin adsorbed layer at intermediate and large pore sizes seems to correspond to a second order thermodynamic phase transition, for the range of parameters used and the thermodynamic conditions studied. However, the results found seem to indicate some relationship between this behavior and the prewetting transition observed in semi-infinite geometries, especially in the vicinity of the critical end point of the prewetting line. The effect of the confinement is very important in this crossover behavior. From the comparison of Fundamental-Measure density functional theory calculations *versus* non-local density functional theory results, we conclude that the

FMT is an excellent tool for the study of the behavior of fluids in confined cylindrical geometries.

In chapter 4 we have applied the FMT in conjunction with a regularization method to estimate the pore-size distribution (PSD) of model porous glasses. We have chosen this particular material because it was developed with molecular modeling techniques, and a direct comparison can be made with the theory used here. An additional advantage of these model materials, *versus* experimental ones, is that in this case the size and shape of the pores is well known, as well as the position of the atoms in the surface, making it a perfect material to check the accuracy of the theoretical characterization methods available. Since there are several solutions of the adsorption integral equation compatible with the experimental adsorption isotherm, and several factors can hide defects of the molecular model, we have done the characterization in a systematic manner: we have first checked the accuracy of the FMT and the independent pore model for predicting the "experimental" adsorption isotherms using the geometrical PSD already known for the materials. This has been done with individual cylindrical and slit-like pores. Secondly, once the adsorption isotherm was successfully reconstructed, we inverted the integral adsorption isotherm with a regularization procedure. The accuracy of the inversion method has also been checked before estimating the PSD of the different materials. Finally, once the method has been proved to be correct, we used it to estimate the PSD of four materials. We have also studied the influence of choosing different values of molecular parameters for the fluid-fluid and the solid-fluid interaction on the adsorption behavior of these systems. We have obtained that the independent pore model is adequate for the four materials investigated here. The slit-like geometry seems to represent the overall adsorption behavior better than the cylindrical geometry. As far as the PSD obtained with our procedure is concerned, the distributions obtained by inversion of the integral are in better agreement with the geometrical distributions than the ones calculated with the Barrett-Joyner-Halenda (BJH) method. The locus of the peak is at the same pore size, and all of them are unimodal, while the BJH distributions show a maximum systematically located at smaller pores, underestimating the PSD of the material, and they are not unimodal. Regarding the geometry of the individual pores that form the material, we can say that, although the PSD is broader than the geometrical ones, the adsorption predicted by a collection of individual slit-like pores is in almost quantitative agreement with the "experimental" adsorption isotherm.

Finally, in chapter 5 we have characterized three different samples of γ-alumina, one of them without treatment and the others two calcined in a furnace during several hours at 823 and 1,023K. For this we have measured adsorption isotherms of nitrogen at 77.35K in a Micromeritics ASAP 2000 apparatus. Additionally, we have used the PSD's provided by the software of the experimental equipment using the BJH method. We have calculated theoretical isotherms by the FMT approach. We have inverted the adsorption integral equations with the regularization method and, finally, we have obtained the PSD's for our three samples of alumina, and the corresponding adsorption isotherms. In this way we have observed the influence of the calcination of alumina on its PSD. Moreover, we have tested the accuracy of the FMT/Regularization method in a systematic way. When we compared the PSD's obtained with the corresponding BJH distributions, we verified that in the two first cases (untreated alumina and alumina calcined at 823K) the BJH method underestimated the size of the pores, giving PSD's shifted to smaller sizes. In the case of alumina calcined at 1,023K, in which the

sintering process has produced the disappearance of the smallest pores, favoring the wider ones, the BJH PSD's and the FMT/regularization PSD's perform very similar. With this, we corroborated the known fact that the BJH method is quite accurate in the macroporous region. Finally, we have predicted an adsorption isotherm of a different fluid (ethane) at a different temperature (333K) in one of the characterized materials (untreated alumina) with the aim of establishing the robustness of the PSD obtained. The agreement obtained shows that it is possible to use this characterization method and extrapolate the results at other conditions, provided that a enough number of different pore sizes are used to calculate the desirable isotherm, and the solid-fluid interaction parameters are well chosen.

RESUMEN

Los materiales porosos se utilizan en muchas ramas de la ciencia y la tecnología, por ejemplo, se usan como catalizadores, en la separación de mezclas, en la purificación de fluidos, y en la fabricación de membranas. Su aplicación adecuada requiere de la caracterización precisa de sus propiedades superficiales y estructurales, además del conocimiento del comportamiento fisicoquímico de los fluidos cuando se encuentran dentro de los poros. Algunos materiales, como las zeolitas, tienen estructuras porosas bien definidas, pero otros en cambio (óxidos porosos, carbones, vidrios porosos con tamaño controlado) son bastante amorfos. Por lo tanto, una caracterización correcta de los materiales porosos es un área de estudio muy importante, la cual en algunos casos es una tarea sencilla pero en la mayoría no. Durante muchos años la adsorción de gases ha sido empleada para estudiar las propiedades de sólidos porosos, dado que es bastante fácil, simple y se puede obtener mucha información. Se han desarrollado muchos métodos para interpretar los datos experimentales y determinar la porosidad, las propiedades superficiales y la distribución de los tamaños de los poros de los materiales a partir de las isotermas de adsorción. En las dos últimas décadas, con la ayuda de las computadoras cada vez más rápidas, se ha extendido mucho el uso las técnicas de la mecánica estadística para realizar esta tarea. En este contexto, el objetivo general de esta tesis consiste en desarrollar herramientas a escala molecular utilizando la mecánica estadística para la caracterización de materiales adsorbentes.

Después de una breve introducción en el tema (capítulo 1), el capítulo 2 está dedicado a hacer una revisión de la metodología básica empleada en este trabajo. En el capítulo 3 hemos implementado la teoría funcional de la densidad de medidas fundamentales (FMT, del inglés *Fundamental-Measure density functional theory*) de Kierlik y Rosinberg para describir la adsorción de moléculas Lennard-Jones dentro de poros cilíndricos. Hasta donde sabemos, ésta es la primera vez que esta teoría es aplicada a geometría cilíndrica. La exactitud de la teoría en predecir las isotermas de adsorción y los perfiles de la densidad es verificada por comparación con simulaciones Monte Carlo en el colectivo Gran Canónico para un amplio intervalo de tamaños de poros, observándose una buena concordancia en todos los casos. Adicionalmente, la teoría ha sido aplicada a la adsorción en poros planos para estudiar la influencia de los poros en esta propiedad. Los resultados indican que el confinamiento de la geometría cilíndrica introduce diferencias significativas en la forma de las isotermas de adsorción y de los perfiles de la densidad. Estas diferencias son relevantes para la caracterización de los materiales porosos. Nuestros resultados indican que un comportamiento de formación de capa tiene lugar en el poro cilíndrico, mientras que la adsorción en un poro plano del mismo tamaño necesita un potencial químico mucho más alto para alcanzar una adsorción significativa. Cuando el tamaño de poro se incrementa, la influencia de la geometría se vuelve menos importante, pero aún se observa un cierto desplazamiento del lugar en el cual se da la transición de la condensación capilar. Adicionalmente, para poros más anchos, tenemos formación de multicapas con condensación capilar a potenciales químicos altos, observándose el mismo comportamiento cualitativo en ambas geometrías. Cuando el diámetro alcanza el límite en donde los efectos de la curvatura ya no son relevantes, el comportamiento cuantitativo de los poros cilíndricos y de los planos es muy similar. La formación de una fina película adsorbida a tamaños de poro grandes e intermedios parece corresponder a una transición de fase

termodinámica de segundo orden, para el intervalo de parámetros usado y a las condiciones termodinámicas estudiadas. Sin embargo, los resultados encontrados parecen indicar que existe una relación entre este comportamiento y el de una transición de pre-mojado observada en geometrías semi-infinitas, especialmente en la vecindad del punto final crítico de la línea de pre-mojado. El efecto del confinamiento es muy importante en este comportamiento de transición. A partir de la comparación de los cálculos hechos con FMT y los hechos con la teoría funcional de la densidad no-local, concluimos que la FMT es una excelente herramienta para el estudio del comportamiento de los fluidos en geometrías cilíndricas confinadas.

En el capítulo 4 hemos aplicado la FMT en combinación con un método de regularización para estimar la distribución de tamaños de poros (PSD, del inglés *Pore-Size Distribution*) de materiales modelo que imitan a los vidrios porosos. Hemos elegido este material en particular porque fue desarrollado con técnicas de modelado molecular, y se puede hacer una comparación directa con la teoría aquí usada. Una ventaja adicional de estos materiales modelo, con respecto a los materiales reales, es que en este caso la forma y tamaño de los poros se conoce exactamente, además de que se sabe la posición de los átomos en la superficie, convirtiéndolo en un material ideal para verificar la exactitud de los métodos de caracterización teóricos disponibles. Dado que existen varias soluciones de la ecuación integral de adsorción compatibles con la isoterma de adsorción experimental, y que varios factores pueden ocultar los defectos del modelo molecular, hemos hecho la caracterización de una manera sistemática: primero hemos probado la exactitud de la FMT y del modelo de poros independientes para predecir las isotermas de adsorción "experimentales" usando la PSD geométrica ya conocida para estos materiales. Esto ha sido hecho tanto con los poros cilíndricos como con los planos. En segundo lugar, una vez que la isoterma de adsorción fue reconstruida, invertimos la isoterma integral de adsorción con un procedimiento de regularización. La exactitud del método de inversión ha sido verificado antes de estimar la PSD de los diferentes materiales. Finalmente, una vez que se ha establecido que el método es correcto, lo usamos para estimar las PSD's de estos cuatro materiales. Hemos estudiado también la influencia de elegir diferentes valores de los parámetros moleculares para la interacción fluido-fluido y para la sólido-fluido en el comportamiento de adsorción en estos sistemas. Los resultados indican que el modelo de poros independientes es adecuado para los cuatro materiales aquí investigados. La geometría plana parece representar el comportamiento de adsorción global mejor que la cilíndrica. En cuanto a lo que las PSD's obtenidas con nuestro procedimiento se refiere, las distribuciones resultantes a través de la inversión de la integral presentan una mejor concordancia con las distribuciones geométricas que las calculadas con el método Barrett-Joyner-Halenda (BJH). El máximo del pico está localizado en el mismo tamaño de poro, y las distribuciones son unimodales, mientras que las BJH's muestran un máximo sistemáticamente localizado a poros más pequeños, subestimando las PSD's del material, y éstas no son unimodales. Respecto a la geometría de los poros individuales que conforman el material, se puede decir, a pesar de que las PSD's son más dispersas que las geométricas, que la adsorción predicha por una colección de poros planos individuales tiene una concordancia casi cuantitativa con la isoterma de adsorción experimental.

Finalmente, en el capítulo 5 hemos caracterizado tres muestras diferentes de γ-alúmina, una de ellas sin ningún tratamiento, y las otras dos calcinadas en un horno durante varias horas a 823 y a 1,023K. Para ello hemos medido isotermas de adsorción de

nitrógeno a 77.35K en un equipo Micromeritics ASAP 2000. Adicionalmente, hemos usado las PSD's calculadas con el método BJH que proporciona el software del mismo equipo experimental para comparar. Hemos calculado las isotermas teóricas utilizando la FMT. Hemos invertido las ecuaciones integrales de adsorción con el método de regularización y, finalmente, hemos obtenido las PSD's para las tres muestras de alúmina, y las correspondientes isotermas de adsorción. De esta manera hemos podido observar la influencia de la calcinación de la alúmina en su PSD. Más aún, hemos probado la exactitud del método combinado FMT/Regularización de una manera sistemática. Cuando hemos comparado las PSD's obtenidas con las correspondientes BJH's, hemos verificado que en los dos primeros casos (alúmina sin tratamiento y alúmina calcinada a 823K) el método BJH subestima el tamaño de los poros, dando PSD's desplazadas a tamaños de poros más pequeños. En el caso de la alúmina calcinada a 1,023K, en la cual el proceso de sinterización ha producido la desaparición de los poros más pequeños en beneficio de los grandes, las PSD's BJH y las PSD's FMT/Regularización son muy similares. Con esto corroboramos el hecho conocido de que el método BJH es bastante exacto en la región de los macroporos. Para terminar, hemos predicho la isoterma de adsorción de un fluido diferente (etano) a una temperatura también diferente (333K) en uno de los materiales caracterizados (alúmina sin tratar) con la idea de comprobar sí la PSD obtenida es transferible a otras condiciones o no. La concordancia observada muestra que es posible usar este método de caracterización y extrapolar los resultados a otras condiciones, procurando que se utilice un número suficiente de tamaños de poro diferentes para calcular la isoterma deseada, y se elijan bien los parámetros de interacción sólido-fluido.

RESUM

Els materials porosos s'utilitzen àmpliament en moltes branques de la ciència i tecnologia modernes com la catàlisi, la separació de mescles, la purificació de fluids i la fabricació de membranes. Per a que els sòlids porosos puguin aplicar-se amb èxit cal disposar d'una caracterització precisa de la superfície i de les propietats estructurals, així com també una bona comprensió del comportament físico-químic dels fluids dins dels porus. Alguns materials, com les zeolites, tenen estructures poroses ben definides, però d'altres, com els òxids porosos, carbons i vidres de porus controlat, són bastant amorfs. Per això, un tema clau i, sovint, complicat, és la caracterització adequada d' aquests tipus de materials. Durant molts anys, l'adsorció de gasos s'ha emprat per estudiar les propietats de sòlids porosos, degut a que és un mètode ràpid, simple i que proporciona prou informació. Es van desenvolupar molts mètodes per extraure dades sobre la porositat i les propietats de la superfície de materials a partir d'isotermes d'adsorció. En les dues últimes dècades, amb l'ajuda dels ordinadors, cada cop més i més ràpids, l'ús de les tècniques de modelat molecular ha anat guanyant rellevància. En aquest context, l'objectiu general d'aquest treball de tesi és desenvolupar eines a escala molecular emprant la mecànica estadística i aplicant-la a la caracterització de materials adsorbents.

Després d'una breu introducció en el tema (capítol 1), en el capítol 2 presentem una revisió de la metodologia bàsica emprada en aquest treball. En el capítol 3 hem implementat la teoria funcional de la densitat de mesures fonamentals o FMT (de l'anglès, Fundamental-Measured density functional theory), publicada per Kierlik i Rosinberg, per descriure l'adsorció de molècules Lennard-Jones en porus cilíndrics. Pel que sabem, aquest és el primer cop que la teoria s'aplica a la geometria cilíndrica. L'exactitud de la teoria en predir isotermes d'adsorció i perfils de densitat de partícules es compara amb simulacions Monte Carlo en el col·lectiu gran canònic per un rang ample de mides de porus. Aquesta comparació mostra que la concordança és molt bona en tots els casos. Addicionalment, s'ha aplicat la teoria a l'adsorció en porus plans per estudiar la influència de la geometria del porus en aquest fenomen. Els resultats indiquen que el confinament de la geometria cilíndrica introdueix diferències significatives en la forma de les isotermes d'adsorció i els perfils de densitat. Aquestes diferències són rellevants a l'hora de caracteritzar materials porosos. Els resultats indiquen que té lloc un comportament per capes en el porus cilíndric més petit que s'ha considerat, mentre que l'adsorció en un porus pla de la mateixa grandària necessita un potencial químic molt més alt per aconseguir una adsorció significant. A mida que el diàmetre del porus augmenta, la influència de la geometria es fa cada cop menys important, encara que es pot observar una certa desviació en la transició de condensació capil·lar. Addicionalment, per porus més amples, obtenim una adsorció multicapa amb condensació capil·lar a potencials químics alts, amb el mateix comportament qualitatiu observat en ambdues geometries. Quan el diàmetre assoleix el límit on els efectes de curvatura ja no són rellevants, el comportament quantitatiu del porus cilíndric es redueix al mateix que el del porus pla. La formació d'una capa fina adsorbent en mides de porus intermèdies i grans sembla correspondre a una transició de fase termodinàmica de segon ordre, per al rang de paràmetres utilitzat i les condicions termodinàmiques estudiades. No obstant, els resultats semblen indicar una interrelació entre aquest comportament i la transició pre-mullada (de la paraula anglesa *prewetting*) que s'observa en geometries

semi-infinites, especialment al voltant del punt final crític de la línia pre-mullada. L'efecte del confinament és molt important en aquest comportament *crossover* (de pas). De la comparació de càlculs FMT amb resultats de la teoria funcional de la densitat no local, concloem que la FMT és una eina excel·lent per a l'estudi del comportament de fluids en geometries cilíndriques.

En el capítol 4 s'explica com hem aplicat la FMT juntament amb un mètode de regularització per estimar la distribució de mides de porus o PSD (de l'anglès, *Pore-Size Distribution*) de vidres porosos model. Hem escollit aquest material perquè va ser desenvolupat mitjançant tècniques de modelat molecular, i es pot comparar directament amb la teoria utilitzada en aquest treball. Un avantatge addicional d'aquests materials model, enfront els experimentals, és que, en el primer cas, la mida i forma dels porus són ben conegudes, així com també la posició dels àtoms en la superfície, esdevenint així un material perfecte per comprovar l'exactitud dels mètodes de caracterització teòrica disponibles. Com que hi ha diferents solucions de l'equació integral d'adsorció compatibles amb la isoterma d'adsorció experimental, i diversos factors poden amagar els defectes del model molecular, hem realitzat la caracterització d'una forma sistemàtica: primer hem comprovat l'exactitud de la FMT i el model de porus independent per predir les isotermes d'adsorció "experimentals" utilitzant la PSD ja coneguda per als materials. Això s'ha efectuat amb porus individuals plans i cilíndrics. En segon lloc, un cop la isoterma d'adsorció va ser reconstruïda amb èxit, vam invertir la isoterma d'adsorció integral amb un procediment de regularització. L'exactitud del mètode d'inversió s'ha comprovat també abans d'estimar la PSD de materials diferents. En últim lloc, un cop demostrat que el mètode és correcte, l'hem utilitzat per estimar la PSD de quatre materials. També hem estudiat la influència d'escollir alguns valors particulars de paràmetres moleculars per les interaccions fluid-fluid i sòlid-fluid en el comportament adsorbent d'aquests sistemes. Hem obtingut que el model de porus independent és adequat per als quatre materials investigats en aquest treball. La geometria plana sembla representar millor que la geometria cilíndrica el comportament adsorbent global. Pel que fa a la PSD obtinguda amb el nostre procediment, s'observa que les distribucions obtingudes mitjançant la inversió de la integral estan en millor concordança amb les distribucions geomètriques que les calculades amb el mètode Barrett-Joyner-Halenda (BJH). El locus del pic està situat a la mateixa mida de por, i tots ells són unimodals, mentre que les distribucions BJH mostren un màxim localitzat sistemàticament a porus més petits, estimant per sota la PSD del material, i no són unimodals. En quan a la geometria dels porus individuals que formen el material podem dir que, encara que la PSD és més ampla que les geomètriques, l'adsorció que es prediu per un conjunt de porus plans individuals està en un acord quasi quantitatiu amb la isoterma d'adsorció experimental.

Finalment, en el capítol 5 exposem com hem caracteritzat tres mostres diferents de γ-alúmina, una d'elles sense tractament i les altres dues calcinades en un forn durant unes hores a 823 i 1023K. Per fer-ho hem mesurat isotermes d'adsorció de nitrogen a 77.35K en un equip Micromeretics ASAP 2000. A més, hem aprofitat les PSD's proporcionades pel programari de l'equip emprant el mètode BJH. Hem calculat isotermes teòriques mitjançant l'aproximació FMT. Hem invertit les equacions integrals d'adsorció amb el mètode de regularització i, finalment, hem obtingut les PSD's per les tres mostres d'alúmina, i les corresponents isotermes d'adsorció pels tres materials. D'aquesta forma hem observat la influència de la calcinació de l'alúmina en la seva PSD. A més, hem comprovat l'exactitud del mètode FMT/de regularització de manera

sistemàtica. Quan comparem les PSD's obtingudes amb les corresponents distribucions BJH, hem verificat que, en els dos primers casos (alúmina no tractada i alúmina calcinada a 823K), el mètode BJH estima per sota la mida dels porus, proporcionant una PSD desviada cap a mides més petites. En el cas de l'alúmina calcinada a 1,023K, en la que el procés de sinterització produeix que els porus més petits desapareguin, afavorint els més grans, les PSD's del mètode BJH i les PSD's de la FMT/regularització són molt semblants. Amb això es corrobora el fet conegut de que el mètode BJH és força acurat en la regió macroporosa. Finalment, hem predit la isoterma d'adsorció d'un fluid diferent (età) a una altra temperatura (333K), en un dels materials caracteritzats (alúmina no tractada), amb l'ànim d'establir la robustesa de la PSD obtinguda. La concordança obtinguda mostra que és possible utilitzar aquest mètode de caracterització i extrapolar els resultats a altres condicions, mentre s'empri un nombre suficient de mides de porus per calcular la isoterma desitjada, i els paràmetres d'interacció sòlid-fluid es triïn adequadament.

TABLE OF CONTENTS

LIST OF FIGURES

LIST OF TABLES

1. INTRODUCTION

1.1 Motivation

Porous materials are widely used in many branches of modern science and technology, such as catalysis, separation of mixtures, purification of fluids and fabrication of membranes. A successful application of porous solids requires a characterization of their surface and structural properties, as well as a good understanding of the physical and chemical behavior of fluids inside the pores. Some materials, such as zeolites and molecular sieves, have well defined porous structures, but others, such as porous oxides, carbons and controlled-porous glasses, are quite amorphous. Therefore, a proper characterization of this kind of materials is an important topic, and more often than not, a complicated one.

For many years, gas adsorption has been used to study properties of porous solids [Rouquerol *et al*., 1999], since it is fast, simple and informative. Many methods were developed to extract information about porosity and surface properties of materials from adsorption isotherm data. In the last two decades, with the aid of the increasingly faster computers, the use of molecular modeling techniques has been gaining relevance.

In molecular modeling of adsorption, one starts from a well-defined molecular model of the system and then calculates the adsorption properties from statistical mechanics. The model is specified by defining equations to describe the fluid-fluid and solid-fluid interactions, and by defining the molecular structure of the solid material; the pore sizes and shapes, positions and species of the wall atoms, and any laws governing motion of the wall atoms. The equations of statistical mechanics for this model are then solved either by theoretical approximations, or by numerical methods (molecular simulation).

This molecular approach has several advantages: firstly, the observed properties are directly related to the underlying molecular model. Secondly, when agreement with experimental data is inadequate, systematic improvement of the molecular model is possible. And finally, such models can be used to investigate the effects of a variety of variables (adsorbate, pore size and shape, nature of material) in a systematic way; such an approach is usually not possible in the laboratory.

The principal difficulties in modeling adsorption processes are usually a lack of precise knowledge of the structure of the porous material and inadequate or unsuitable experimental results with which to refine the models and to compare with calculations.

The inappropriate experimental measurements arise in part due to the fact that many workers still use older and more classical methods of interpretation. Some examples of this are the Brunauer-Emmett-Teller equation for surface area, Kelvin-based methods for pore-size distributions, *etc*. [Rouquerol *et al*., 1999]. These methods have little molecular basis, and in particular do not rely on any model of the intermolecular interactions. Molecular-based methods of interpretation require low-pressure adsorption measurements to check the solid-fluid interaction models, and also rely on knowledge of the molecular nature of the surfaces involved. Thus, while molecular methods are more difficult to apply and may require more careful measurements, they provide fundamental insight into the adsorption processes.

1.2 Objectives

The general objective of this thesis is to develop tools on a molecular scale from a statistical mechanics perspective in order to apply them to the characterization of porous materials. We will use two techniques, density functional theory and Monte Carlo simulations applied to some selected materials.

The particular objectives are enumerated as follows:

- Implementation of the Fundamental-Measured density functional theory due to Kierlik and Rosinberg [1990] to describe the adsorption of Lennard-Jones molecules in cylindrical pores.
- To test the accuracy of the theory *versus* Monte Carlo simulation.
- Comparison of the adsorption behavior in cylindrical and slit-like pores.
- Implementation of a technique to obtain pore-size distributions by means of the regularization inversion method of the adsorption integral equation.
- To verify the hypothesis of the independent pores model using two simple geometries for individual pores: cylindrical and slit-like shapes; well-characterized porous materials (controlled-porous glasses), and density functional theory.
- Characterization of γ-alumina to obtain the pore-size distribution using density functional theory and to study the effect of the calcination of the material in the pore-size distribution.
- To establish the prediction capability of the pore-size distribution obtained to calculate the adsorption isotherm of the ethane on γ-alumina at different thermodynamic conditions.

1.3 Methodology

1.3.1 Density functional theory

In density functional theory the first step is to define the molecular model of the system of interest, to construct the equations of statistical mechanics for this model, and to solve them by some approximation method. In this approach a van der Waals type

approximation is made for the free energy; that is, an approximate expression for the free energy is written as a sum of a short-range repulsive (hard-sphere) contribution and a long-range attractive contribution. This expression involves the density profile, $\rho(\boldsymbol{r})$, and the free energy is then minimized with respect to $\rho(\boldsymbol{r})$ in order to find the true equilibrium density profile. Once this is known, it is possible to calculate the free energy, adsorption isotherm, and other equilibrium properties. Density functional theory is easy to apply to systems of simple geometry and to pure and mixed fluids composed of spherical molecules. The principal disadvantages of such an approach are that it is difficult to apply to complex systems, *e. g*. non-spherical molecules, pores of complex geometry, or heterogeneous surfaces and, that some approximations need to be made. Molecular simulations are much more flexible in these regards.

1.3.2 Molecular simulation

An alternative approach is molecular simulation, in which the rigorous equations of statistical mechanics are written down for the model system, and then solved numerically. Provided that the solution is correctly carried out (*e. g*. large enough system, long enough runs, boundary conditions and long-range corrections applied properly) the simulation will yield an exact answer (within some statistical uncertainty that can be estimated) for the model system. There are two principal methods: Monte Carlo and molecular dynamics. The Monte Carlo approach relies on the development of a Markov chain, by randomly trying different types of moves, and applying suitable acceptance criteria to these movements. Equilibrium properties of the system, such as adsorption, density profiles, isosteric heats of adsorption, selectivities, *etc*., can be obtained by averaging over the Markov chain using the laws of statistical mechanics.

1.4 Contents

The rest of this thesis is organized as follows. In chapter 2 we review the fundamentals of the different molecular modeling tools used in this work. Chapter 3 is devoted to the Fundamental-Measured density functional theory applied to cylindrical and slit-like pores, along with a comparison with Monte Carlo simulation results of cylindrical pores. In chapter 4 we present and discuss our results of the pore-size distribution obtained with the independent pore model using cylindrical and slit-like pores of controlled-pore glasses. In chapter 5 we discuss the pore-size distribution of γ-alumina calculated using experimental adsorption isotherms of nitrogen at 77.35K and the inversion of the adsorption integral equation. Also, we study the effect of the calcination of the alumina over the pore-size distribution, and the capability to predict of the adsorption isotherms of ethane on alumina at other thermodynamic conditions using this pore-size distribution. Finally, chapter 6 gives a briefly summary of this work and gives some recommendations for future work.

1.5 References

Kierlik, E.; Rosinberg, M. L. *Phys. Rev. A* **42**, 3382 (1990).

Rouquerol, F.; Rouquerol, J.; Sing, K. *"Adsorption by Powders & Porous Solids"*, (Academic Press, London, 1999).

2. METHODOLOGY

2.1 Introduction

Three primary methods exist for studying nearly any basic problem in science: experimentation, theoretical calculations, and molecular scale computer simulations. When performing an experiment, the researcher is able to directly measure the properties of the real system. However, most of the times the range and the amount of the data, which may be obtained, are limited by several situations, such as the difficulty to achieve some experimental conditions, the cost of equipment, *etc*. Additionally, sometimes a model to interpret the experimental data is necessary due to the measurement of the desired property is not directly extracted.

In this sense, adsorption data and mercury porosimetry are widely used to characterize porous materials [Gregg and Sing, 1982], the classical methods for interpreting such data rely on equations that are more than 50 years old, and are of uncertain validity, particularly for micropores and small mesopores. The most important of these equations are those of Brunauer, Emmet and Teller (BET), Kelvin, and Dubinin and Radushkevitch (DR) and their modified forms [Gregg and Sing, 1982]. The BET equation neglects adsorbate-adsorbate interactions, heterogeneity of the surface, and variations in properties of adsorbed layers after the first; nevertheless, it usually gives a good account of low-pressure adsorption, especially for nonporous materials. The Kelvin equation assumes a) the vapor phase is ideal, b) the liquid phase is incompressible, with a molar volume that is negligible compared to the gas, and c) the system is large enough for the surface tension to be defined. Assumptions a) and b) will lead to significant errors at higher temperatures, especially as the capillary critical point is approached, while approximation c) will lead to increasing errors as the pore size decreases. As well, a breakdown occurs in using the Kelvin equations as the pore size decreases [Thompson *et al*., 1984] The DR equation introduces a single adjustable parameter to characterize the pore-fluid system, and is essentially empirical in nature.

Statistical mechanics provides a more reliable and general approach for the interpretation of adsorption and porosimetry experiments. At the present time the two most promising approaches are density functional theory (DFT) and direct molecular simulation. The simulation approach has the advantage that the statistical mechanical equations are solved exactly for the prescribed model of the pore geometry and intermolecular interactions; it is relatively easy to incorporate surface structure and heterogeneity, and a variety of pore geometries and irregularities. The DFT approach involves some approximations, but provides a more systematic procedure to study the physical behavior of systems. In general, applications of the DFT have until recently

been limited to problems where the density profiles are uniform in two dimensions. The result is a 1D numerical problem that must be solved. This is an important limitation to apply DFT to structured walls, where the heterogeneity of the walls produces a 3D problem, with the need to perform nested integrals. These integral equations are expensive both in evaluation time and in memory requirements; however, intelligent algorithms and the use of parallel computers can mitigate the expense [Douglas Frink and Salinger, 2000]. In synthesis, both methods, the molecular simulation and DFT calculations give more detailed insight and higher accuracy than the classical methods currently in use to characterize porous materials.

In this chapter we briefly explain the fundamentals underlying on the molecular model techniques used in this work. First, the density functional theories, and in second place, the molecular simulation Monte Carlo method in the Grand Canonical ensemble. After that, we defined the pore-size distribution and we expose the methodology used to obtain it. At the end, we present the details of the procedure used, at which the experimental adsorption isotherms were measured.

2.2 Fundamental Measure density functional theory (FMT)

In the formulation of the DFT used along this work we essentially follow the work of Kierlik and Rosinberg [1990]. The free energy density, $F[\rho(\mathbf{r})]$, is expressed as [Evans, 1979]

$$F\left[\rho(\mathbf{r})\right] = k_B T \int d\mathbf{r}\rho(\mathbf{r})\left[\ln\left(\Lambda^3\rho(\mathbf{r})\right)-1\right]+F_{ex}\left[\rho(\mathbf{r})\right], \tag{2.1}$$

where the first term on the right-hand side represents the ideal contribution, while the second term is the excess free energy density. In this expression

$$\Lambda \equiv \left(\frac{2\pi\hbar^2}{mk_BT}\right)^{1/2}, \tag{2.2}$$

where Λ is the de Broglie wavelength, $\hbar$ is Planck's constant over 2π, m is the mass of the particle, k_B is Boltzmann's constant and T is the absolute temperature. In fluids with interactions such as those described through the Lennard-Jones (LJ) intermolecular potential, the excess free energy is further decomposed into a contribution of a reference system of hard spheres plus the contribution due to the attractive interactions, usually treated under a mean-field approximation, according to

$$F_{ex}\left[\rho(\mathbf{r})\right] = F_{HS}\left[\rho(\mathbf{r})\right]+F_{att}\left[\rho(\mathbf{r})\right]. \tag{2.3}$$

In the FMT formulation, the excess free energy contribution of the reference system of hard spheres is further expressed in terms of fundamental geometrical measures of the particles [Kierlik and Rosinberg, 1990; Rosenfeld, 1989]. In particular, the functional proposed for the excess free energy of the hard-sphere fluid, $F_{HS}[\rho(r)]$, yields the Percus-Yevick (PY) compressibility equation of state for an homogeneous fluid [Wertheim, 1963; Thiele, 1963; Lebowitz, 1964], or the scaled particle theory (SPT) [Reiss *et al*., 1959; Helfand *et al*., 1961]. In choosing this particular recipe of DFT, we take into account the fact that its predictions of the structural and thermodynamic

properties of the fluid are obtained as consequences of the theory itself, without further assumptions common to other theories [Evans, 1992]. This DFT for the hard-sphere fluid might be considered as a generalization of the SPT free energy to non-uniform situations. Another advantage of this DFT recipe is that the density-independent expression of the weighting functions avoids the need to calculate them anew for each point in the pore. Moreover, the extension to mixtures is straightforward, and specific versions are designed to deal with the crossover to one and zero-dimensional systems [Rosenfeld *et al*., 1997; Tarazona, 2000].

With the aim at studying the adsorption of LJ particles on pores, it is convenient to work under constant chemical potential μ. Therefore, we will focus our attention on the grand potential of the system, defined from the Helmholtz free energy according to

$$\Omega[\rho(\mathbf{r})] \equiv F[\rho(\mathbf{r})] - \int dr\, \rho(\mathbf{r})[\mu - \phi_{ext}(\mathbf{r})], \tag{2.4}$$

where the first term on the right-hand side is the intrinsic Helmholtz free energy functional, and in the second term the expression $\phi(r)_{ext}$ takes into account the potential imposed by the wall.

In the FMT formulation the grand potential hence takes the form

$$\begin{aligned}\Omega[\rho(\mathbf{r})] = k_B T \int d\mathrm{r}\rho(\mathrm{r})\left[\ln\left(\Lambda^3\rho(\mathrm{r})\right)-1\right] + k_B T \int d\mathrm{r}\Phi\left(\{\bar{n}_\alpha(\mathrm{r})\}\right) \\ + \tfrac{1}{2}\int d\mathrm{r}\int d\mathrm{r}'\,\rho(\mathbf{r})\rho(\mathbf{r}')\phi_{att}\left(|\mathrm{r}-\mathrm{r}'|\right) - \int d\mathrm{r}\rho(\mathrm{r})[\mu - \phi_{ext}(\mathrm{r})].\end{aligned} \tag{2.5}$$

In this expression, the first term stands for the ideal gas contribution to the free energy. The second term is the excess free energy of the hard-sphere reference system in a weighted density approximation [Kierlik and Rosinberg, 1990]. The third term describes the effect of the attractive interactions between particles, ϕ_{att}, introduced in a mean-field way. The functional dependence of ϕ_{att} stresses the fact that we will only consider here isotropic interactions. The last term represents the contribution of the bulk chemical potential as well as the effect due to the walls of the pore, introduced through the external field $\phi_{ext}(\boldsymbol{r})$.

According to Kierlik and Rosinberg [1990] the excess free-energy density of the reference system of hard spheres, $k_B T\Phi(\{\bar{n}_\alpha(\boldsymbol{r})\})$, is assumed to be a function of the weighted densities, the latter defined as

$$\bar{n}_\alpha(\mathbf{r}) = \int d\mathbf{r}'\,\omega^{(\alpha)}(\mathbf{r}-\mathbf{r}')\rho(\mathbf{r}'), \tag{2.6}$$

with α = 0, 1, 2, and 3. The four weight functions $\omega^{(\alpha)}(r)$ are related to the Heaviside step function, $\Theta(r)$, and its derivatives. These weight functions are independent of the density and are given by

$$\begin{aligned}
\omega^{(3)}(\mathrm{r}) &= \Theta(R-\mathrm{r}) \\
\omega^{(2)}(\mathrm{r}) &= \delta(R-\mathrm{r}) \\
\omega^{(1)}(\mathrm{r}) &= \frac{1}{8\pi}\delta'(R-\mathrm{r}) \\
\omega^{(0)}(\mathrm{r}) &= -\frac{1}{8\pi}\delta''(R-\mathrm{r}) + \frac{1}{2\pi\mathrm{r}}\delta'(R-\mathrm{r}),
\end{aligned} \tag{2.7}$$

where R is the effective radius of the hard-sphere reference fluid, $\delta(r)$ is the isotropic Dirac delta function, and the primes denote successive derivatives of the delta function with respect to r. In particular, the hard-sphere excess free energy has the form [Kierlik and Rosinberg, 1990]

$$\Phi(\{\bar{n}_\alpha\}) = -\bar{n}_0 \ln(1-\bar{n}_3) + \frac{\bar{n}_1\bar{n}_2}{1-\bar{n}_3} + \frac{1}{24\pi}\frac{\bar{n}_2^3}{(1-\bar{n}_3)^2}. \tag{2.8}$$

At this point, the equilibrium properties of the fluid can be obtained by minimizing the grand potential functional, Eq. 2.5, with respect to the local density, according to

$$\frac{\delta\Omega[\rho(\mathbf{r})]}{\delta\rho(\mathbf{r})} = 0, \tag{2.9}$$

at constant chemical potential, μ, and under appropriate boundary conditions [Evans, 1979]. The above requirements result in the Euler-Lagrange equation

$$\mu = k_B T \ln\left(\Lambda^3 \rho(\mathbf{r}'')\right) + \int d\mathbf{r} \sum_\alpha \omega^{(\alpha)}(|\mathbf{r}-\mathbf{r}''|)\frac{\partial\Phi}{\partial\bar{n}_\alpha(\mathbf{r})} + \int d\mathbf{r}\rho(\mathbf{r})\phi_{att}(|\mathbf{r}-\mathbf{r}''|) + \phi_{ext}(\mathbf{r}''), \tag{2.10}$$

which is an implicit relationship to be satisfied at every space point $\boldsymbol{r''}$, whose functional inversion yields the density profile in terms of the chemical potential, the attractive and external potential fields and the geometry of the particles.

2.3 Non-local density functional theory

The most advanced non-local version of DFT (NLDFT) was first developed by Tarazona [1985], who introduced the smoothed (or weighted) densities, and thereafter modified by Tarazona *et al*. [1987], Rosenfeld [1989], Denton and Ashcroft [1991], Kierlik and Rosinberg [1990], and Patra and Ghosh [1993]. NLDFT has recently been successfully employed for analyses of a number of quite complicated problems in interfacial and adsorption equilibrium, phase transition, complex fluids, *etc*. A brief review of most of its applications in confined fluids is described in the next chapter.

The Tarazona DFT gives good results for the hard sphere direct correlation function, the results being only very slightly different from the PY values at a high (liquid-like) reduce density $\rho\sigma^3$ = 0.8, while at lower densities the two theories are usually indistinguishable. This DFT has the advantages of being both quite accurate and relatively easy to use in numerical calculations for realistic intermolecular potentials such as Lennard-Jones. It is also able to predict solid-fluid transitions, in contrast to some other forms of DFT. However, it also has several shortcomings:

- It is difficult to use for mixtures, since the extension to several components involves some ambiguity in the definition of the weighting functions [Tan *et al.*, 1989].
- The weighting factors depend on the smoothed density, and so must be calculated afresh for each point in the pore.

In this approximation [Tarazona, 1985; Tarazona *et al*., 1987] the free energy of the hard-sphere fluid is evaluated at the smoothed density $\bar{\rho}(\mathbf{r})$

$$F_{HS}[\rho(\mathbf{r})] = \int d\mathbf{r}\rho(\mathbf{r}) f_{HS}[\bar{\rho}(\mathbf{r})]. \tag{2.11}$$

Here $f_{HS}[\bar{\rho}(\mathbf{r})]$ is the excess free energy per particle, which is calculated from the Carnahan-Starling equation of state [Carnahan and Starling, 1969]. The smoothed density is defined as

$$\bar{\rho}(\mathbf{r}) = \int d\mathbf{r}'\, \rho(\mathbf{r}') w(|\mathbf{r}-\mathbf{r}'|, \bar{\rho}(\mathbf{r})), \tag{2.12}$$

where $w(|\mathbf{r}-\mathbf{r}'|, \bar{\rho}(\mathbf{r}))$ is the weighting function. Tarazona proposed the following expansion for the weighting function

$$w(r,\rho) = w_0(r) + w_1(r)\rho + w_1(r)\rho^2. \tag{2.13}$$

The coefficients $w_0(r)$, $w_1(r)$, and $w_2(r)$ were found from the requirements that the functional approximates the PY two-particle direct correlation function of the homogeneous hard-sphere fluid [Hansen and McDonald, 1991]. Explicit expressions for the weighting functions are given by the follow equations and are taken from Tarazona *et al*. [1987]

$$w_0(r) = \begin{cases} \dfrac{3}{4\pi\sigma^3}, & r < \sigma, \\ 0, & r > \sigma, \end{cases}$$

$$w_1(r) = \begin{cases} 0.475 - 0.648\left(\dfrac{r}{\sigma}\right) + 0.113\left(\dfrac{r}{\sigma}\right)^2, & r < \sigma, \\ 0.288\left(\dfrac{\sigma}{r}\right) - 0.924 + 0.764\left(\dfrac{r}{\sigma}\right) - 0.187\left(\dfrac{r}{\sigma}\right)^2, & \sigma < r < 2\sigma, \\ 0, & r > 2\sigma, \end{cases} \tag{2.14}$$

$$w2(r) = \begin{cases} \dfrac{5\pi\sigma^3}{144}\left(6 - 12\left(\dfrac{r}{\sigma}\right) + 5\left(\dfrac{r}{\sigma}\right)^2\right), & r < \sigma, \\ 0, & r > \sigma. \end{cases}$$

2.4 Monte Carlo simulation method

In the past three decades, computer "experiments" have come to play a major role in fluid-state physics. Their importance, from the theoretician's point of view, rests on the fact that they provide essentially exact, quasi-experimental data on well-defined models. As there is no uncertainty about the form of the interaction potential, theoretical results can be tested unambiguously in a manner that is generally impossible with data obtained in experiments of real systems. It is also possible to obtain information on quantities of theoretical importance that are not readily measurable in the laboratory [Hansen and McDonald, 1991].

Simulation studies have been used in two ways. On the one hand, the results can be compared with those from an approximate theory based on statistical mechanics and using the same set of intermolecular forces. This provides a test of the approximations made in the latter theory, which does not depend upon knowledge of the forces, or on experimental artifacts. Simulations used in this way to furnish exact data for a model are often referred to as "machine experiments". On the other hand, the simulation results may be compared with real (physical) experiments, when they provide a test of the assumptions employed in the model and, in particular, those concerning the intermolecular forces. Machine experiments are often limited by the existence or otherwise of suitable materials for study. In both cases it is, of course, nature that is the source of inspiration and ultimate object of interest as in any other scientific work.

Two distinct methods are available [Hansen and McDonald, 1991], and have been widely used: the Monte Carlo method of Metropolis *et al*. [1953] and the method of molecular dynamics pioneered by Alder and Wainwright [1959]. This type of calculation provides what may be regarded as essentially exact results for a given intermolecular force law, thereby eliminating the ambiguity that invariably arises in the interpretation of experimental data on real systems. Their usefulness rests ultimately on the fact that a model containing a relatively small number of particles, typically several hundreds is in most cases sufficiently large to simulate the behavior of a macroscopic system.

In the method of molecular dynamics, the classical equations of motion of a system of interacting particles are solved, and equilibrium properties are determined from time averages taken over a sufficiently long time interval. The Monte Carlo method involves the generation of a series of configurations of the particles of a model in a way that ensures that the configurations are distributed in phase space according to some prescribed probability density. The mean value of any configurational property determined from a sufficiently large number of configurations provides an estimate of the ensemble-averaged value of that quantity, the character of the ensemble average being independent on the particular sampling procedure that is used. The major advantage of molecular dynamics is that it allows the study of time-dependent processes [Hansen and McDonald, 1991]. For the calculation of thermodynamic properties, however, the Monte Carlo method is often more suitable. We are interested in equilibrium thermodynamic and structural properties; therefore, we use Monte Carlo in this work.

As the name suggests, a probabilistic element is an essential part of any Monte Carlo computation. In a classical Monte Carlo calculation, a system of N particles interacting through some known potential is assigned a set of arbitrarily chosen initial coordinates; a sequence of configurations of the particles is then generated by successive random displacements. Not all configurations that occur are accepted, the decision whether to "accept" or "reject" a particular configuration is been made in such a way as to ensure that, asymptotically, the configuration space is sampled according to the equilibrium probability density appropriate to a chosen ensemble. The ensemble average of a function of the coordinates of the particles, such as the potential energy, is then obtained as an unweighted average over the resulting set of configurations. The particle momenta do not enter the calculation, there is no time scale involved, and the order in which the configurations occur has no special significance [Hansen and McDonald, 1991].

The only input information in a computer simulation, apart from the fixed parameters and the chosen initial conditions, are the details of the particle interactions. There is no restriction on the form of the inter-particle potential, but in practice it is nearly always assumed to be pair-wise additive. For economy in computing time, it is customary to truncate the interaction at a separation $r = r_c \leq \frac{1}{2}L$, where r_c is the cut-off radius and L is the length of the simulation box. The effect of the neglected interactions on bulk properties of the system can be allowed for by making an appropriate "tail corrections" (long-range corrections) [Hansen and McDonald, 1991].

Grand Canonical Monte Carlo (GCMC)

The GCMC method simulates an open system specified by fixed temperature T, volume V and chemical potential μ. It is the staple technique for the simulation of an adsorbed fluid (or fluid mixture) in equilibrium with a bulk fluid reservoir, which is frequently the situation encountered in experimental studies of confined fluids. The method was first used in studies of bulk fluids [Adams, 1975; Norman and Filinov, 1969], and was quickly extended to adsorbed systems [Van Megen and Snook, 1982; 1985].

GCMC, like the rest of the Monte Carlo methods used in molecular simulation, is based on the use of a Markov chain to generate a series of molecular configurations [Ross, 1997] with the correct distribution of energy and density. In the grand canonical ensemble, the probability associated with any given (classical) state s of the system is [Allen and Tildesley, 1987]

$$P(s) \propto \exp\left[-\beta\left(\nu(s) - N\mu\right) - \ln N! - 3N\ln\Lambda + N\ln V\right], \qquad (2.15)$$

where Λ is the de Broglie wavelength, $\beta = 1/k_BT$, $\nu(s)$ is the total intermolecular potential energy of the system, and N is the number of molecules in the system. Most simulators use the original prescription for generating the Markov chain proposed by Norman and Filinov [Norman and Filinov, 1969; Allen and Tildesley, 1987], In this method [Allen and Tildesley, 1987; Frenkel and Smit, 1996], subsequent steps in the chain are generated by modifying the current molecular configuration in one of three ways: either creating a new molecule at a random position, destroying an existing molecule, or displacing an existing molecule by a random vector. These "moves" are then accepted or rejected according to the following criteria based on the temperature and chemical potential

$$\begin{aligned} P_{displace} &= min\left[1, \exp\left(-\beta\Delta v\right)\right] \\ P_{create} &= min\left[1, \exp\left(-\beta\Delta v\right) + \mu - \ln\left(N+1\right)\right], \\ P_{destroy} &= min\left[1, \exp\left(-\beta\Delta v\right) - \mu + \ln\left(N\right)\right] \end{aligned} \tag{2.16}$$

where P_i, the probabilities of each type of "move" are equal. Thermodynamic quantities of interest can be estimated by averaging their microscopic counterparts over a large number, M, of these configurations, for instance, the average internal energy $<U>$ is estimated by the average of the instantaneous potential energy, $1/M \sum_i^M v(\boldsymbol{s})$. In general, there is considerable freedom in choosing the parameters controlling the simulation, and statistically efficient choices of these parameters, as well as the total simulation length, vary widely between different systems.

The thermodynamic potential appropriate to the grand canonical ensemble is the grand free energy, Ω, given by

$$\Omega = F - \mu\langle N\rangle, \tag{2.17}$$

where F is the Helmholtz free energy, $F = U\text{-}TS$ and $<N>$ is the average number of molecules (for a mixture the last term on the right-hand side of Eq. 2.17 is replaced by sum over all components, $\sum_\alpha \mu_\alpha \langle N_\alpha \rangle$). For a pore of general shape the exact differential of Ω is given by

$$d\Omega = -SdT - P_b dV - \langle N\rangle d\mu + \gamma dA, \tag{2.18}$$

where S is the entropy, P_b is the bulk phase pressure, γ is the solid-fluid interfacial tension and A is the surface area. From this equation the form of the Gibbs adsorption isotherm is obtained

$$\left(\frac{\partial\Omega}{\partial\mu}\right)_{T,V,A} = -\langle N\rangle. \tag{2.19}$$

In this work, adsorption isotherms and density profiles have been obtained through a GCMC scheme. The temperature T, the volume V, and the chemical potential μ inside the pore are thus fixed. To obtain the adsorption isotherms, we ran the simulation at values of the activity, defined as

$$z = \frac{\exp\left(\mu/k_B T\right)}{\sigma}, \tag{2.20}$$

corresponding to bulk chemical potential, equal to those used in the density functional theory calculations.

2.5 Pore-Size Distribution (PSD)

As we mentioned in the beginning of this section, there exist two main classes of methods to interpret adsorption data with the aim to obtain PSD information. The methods based on classical thermodynamics and the methods based on statistical

mechanics. In this work, we are dealing only with the last methods, although, we use the Barrett-Joyner-Halenda (BJH) method for comparison.

2.5.1 Methods to obtain PSD by statistical mechanics

The behavior of the experimentally measured adsorption isotherms can be related in a simple way using an independent pore model [Seaton *et al*., 1989]. This means that an experimental adsorption isotherm can be represented as a set of independent, non-interconnected pores of ideal and simple geometry of different sizes; usually these are of slit shape for activated carbons, and of cylindrical geometry for glasses, oxides, silicas, *etc*. Therefore an experimental adsorption isotherm $\Gamma(P)$ represents an average over all values of the pore sizes existing on the porous material

$$\Gamma(P) = \int_{H_{min}}^{H_{max}} \rho^{E}(P,H) f(H) dH \,, \tag{2.21}$$

where $\rho^{E}(P,H)$ represents the theoretical isotherm at some specific size (H), $f(H)$ is the PSD and the sum is over the range of pore sizes (H_{min} to H_{max}). To obtain the PSD is necessary to invert this integral equation. In this section we briefly expose a review of the various methods available in the literature for carrying out this inversion process.

It is important to stress at the outset that the integral equation relating the adsorption isotherm to the local isotherm and the distribution function (Eq. 2.21) when applied to a set of experimental points provides an "ill-posed" set of simultaneous equations. Their solution can be performed reliably to obtain stable results only if highly accurate experimental adsorption isotherms are available, covering a wide range of pressures: four or five orders of magnitude are usually considered necessary. Since all experimental points are subject to inherent random errors, the experimental data usually need to be smoothed before subjecting them to numerical analysis. Smoothing of experimental data is often achieved by a least squares quadratic fit to a quadratic curve. Alternatively the smoothing may be carried out using spline-fitting techniques.

The methods available for the evaluation of PSD functions fall into two main groups: those in which a general analytical form of the distribution function is postulated, and the parameters describing it are calculated from the experimental data, and those in which no *a priori* assumption is made about the shape of the distribution. An excellent source with the details of these methods is the book of Rudzinski and Everett [1992] applied to adsorption energy distributions, but the integral equations are essentially the same.

The work of Seaton *et al*. [1989] was the first one in which nitrogen adsorption measurements were used to determine PSD in porous carbons using a molecular model. In this study, they used local DFT [Evans and Tarazona, 1984; Evans *et al*., 1986a; 1986b] to model nitrogen isotherms, and it is an example of the application of the first kind of methods described above to obtain PSD. They fitted a bimodal log-normal distribution. Following this work, later, Lastoskie *et al*. [1993] used a log-normal

distribution and a gamma distribution to describe microporous carbons using nitrogen isotherms. In this work they demonstrated that NLDFT provides a more accurate interpretation of the PSD that classical methods and the local DFT, and they found that a sufficiently large sample data (typically 30-50 points) constraints the shape of *f(H)*. Of such a way that the numerical values of the pore-size distribution will essentially be the same, provided a sufficiently flexible functional form is chosen for the PSD. They used two different functional forms to test the numerical uniqueness of PSD of carbons, obtaining the same distribution. El-Merraoui *et al*. [2000] used a bimodal log-normal function to describe the PSD of activated carbon fiber.

Included in the second group using the Tikhonov regularization method we can find the work of Neimark *et al*. [1998], in which they obtain the PSD of MCM-41 type adsorbents (cylinder pores) by means of nitrogen and argon adsorption using NLDFT. Additionally the work of Ravikovitch *et al*. [2000] in where they show that using N_2, Ar, and CO_2 adsorption isotherms with the same methods (NLDFT and Tichonov regularization) obtain very similar PSD of microporous carbonaceous materials (slit-shaped pores). Gusev and coworkers [1997], and Davies and Seaton [2000] have used GCMC simulations combined with regularization method to obtain PSD of activated carbons. Davies *et al*. [1999] and Davies and Seaton [1999] have addressed in detail the problem of calculating PSD's from adsorption data. They have stressed the importance of the identification of an optimal smoothing parameter to be used in the analysis.

2.5.2 The BJH method

The BJH method for calculating PSD [Barrett *et al*., 1951] is one of a family of methods [Gregg and Sing, 1982] based on a model of the adsorbent as a collection of cylindrical pores. The method accounts for capillary condensation in the pores using the classical Kelvin equation. In each pore the total excess adsorption is given by a surface layer thickness *t(P)* plus a pore-filling term; the pore is filled if the pressure satisfies

$$Ln\frac{P}{P_0} \geq \frac{-2\gamma\ V_L}{RT}\frac{1}{r_c}, \tag{2.22}$$

where $r_c = r - t(P)$ and r is the radius of the pore. V_L is the molecular volume of the liquid, γ is the surface tension, and P_0 is the vapor pressure. Thus, the Kelvin equation is only applied to the "core" fluid in this treatment. In the original BJH formulation, a simplification was introduced in which the parameter c, the ratio of core radius to pore radius, is assumed constant. In the results taken from literature [Gelb and Gubbins, 1999] and shown here (section 4.4) for comparison, this assumption is relaxed and therefore this is their only deviation from the original approach [Barrett *et al*., 1951].

This analysis requires independent determination of γ, V_L, P_0, and the reference isotherm *t(P)*. Gelb y Gubbins [1999] have determined V_L and P_0 using Gibbs Ensemble Monte Carlo simulations of the bulk fluid. The surface tension was interpolated from previous simulations of a LJ liquid [Holcomb *et al*., 1993; Chapela *et al*., 1977]; the value used were $\gamma^* = 0.389$ at $T^* = 0.809$, in reduced units [Gelb y Gubbins, 1998]. These data were fitted with a modified BET isotherm [Brunauer *et al*., 1969] to provide an analytical function of *t(P)*.

2.6 Experimental adsorption isotherm

All equipment designed to measure surface area, adsorption/desorption isotherms or pore volume by adsorption actually determines the quantity of gas condensed on a solid surface at some equilibrium vapor pressure [Lowell and Shields, 1991]. The surface area or pore volumes and pore sizes are then calculated by means of an appropriate theory used to treat the adsorption and/or desorption data. Depending on the apparatus employed, the adsorbed quantity is measured as volume or weight. The accuracy of an adsorption apparatus is, therefore, dependent upon its ability to measure correctly either of these quantities.

Many types of vacuum adsorption apparatus have been developed. However, all vacuum adsorption systems have certain essential features, including a vacuum pump, two gas supplies, a sample container, a calibrated volume, manometer and a coolant. Micromeritics house builds two very different types of instruments, which employ very different techniques. They are identified as static volumetric method and the flowing gas, or dynamic, method [Webb and Orr, 1997].

Static volumetric methods are those by which adsorption is measured using mass balance equations, appropriate gas equation of state, and measured pressures. During analysis the sample most frequently is maintained at cryogenic temperature, generally that of liquid nitrogen. Gas usually is supplied at near ambient temperature and at precise pressures through a manifold having accurately known volume and temperature. The molar quantity of gas adsorbed at equilibrium is computed by following gas pressure changes as quantities of gas are admitted from a manifold to a sample [Webb and Orr, 1997].

Figure 2.1 shows a schematic diagram of the essential elements of a volumetric adsorption apparatus. It consists basically of three valves, one to admit the adsorptive, one to connect to an evacuation system, and one to isolate the sample; three transducers to permit measuring gas pressures from very low to above ambient; the sample holder which can either be heated or cooled (the cryogenic bath is shown); and interconnecting passageways which, collectively, comprise what is called the manifold [Webb and Orr, 1997].

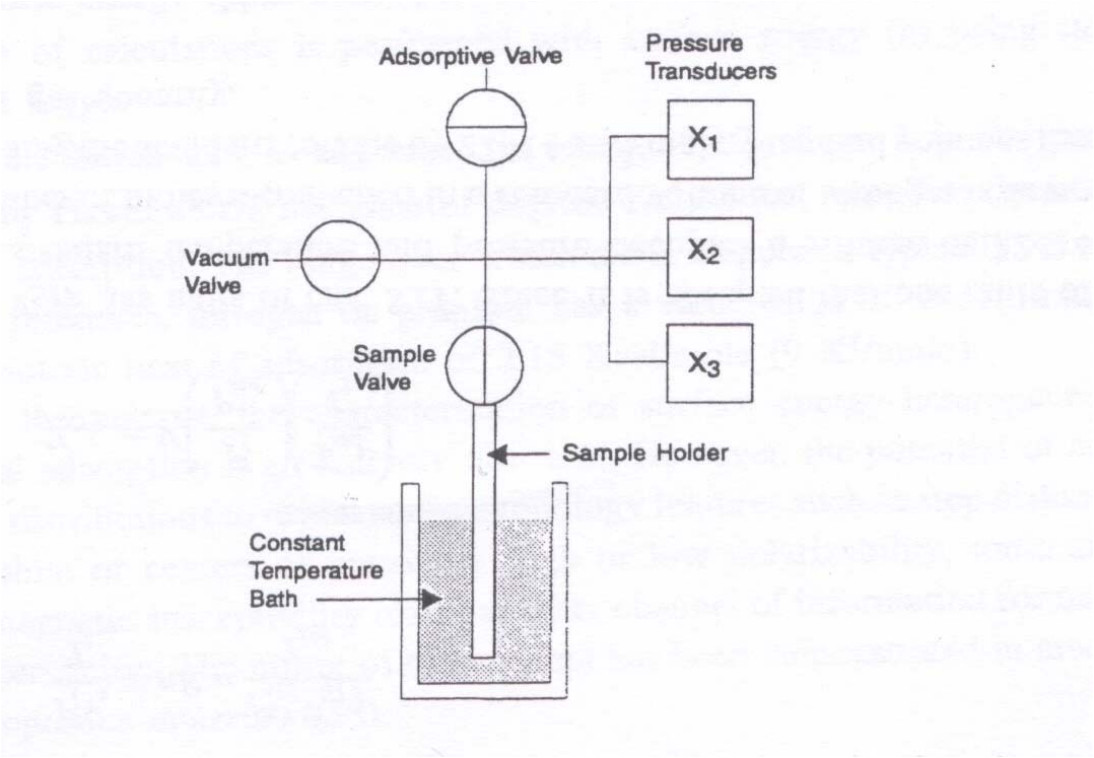

Fig. 2.1. Schematic diagram of the elements of a volumetric adsorption apparatus (taken from Ref. Webb and Orr, 1997.

Sample holders come in various sizes and shapes to accommodate materials of different quantities and forms, which displace various volumes. Therefore to know accurately the free volume within a particular sample holder, both the sample holder and sample volumes must be known or the free space must be determined. This determination is accomplished by following gas pressure changes as quantities of gas are exchanged between the gas manifold and the sample holder at the same temperature. Only after all system volumes are firmly established can the quantity of gas adsorbed by the sample be established with accuracy. Precise measurements require careful accounting of gas quantities and close attention to each and every step [Webb and Orr, 1997].

2.7 References

Adams, D. J. *Mol. Phys*. **29**, 307 (1975).

Alder, B. J.; Wainwright, T. E. *J. Chem. Phys.* **31**, 459 (1959).

Allen, M. P.; Tildesley, D. J. *"Computer simulation of liquids"* (Clarendon Press, Oxford, 1987), Chap. 4, p.110.

Barrett, E. P.; Joyner, L. G.; Halenda, P. P. *J. Am. Chem. Soc.* **73**, 373 (1951).

Brunauer, S.; Skalny, J.; Bodor, E. E. *J. Colloid Interface Sci*. **30**, 546 (1969).

Carnahan, N. F.; Starling, K. E. *J. Chem. Phys.* **51**, 635 (1969).

Chapela, G. A.; Saville, G.; Thompson, S. M.; Rowlinson, J. S. *J. Chem. Soc., Faraday Trans. 2* **73**, 1133 (1977).

Davies, G. M.; Seaton, N. A.; Vassiliadis, V. S. *Langmuir* **15**, 8235 (1999).

Davies, G. M.; Seaton, N. A. *Langmuir* **15**, 6263 (1999).

Davies, G. M.; Seaton, N. A. *AIChE J.* **46**, 1753 (2000).

Denton, A. R.; Ashcroft, N. W. *Phys. Rev. A* **44**, 8242 (1991).

Douglas Frink, L. J.; Salinger, A. G. *J. Comput. Phys.* **159**, 407 (2000).

El-Merraoui, M.; Aoshima, M.; Kaneko, K. *Langmuir* **16**, 4300 (2000).

Evans, R. *Adv. Phys.* **28**, 143 (1979).

Evans, R.; Tarazona, P. *Phys. Rev. Lett.* **52**, 557 (1984).

Evans, R.; Marini Bettolo Marconi, U.; Tarazona, P. *J. Chem. Phys*. **84**, 2376 (1986a).

Evans, R.; Marini Bettolo Marconi, U.; Tarazona, P. *J. Chem. Soc., Faraday Trans. 2* **82**, 1763 (1986b).

Evans, R. in *"Fundamentals of inhomogeneous fluids"*, edited by D. Henderson (Marcel Dekker, Inc., New York, 1992), Chap. 3, p.85.

Frenkel, D.; Smit, B. *"Understanding molecular simulation: from algorithms to applications"* (Academic Press, San Diego, 1996), Chap. 3, p.19.

Gelb, L. D.; Gubbins, K. E. *Langmuir* **14**, 2097 (1998).

Gelb, L. D.; Gubbins, K. E. *Langmuir* **15**, 305 (1999).

Gelb, L. D.; Gubbins, K. E.; Radhakrishnan, R.; Sliwinska-Bartkowiak, M. *Rep. Prog. Phys.* **62**, 1573 (1999).

Gregg, S. J.; Sing, K. S. W. *"Adsorption, surface area and porosity"*, 2nd edition (Academic Press Inc., London, 1982).

Gusev, V. Y.; O'Brien, J. A.; Seaton, N. A. *Langmuir* **13**, 2815 (1997).

Hansen, J. P.; McDonald, I. R. *Theory of simple liquids*, 2nd edition (Academic Press, London, 1991).

Helfand, E.; Frisch, H. L.; Lebowitz, J. L. *J. Chem. Phys.* **34**, 1037 (1961).

Holcomb, C. D.; Clancy, P.; Zollweg, J. A. *Mol. Phys.* **78**, 437 (1993).

Kierlik, E.; Rosinberg, M. L. *Phys. Rev. A* **42**, 3382 (1990).

Lastoskie, C.; Gubbins, K. E.; Quirke, N. *J. Phys. Chem.* **97**, 4786 (1993).

Lebowitz, J. L. *Phys. Rev.* **133**, A895 (1964).

Lowell, S.; Shields, J. E. *"Powder surface area and porosity"*, 3rd edition (Chapman & Hall, The Netherlands, 1991), Part 2, p. 153.

Metropolis, M.; Rosenbluth, A. W.; Rosenbluth, M. N.; Teller, A. N.; Teller, E. *J. Chem. Phys.* **21**, 1087 (1953).

Neimark, A. V.; Ravikovitch, P. I.; Grün, M.; Schüth, F.; Unger, K. K. *J. Colloid Interface Sci.* **207**, 159 (1998).

Norman, G. E.; Filinov, V. S. *High Temp. (URSS)* **7**, 216 (1969).

Patra, C. N.; Ghosh, S. K. *Phys. Rev. E* **47**, 4088 (1993); *Ibid.* **48**, 1154 (1993).

Ravikovitch, P. I.; Vishnyakov, A.; Russo, R.; Neimark, A. V. *Langmuir* **16**, 2311 (2000).

Reiss, H.; Frisch, H. L.; Lebowitz, J. L. *J. Chem. Phys*. **31**, 369 (1959).

Rosenfeld, Y. *Phys. Rev. Lett*. **63**, 980 (1989).

Rosenfeld, Y.; Schmidt, M.; Löwen, H.; Tarazona, *P. Phys. Rev. E* **55**, 4245 (1997).

Ross, S. M. *"Simulation"*, 2nd edition (Academic, San Diego, CA, 1997).

Rudzinski, W.; Everett, D. H. *"Adsorption of gases on heterogeneous surfaces"* (Academic Press, London, 1992), Chap. 11, p. 420.

Seaton, N. A.; Walton, J. P. R. B.; Quirke, N. *Carbon* **27**, 853 (1989).

Tan, Z.; Marini Bettolo Marconi, U.; van Swol, F.; Gubbins, K. F. *J. Chem. Phys.* **90**, 3704 (1989).

Tarazona, *P. Phys. Rev. A* **31**, 2672 (1985); *Ibid.* **32**, 3148 (1985) (*erratum*).

Tarazona, P.; Marini Bettolo Marconi, U.; Evans, R. *Mol. Phys*. **60**, 573 (1987).

Tarazona, P. *Phys. Rev. Lett*. **84**, 694 (2000).

Thiele, E. *J. Chem. Phys.* **39**, 474 (1963).

Thompson, S. M.; Gubbins, K. E.; Walton, J. P. R. B.; Chantry, R. A. R.; Rowlinson, J. S. *J. Chem. Phys*. **81**, 530 (1984).

Van Megen, W.; Snook, I. K. *Mol. Phys*. **45**, 629 (1982).

Van Megen, W.; Snook, I. K. *Mol. Phys*. **54**, 741 (1985).

Webb, P. A.; Orr, C. *"Analytical methods in fine particle technology"* (Micromeritics Instrument Corp., U. S. A., 1997), Chap. 3, p. 94.

Wertheim, M. S. *Phys. Rev. Lett*. **10**, 321 (1963).

3. ADSORPTION IN PORES[♣]

3.1 Introduction

The thermodynamic and structural properties of inhomogeneous classical fluids constitute a fundamental problem for physics and chemistry. During the last years a great effort has been devoted to the molecular modeling of these properties within the framework of interfacial phenomena, freezing, fluids in confined geometry, *etc*. Despite the important advances achieved with the combination of modern theories and computer molecular simulations, inhomogeneous situations are not yet completely understood. Even simple spherical fluids show a complex behavior when confined in well-defined geometries. When the pore size is on the order of the correlation length, the presence of walls causes a dramatic change in the behavior of these confined systems compared to that exhibited in the bulk phase. In particular, energetic interactions and geometrical confinement modify the character of phase transitions, shift critical points, and new observable metastable states and hysteresis phenomena appear, among other features [Gelb *et al*., 1999].

A very successful and general method for determining the thermodynamic and structural properties of inhomogeneous fluids is undeniably density functional theory [Evans, 1992]. This method is based on the formulation of the free energy for an inhomogeneous fluid as a functional of the spatially varying one-particle density $\rho(\boldsymbol{r})$. The density functional approach provides all relevant thermodynamic functions, such as surface tension, solvation forces, adsorption isotherms, density profiles, *etc*. Unfortunately, the exact free energy functional is only known for a few simple models and, consequently, the cornerstone of the theory is to provide suitable approximations for the free energy [Evans, 1992].

It is customary to separate the ideal from the excess contributions to the free energy. Moreover, the excess free energy functional is further split, somewhat arbitrarily, into two parts: the hard-sphere contribution and the attractive part usually treated under the mean-field approximation. Within this framework, density functional approaches are further classified into local and non-local theories, depending on how the hard-sphere contribution to the excess free energy density is modeled. In the local approximation, the excess free energy density at a point $\boldsymbol{r}$ is formulated as dependent on the local particle density at the same position $\boldsymbol{r}$**.** Although local theories can adequately describe

---

[♣] The results presented in this chapter are in press (Journal of Chemical Physics, Issue: 22 Dec. 2002).

relevant properties in inhomogeneous situations [Sullivan and Telo da Gama, 1986; Dietrich, 1988; Evans, 1990; Tarazona and Evans, 1983; Tarazona *et al*., 1983; Tarazona and Evans, 1982; Evans and Parry, 1989] this formulation fails when predicting oscillatory density profiles, such as those observed in confined fluids, since short-range correlations are neglected [Evans, 1992]. On the other hand, in the non-local or weighted density functional theories, the excess free energy for the hard-sphere reference system is function of the particle density in the neighborhood of the point $\boldsymbol{r}$, through smoothed densities. The latter are constructed from appropriate averages of the particle density over a given local volume, thus accounting for the short-range correlations. Different recipes of the weighted density can be found in the literature [Nordholm *et al*., 1980; Johnson and Nordholm, 1981; Freasier and Nordholm, 1983, 1986; Tarazona, 1984; 1985; Curtin and Ashcroft, 1985; Meister and Kroll, 1985; Percus, 1981; 1982; 1988; Robledo and Varea, 1981].

A new kind of non-local free energy density functionals has been developed in the last two decades. The Fundamental-Measure theory free energy functional was originally proposed by Rosenfeld in 1989 [Rosenfeld, 1989]. This procedure is based on the convolution decomposition of the excluded volume for a pair of convex hard spheres in terms of characteristic functions for the geometry of the two individual bodies. In the original formulation [Rosenfeld, 1989], the excess free energy density of the hard-sphere fluid is obtained from four scalar and two vector weighting density-independent functions. Later on, Kierlik and Rosinberg [1990] proposed a new fundamental-measure functional, defined by only four scalar weighting functions. Although the functional forms of the Rosenfeld and Kierlik and Rosinberg theories are different, it has been proved that both approaches represent the same fundamental density functional [Phan, *et al.*, 1993].

Most of the initial studies on confined fluids for slit-like and cylindrical pores were based on the local approximation for the repulsive part of the Helmholtz free energy [Evans and Tarazona, 1984; Evans and Marini Bettolo Marconi, 1985a; 1985b; 1987; Peterson *et al*., 1985; 1986; Evans *et al*., 1986a; 1986b; Tarazona *et al*., 1987]. After the work of Nordholm and co-workers [Nordholm *et al*., 1980; Johnson and Nordholm, 1981; Freasier and Nordholm, 1983; 1986] and Tarazona [1985], in which the non-local approach was introduced, a great number of studies based on this approximate method have been undertaken [Peterson *et al.*, 1988; 1990; Balbuena and Gubbins, 1993; Lastoskie *et al*., 1993a]. In the past decade, following the work of Rosenfeld and that of Kierlik and Rosinberg, a number of analyses have been directed to study the adsorption behavior of spherical fluids and their mixtures, all of them, however, restricted to slit-like pores [Kierlik and Rosinberg, 1991; Kierlik *et al*., 1992; 1994; Jiang *et al*., 1994; Phan *et al*., 1995; Kierlik *et al*., 1995; Sowers and Gubbins, 1995; Sliwinska-Gartkowiak *et al*., 1997; Bryk *et al*., 1998; Ravikovitch *et al*., 2001]. As far as dimensional crossover is concerned, more recently Gonzalez *et al.* [1998] studied the behavior of a system confined in a spherical cavity with an analysis based on the modifications introduced by Rosenfeld *et al.* [1997] on the original work of Rosenfeld [1989]. Tarazona [2000], in turn, developed a FMT functional that is able to correctly account for dimensional crossover. To our knowledge, none of the Fundamental-Measure approach versions has ever been used to describe the behavior of confined fluids in cylindrical geometries. This application, however, has a particular importance since DFT is currently being used to obtain the pore-size distribution from adsorption

isotherms in porous materials, in which cylindrical pores are common [Rouquerol *et al*., 1999]. Thus, to establish the validity of this kind of functionals for predicting the adsorption behavior in cylindrical pores becomes a matter of fundamental interest.

The main goal of this part of the work is to analyze the ability of the FMT free energy functional, proposed by Kierlik and Rosinberg, to describe the thermodynamic and structural properties of a Lennard-Jones spherical fluid confined in cylindrical pores. In particular, the accuracy of the FMT results is tested by comparing them to those obtained from Grand Canonical Monte Carlo simulations using the same molecular model and for a wide range of pore sizes, from micropores to mesopores. In addition, the effect of the geometrical confinement on the adsorption properties is studied comparing the FMT results for cylindrical pores with the data obtained for slit-like pores of similar width.

The rest of the chapter is organized as follows. In section 3.2 we briefly review some details of the FMT, we set out the model potentials and approximations used in this work, we define the pore properties, and finally, we give details about the molecular simulations performed. In section 3.3 we present and discuss our results. Finally, section 3.4 is dedicated to summarize the main conclusions that can be drawn from this work.

3.2 Molecular model

3.2.1 Density functional theory

This part was already explained in detail in section 2.2. Here we will only add some specific details of the model used in this work. The inversion of the Euler-Lagrange equation (Eq. 2.10) in the case of a fluid adsorbing onto cylindrical walls of diameter *H*, unbounded in the axial direction, requires the calculation of a series of convolution and constitutes the main computational effort of this work. These convolutions are generically expressed as

$$\int d\mathbf{r}\psi\left(\left|\mathbf{r}-\mathbf{r}''\right|\right)f(\mathbf{r}), \tag{3.1}$$

where $\psi(|\mathbf{r}|)$ is an arbitrary isotropic kernel, and $f(\mathbf{r})$ a given function of the position which, for symmetry requirements, depends only on the distance to the axis of the cylinder $\boldsymbol{r}_\perp$. Identically and also due to symmetry requirements, the result of each of these convolutions is a function of the distance to the axis of the cylinder, $\boldsymbol{r}''_\perp$.

To take advantage of the isotropy of the kernel, we have introduced a local coordinate system around the space point $\boldsymbol{r}''$. The *z*-axis is perpendicular to the cylinder's axis pointing outward in the radial direction, the *y*-axis is parallel to the cylinder's axis, and the *x*-axis is correspondingly oriented [see Fig. 3.1]. Adopting spherical coordinates with respect to this local reference system, the distance $\boldsymbol{r}_\perp$ of a given space point can be obtained according to the transformation

$$r_{\perp}(r,\theta,\varphi;r_{\perp}'') = \sqrt{(r_{\perp}'' + r\cos\theta)^2 + r^2 sin^2\theta\ sin^2\varphi}\ , \tag{3.2}$$

which permits the evaluation of the function $f(\boldsymbol{r}_{\perp})$. The convolutions are then calculated by repeated one-dimensional integration, taking advantage of Gaussian quadratures to increase the velocity of the numerical evaluation. We have not introduced here a reduction of the multidimensional integration by an appropriate (although cumbersome for non-planar geometries) coordinate change, as it is the case in the adsorption on a flat wall [Kierlik and Rosinberg, 1990]. However, there is not a significant increase in the computational time, since the problem is still one-dimensional, due to the fact that the density profile is a function which depends only on the distance to the axis of the cylinder, $\boldsymbol{r}_{\perp}$. As a result, the comparison between the density profiles in slit-like and cylindrical pores shows significant differences near the axial region due, precisely, to these curvature effects.

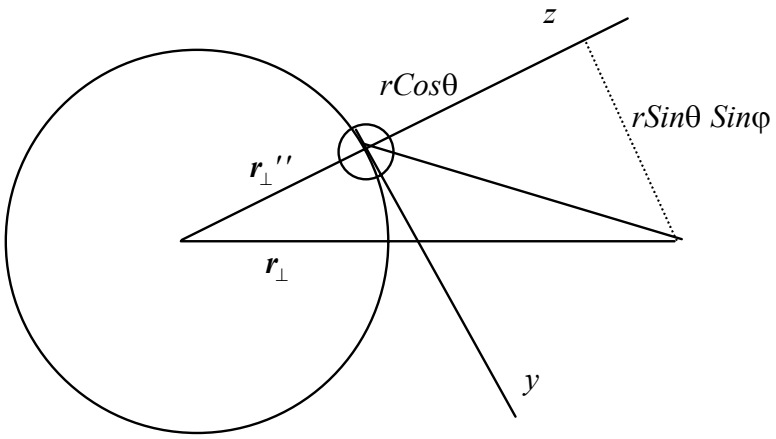

Fig. 3.1. Projection of the cylindrical pore on a plane orthogonal to cylinder axis following Eq. 3.2.

It is important to realize that our procedure respects the geometrical properties of the system, which is especially relevant near the axis of the cylinder, where the radius of curvature of the "slices" of constant density is of the same order of magnitude as the radius of the particles themselves.

We have performed FMT density functional calculations as well as GCMC simulations of adsorption in cylindrical pores of different diameter sizes. We have also calculated adsorption properties in slit-like pores using FMT. The molecular parameters used were the same as in the simulation of nitrogen adsorption on model porous glasses of silica [Gelb and Gubbins, 1998; 1999]. Adsorption was assumed to take place on standard conditions for the nitrogen at the normal boiling temperature of 77K. The reason of such a choice is the interest of further applications of our methodology to the determination of the pore-size distribution in this kind of materials. In some specific cases, we have calculated the adsorption, desorption and stable branches, as discussed later. For the rest of the cases we have calculated only the adsorption branch.

3.2.2 Fluid-fluid interactions

In this work, the nitrogen molecule is modeled as a spherical LJ particle, with a "cut-and-shifted potential", $\phi^{LJ}(r)$. The LJ parameters ε and σ have been taken from literature [Maddox *et al.*, 1997] (see also table 3.1). In addition, all the LJ interactions were truncated at a cutoff radius $r_c = 2.52\sigma$.

We divide the potential into repulsive (reference) and attractive (perturbative) components, following the conventional Weeks, Chandler, and Andersen (WCA) perturbation scheme [Week *et al*., 1971], splitting the potential at the minimum,

$$\phi_{ref} = \begin{cases} \phi^{LJ}(r) + \varepsilon & r < r_{min} \\ 0 & r \geq r_{min} \end{cases}, \tag{3.3}$$

and

$$\phi_{att} = \begin{cases} -\varepsilon & r < r_{min} \\ \phi^{LJ}(r) & r \geq r_{min} \end{cases}, \tag{3.4}$$

with $r_{min} = 2^{1/6}\sigma$. In this approach, the reference system is replaced by a system of hard spheres with a temperature-dependent diameter $d(T^*)$. We have used the mapping from LJ to hard spheres developed by Verlet and Weis [1972] and Lu *et al*. [1985], described as follows

$$\frac{d(T^*)}{\sigma} = \frac{\eta_1 T^* + \eta_2}{\eta_3 T^* + \eta_4} \tag{3.5}$$

with the reduced temperature, $T^* = k_B T/\varepsilon$, and the coefficients $\eta_1 = 0.3837$, $\eta_2 = 1.035$, $\eta = 0.4249$, $\eta_4 = 1$, fitted by Peterson *et al*. [1986] to match the bulk phase diagram of the LJ fluid.

The excess Helmholtz free energy per particle of the reference system, Φ, is taken from the SPT [Reiss *et al.*, 1959; Helfand *et al.*, 1961], or PY equation of state for the uniform hard-sphere fluid [Wertheim, 1963; Thiele, 1963; Lebowitz, 1964] (Eq. 2.8), where $\rho(\boldsymbol{r}) \equiv \rho$. Moreover, the weighted densities defined in Eq. 2.6, which coincide with the variables of the SPT [Reiss *et al.*, 1959; Helfand *et al.*, 1961], can be written in terms of fundamental measures characterizing the particle

$$\bar{n}_0 = \rho, \qquad \bar{n}_1 = R\rho, \qquad \bar{n}_2 = 4\pi R^2 \rho, \qquad \bar{n}_3 = \tfrac{4}{3}\pi R^3 \rho \tag{3.6}$$

3.2.3 Solid-fluid interactions

The LJ parameters for the substrate atoms are those used by Gelb and Gubbins [1998; 1999] following the work from Brodka and Zerda [1991], and they can be found in table 3.1. These parameters represent bridging oxygen atoms in silica, since previous simulations of adsorption on silica gels show that the omission of the silicon atoms is an

acceptable approximation [Brodka and Zerda, 1991; MacElroy, 1993]. The LJ solid-fluid parameters (table 3.1) follow the Lorentz-Berthelot mixing rules.

Parameter	Fluid-fluid[a]	Solid-solid[b]	Solid-fluid
σ (Å)	3.75	2.70	3.22
ε/k_B (K)	95.20	230.00	147.90

Table 3.1. LJ parameters of nitrogen and of porous glasses. [a] From the work of Maddox *et al*. [1997]; [b] from the Ref. Gelb and Gubbins 1998; 1999.

We have represented each pore as an infinite cylinder where the atoms are single spherical LJ sites. These LJ spheres are laid out in 6 concentric layers separated by a distance Δ. Each layer is arranged in such a way that consecutive rows of solid atoms are displaced 0.15nm in the angular and axial directions. The distance between the axes that define the successive rows is called *d*. The resulting overall configuration of each layer can be described as a hexagonal lattice. The values of these parameters are fixed (d = 2.77 Å and Δ = 3.0 Å), so that the total density of oxygen atoms in our model, 44.1 atoms/nm^3, and a material porosity of 30%, are approximately mimicked [Gelb and Gubbins, 1999]. The pore diameter *H* is defined from the center of the particles on opposite sides of the innermost layer. An example of this cylinder and the disposition of the atoms can be seen in figure 3.2(a). In the case of slit-like pores, the material is modeled applying the same principles to a planar geometry, where the parameter *H* represents the distance between two identical parallel walls. In figure 3.2(b) a representation of this pore can be found.

The total potential energy between a fluid molecule probe and the wall is calculated as the sum of the contributions of all the substrate atoms. However, we have considered an averaged potential, constructed from the previous one by integrating with respect to the angular and axial directions, preserving only the radial functional dependence. For slit-like pores, the potential is averaged over translations parallel to the walls.

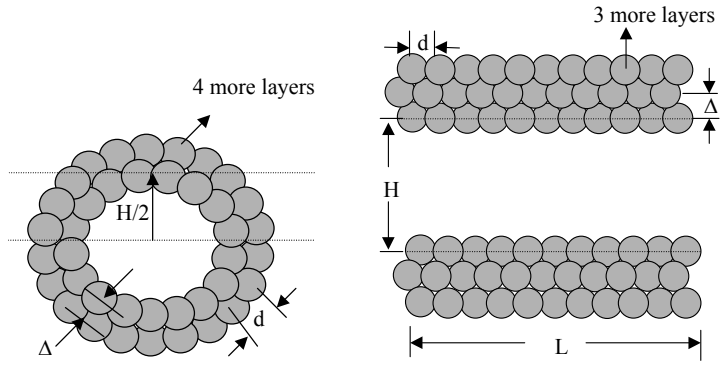

a) b)

Fig. 3.2. Structure of the (a) cylindrical and (b) slit-like pores, and the definitions of geometrical parameters.

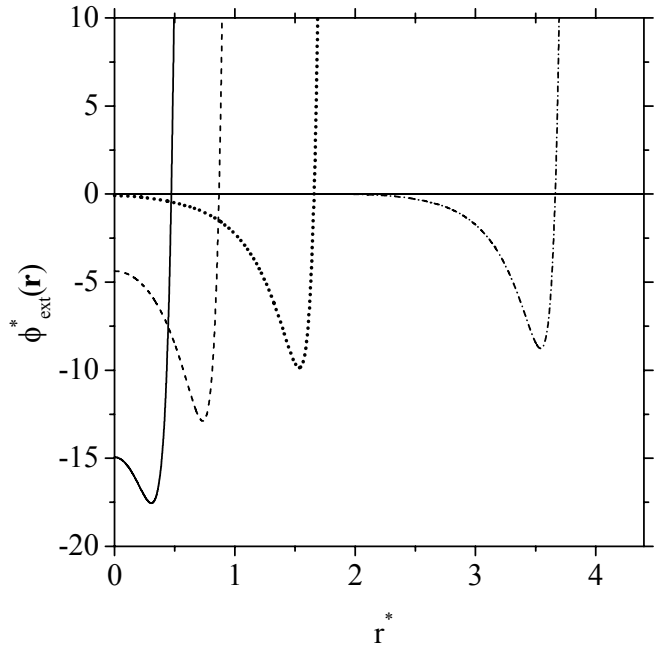

a)

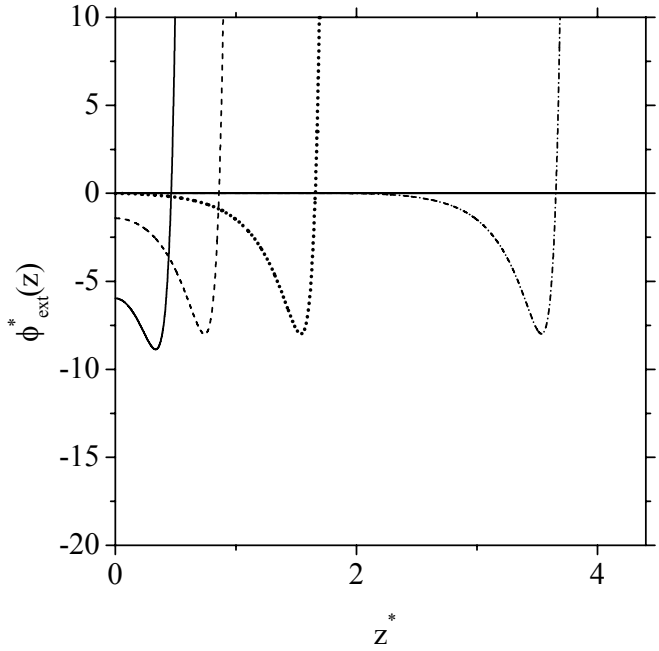

b)

Fig. 3.3. Dependence of the wall potential as a function of the distance for (a) cylindrical and (b) slit-like pores of different size: H = 2.4σ, 3.2σ, 4.8σ, and 8.8σ, starting from left to right.

In Figure 3.3(a) we have shown the radial dependence of the cylindrical wall potential, $\phi_{ext}(r)$, for several pore size diameters. As it can be seen in the figure, the influence of the wall on the adsorption is expected to be very important for pores whose width is comparable with the range of the attractive potential of the wall. In particular, for such narrow pores the adsorbed fluid will have properties significantly different from those

of the bulk fluid. Conversely, for wider pores one expects the effect of the pore walls to be important only at low coverage, and capillary condensation to occur at a given critical pressure. In figure 3.3(b) we present the wall potential as a function of the distance in the direction perpendicular to the parallel walls, $\phi_{ext}(z)$, for slit-like pores of different width.

The mean pore fluid density, $<\rho>$, is defined from the relation

$$\langle \rho \rangle = \frac{\int d\mathbf{r} \rho(\mathbf{r})}{\int d\mathbf{r}}, \tag{3.7}$$

where the integral is extended over the volume of the pore and this volume is considered a function of H. The excess density is defined as the deviation of the average density with respect to the bulk values, that is

$$\langle \rho^{E} \rangle \equiv \langle \rho \rangle - \rho_{bulk}. \tag{3.8}$$

3.2.4 Monte Carlo simulations

Aiming at a quantitative comparison between the FMT and Monte Carlo simulations, we have chosen to apply the same molecular parameters for both procedures. It is well known that the bulk properties predicted by each methodology are different. However, since both theories are molecular in nature, we have decided to compare the bare results from the same molecular model and analyze the differences later on. Other authors have compared DFT results with Monte Carlo simulations based on the same bulk properties [Lastoskie *et al*., 1993a; Ravikovitch *et al.*, 2000], although such a procedure implies the use of different molecular parameters for each approach. Despite the fact that the latter point of view is legitimate, the different sets of molecular parameters used in that case represent in fact different systems, although very close in their properties. In our simulations, adsorption isotherms and density profiles have been obtained through a GCMC scheme. The values of activities at which the points were obtained correspond to bulk chemical potential, equal to those used in the density functional theory calculations.

Three different types of Monte Carlo trials were used in the simulations: creation of a new adsorbate molecule at a random position inside the pore, removal of a randomly chosen adsorbate molecule, and move of a randomly chosen adsorbate particle. The maximum move for a particle translation was fixed at 0.20σ, and the ratio between trials was fixed to be a 50% for translation moves and the remaining 50% for creation-destruction moves. The length of the simulation box was changed from 60 to 1,000 Å, depending on the pore diameter size, to ensure a sufficient number of particles inside. In the axial and angular directions, periodic boundary conditions and minimal image convention were applied. The LJ potential was cut and shifted at a radius of $r_c = 2.52\sigma$; no long-range corrections were used. To equilibrate the system, the simulations were run for at least $3\text{x}10^6$ moves. Averages were then collected from runs over at least

$20x10^6$ configurations after equilibration. The block size to compute averages was fixed at 500,000 moves.

The excess pore fluid density in this case is defined as

$$\left\langle \rho^{E} \right\rangle = \frac{\langle N \rangle}{V} - \rho_{bulk}, \tag{3.9}$$

where $\langle N \rangle$ is the mean number of particles inside pore and V is the pore volume, defined in the same way as in Eq. 3.7.

3.3 Results and discussion

We have calculated density profiles and adsorption isotherms for cylindrical pores of different sizes by means of two approaches, FMT and GCMC. All the calculations were done at 77K. In addition, FMT calculations for slit-like pores of the same width will serve us to discuss as well the main differences introduced by the dissimilarity in the geometry. The pore diameters studied here are in the range from $H = 3.2\sigma$ to $H = 17.6\sigma$, which covers the region from micropores (whose diameter is less than 20 Å), to larger pores (mesopores, with a diameter between 20 Å and 500 Å). We have found that our numerical implementation of the FMT model used here fails to converge for very narrow pores ($H<3.2\sigma$, corresponding to $H<12$ Å) which constitutes the limit of the applicability of our procedure. An analysis of the strictly 1D [Rosenfeld *et al.*, 1997; Tarazona, 2000] adsorption is out of the scope of this work. The main points to be discussed in this section will be, on one hand, the comparison of the excess density and density profiles between FMT and GCMC, to elucidate the limits of the agreement of both procedures in the analysis of the adsorption in cylindrical pores, when the same molecular model is used. On the other hand, the effect of the geometry in the profiles and adsorption isotherms will be briefly discussed by comparing the FMT results for cylindrical and slit-like pores. This latter point is of relevance in the calculation of pore-size distributions of real materials from experimental data of adsorption isotherms.

Fig. 3.4(a) shows the adsorption isotherm obtained from FMT corresponding to cylindrical and slit-like pores of size $H = 3.2\sigma$, as well as the simulation results for the cylindrical geometry. As it can be seen, the agreement between predictions from the theory and simulation data is excellent in the whole range of chemical potentials considered (from $\mu^* = -12.479$ to $\mu^* = -3.338$), although theoretical predictions slightly underestimate the amount of fluid adsorbed along the whole adsorption isotherm. Results corresponding to the adsorption in the slit-like pore are significantly different from those obtained for the cylindrical geometry. In the former, a very pronounced jump in the average density is observed at chemical potentials around $\mu^* = -8.0$, followed by a continuous increase of the density as the chemical potential is raised. For the cylindrical pore, the jump in the density is displaced towards lower chemical potentials. At higher chemical potentials, the continuous increase in the density is smoother than in the case of planar geometry. The insets in Fig. 3.4(a) show the hysteresis existing around the sudden density jump, indicating that it corresponds in both cases to a *first order phase transition* inside the pore. A higher degree of

confinement in cylindrical pores is responsible for the appearance of the mentioned transition at chemical potentials significantly lower than in slit-like pores. As seen in Fig. 3.4(b), only one rather localized annular layer is formed at the wall inside the pore, in the whole chemical potential range studied. Thus, once this layer is build, the increase of the chemical potential only introduces changes in the height of the density profile, yielding to the observed continuous increase of the excess adsorption after the transition in both geometries. The nature of such a transition is not completely clear, since the confinement of the fluid, the curvature of the wall, as well as the solid-fluid potential interactions influence the kind of the transition as well as its location in the space of thermodynamic parameters. However, we attribute this phase transition to the so-called 0→1 layering transition, previously found by different authors [Ball and Evans, 1988; Balbuena and Gubbins, 1993; Lastoskie *et al*., 1993b]. We will come back to this point later on.

The agreement between theoretical FMT predictions and GCMC simulation results in Figs. 3.4(a) and 3.4(b) is very good for all thermodynamic conditions, with special emphasis on the localization and the height of the density peaks at different chemical potentials. It must be noted, however, that the agreement between both sets of results is better at low chemical potentials (*i.e.* pressures). This effect is a consequence of the lack of accuracy of the FMT approach used in this work to predict the adsorption behavior for very narrow pores (which would confine the fluid to an almost one-dimensional behavior). In Fig. 3.4(a) the differences between the adsorption isotherms of cylindrical and planar pores can be ascribed to the geometrical constraints that crucially determine the way in which molecules accommodate inside confined geometries.

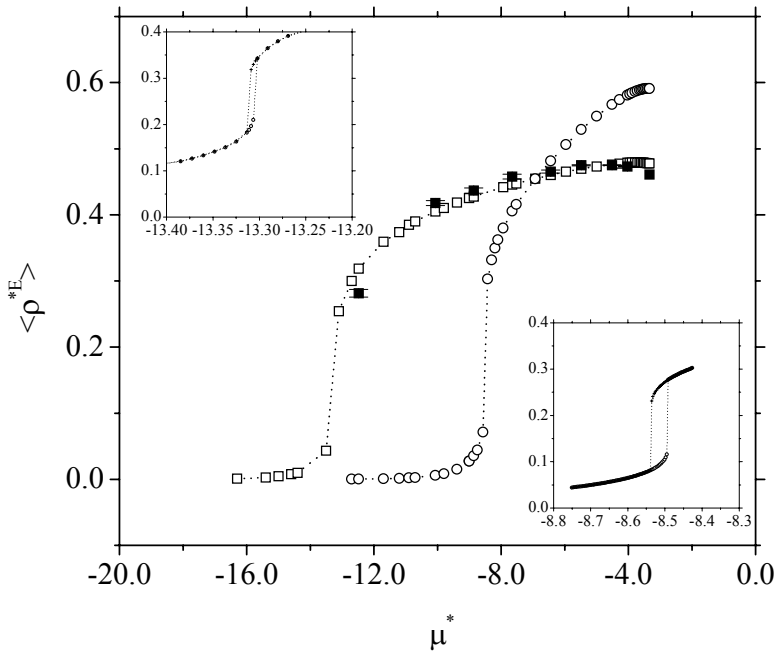

a)

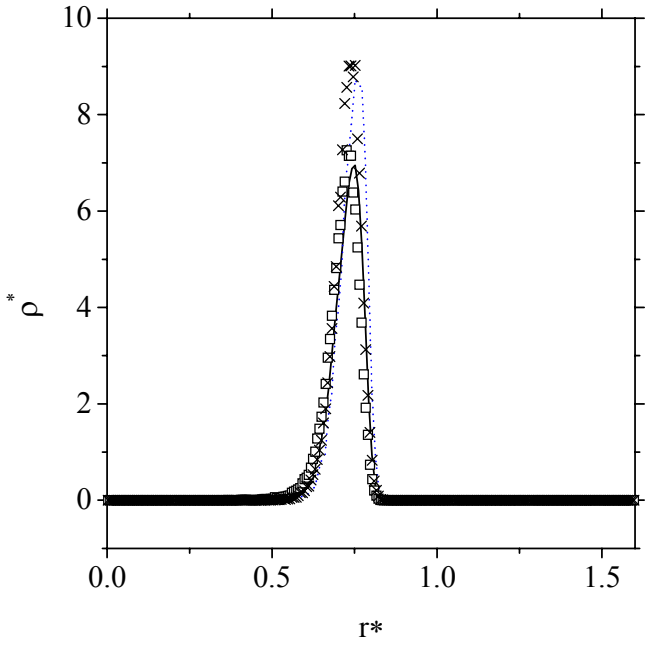

b)

Fig. 3.4. (a) Adsorption isotherms in $H = 3.2\sigma$ cylindrical and slit-like pores; (open squares) FMT calculations, (closed squares) GCMC simulations, both in the cylindrical pore; (open circles), FMT calculations in the slit-like pore. The lines are only visual aid. The insets show the hysteresis FMT results in the slit-like pore in the right-hand side and in the cylindrical pore in the left-hand side. (b) Density profiles from (lines) FMT calculations and (symbols) GCMC simulations (symbols) in the cylindrical pore at $\mu^* = -10.065$ (solid line and open squares), and -4.031 (dotted line and crosses).

Regarding the adsorption isotherms and density profiles in wider pores, Fig. 3.5(a) shows the excess adsorbed density *versus* the chemical potential (adsorption isotherm) of cylindrical and slit-like pores of size $H = 4.8\sigma$. The adsorption isotherm corresponding to the cylindrical pore has also been obtained from Monte Carlo simulation. As it can be seen, the theory is able to provide a realistic description of the excess density *versus* the chemical potential since an almost quantitative agreement between FMT and GCMC results is found in all the range of chemical potentials studied.

More in detail, at low chemical potentials ($\mu^* < -7.0$) a monolayer is formed in both pores. As the chemical potential is increased a second layer is adsorbed in both cylindrical and slit-like pores without the appearance of additional layers. However, important differences between the adsorption isotherms can be observed. The excess density in the cylindrical pore is higher than that corresponding to the planar geometry in practically the whole range of chemical potential values (except at the highest chemical potentials). Also, the increase in density observed when a new layer is formed is more pronounced in the case of the slit-like geometry; this is especially true in the formation of the second adsorbed layer. To elucidate the reasons for this behavior we have also examined the density profiles corresponding to both geometries. Fig. 3.5(b) shows the density profiles, at two different chemical potentials, inside the cylindrical

pore. At the lowest chemical potential only a single annular layer is adsorbed, with the density peak located at $r^* = 1.5$. This position is consistent with the location of the solid-fluid potential minimum for a cylindrical pore of $H = 4.8\sigma$ (see Fig. 3.3(a)). As the chemical potential is increased, a second adsorbed layer appears close to the center of the cylinder, in agreement with the slight increase of the adsorption isotherm observed in Fig. 3.5(a).

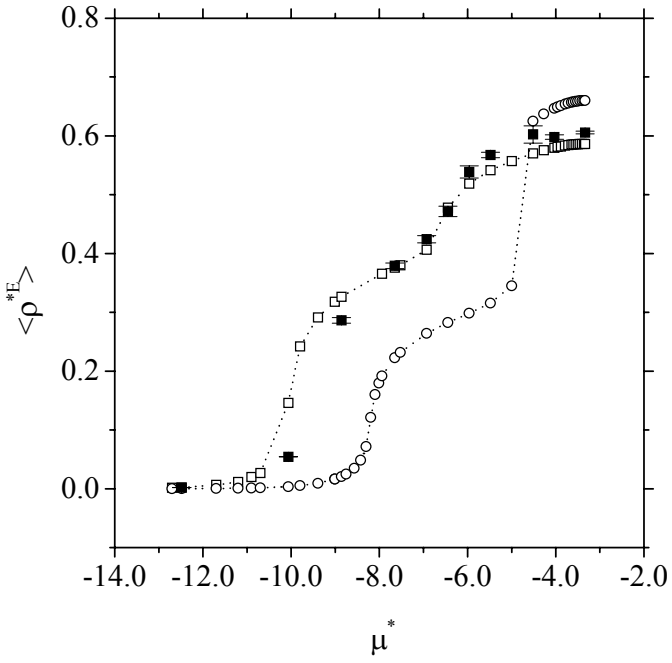

a)

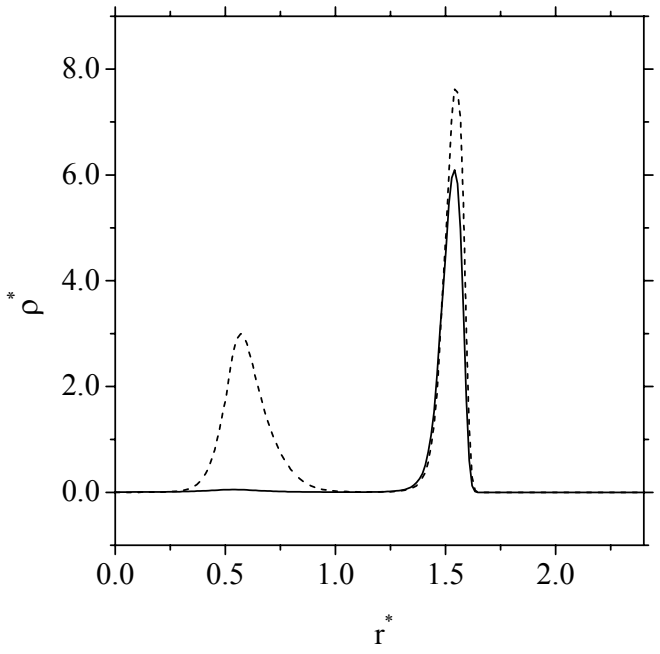

b)

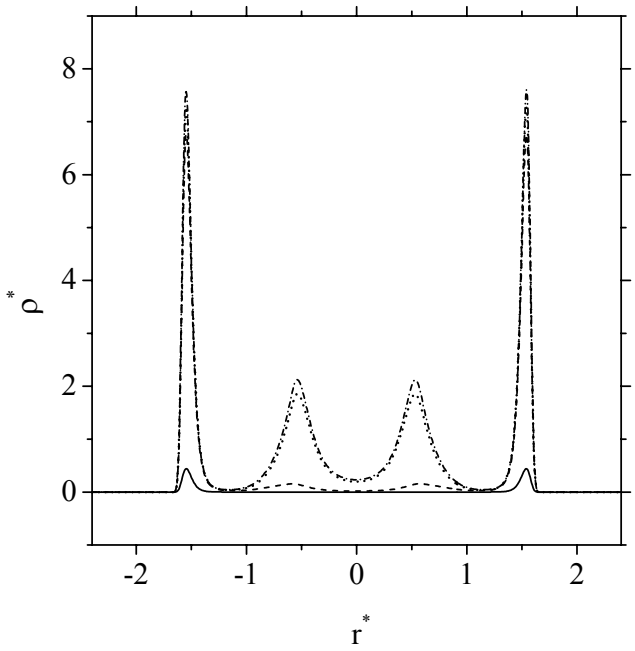

c)

Fig. 3.5. (a) Adsorption isotherms in $H = 4.8\sigma$ cylindrical and slit-like pores; the notation is the same as in Fig. 3.4(a). (b) Density profiles from FMT calculations in the cylindrical pore at $\mu^* = -7.651$ (solid line), and -4.031 (dashed line). (c) Density profiles from FMT calculations in the slit-like pore at six different μ^*, from bottom to top: -10.065, -8.858, -7.651, -4.995, -4.513, -3.338.

The isotherm for the planar geometry case, although apparently similar, is in fact qualitatively different from that of the cylindrical pore. Notice, for instance, that in the slit-like pore there are particles in the center of the pore at high chemical potential values (see Fig. 3.5(c)), whereas molecules are strongly excluded from the axial region of the cylinder. This effect indicates that capillary condensation is likely to occur in the planar geometry but not in the cylinder of the same dimensions $H = 4.8\sigma$, in the range of chemical potentials studied here. A detailed analysis of the hysteresis cycle as well as of the free energy indicates that the jump in the excess density in the planar geometry corresponds to a first order phase transition that can be described as capillary condensation [Evans, 1990]. In the case of cylindrical geometry, the formation of the second layer does not correspond to thermodynamic phase transition but merely to a continuous filling of the second layer. In fact, it is worth noting that the average density is proportional to the first derivative of the free energy, (Eq. 2.5) with respect to the chemical potential, but the average density does not present a discontinuity, nor does its slope diverge.

In the planar pore one can also notice the formation of the first layer around $\mu^* = -8$, a slightly higher chemical potential than in the $H = 3.2\sigma$ pore. This effect is dominated by the solid-fluid interaction as it can be seen by the fact that it appears at the same chemical potential for all slit-like pores of larger width. However, this transition cannot be considered as being of first order. In fact, in this case, no hysteresis in the average density is observed around this value of chemical potential, being this quantity (related

to the first derivative of the free energy) continuous across the transition, up to the accuracy of our numerical method. The sharp slope observed, however, could indicate that the behavior could correspond to a continuous second order phase transition. In the case of the cylindrical geometry, the transition is observed at lower chemical potential and seems to also display such a continuous character.

In the mesopore range we present results for two pore sizes, $H = 8.8\sigma$ and $H = 17.6\sigma$, which correspond, respectively, to the series of Figs. 3.6(a,b,c) and 3.7(a,b,c,d). In Fig. 3.6(a) we show the adsorption isotherms for cylindrical and slit-like pores of width $H=8.8\sigma$. The agreement between the theoretical adsorption isotherm and simulation data corresponding to this cylindrical pore is better than that obtained for narrower pores, as expected. The adsorption isotherms for both geometries exhibit the same qualitative behavior. One observes, on one hand, the crossover from an empty pore to the formation a monolayer at low chemical potentials, as in the previous cases. This increase in the adsorbance in planar geometries is located at the same chemical potential of about $\mu^* = -8.2$ in all the studied pores with $H>3.2\sigma$. However, the local curvature of the walls in cylindrical geometry shifts the transition region towards lower chemical potentials as the diameter decreases. In both cases, however, the formation of the thin layer at the wall seems to be continuous and, as before, such a behavior cannot be attributed to a first order phase transition.

On the other hand, the sudden increase in the excess density as the chemical potential is increased corresponds to capillary condensation in both, cylindrical as well as planar geometries. It is important to note that capillary condensation is shifted towards the region of lower chemical potential as the degree of confinement increases, due to both, the change in the geometry (from planar to cylindrical) and by the change in the pore size [Evans and Tarazona, 1984; Evans and Marini Bettolo Marconi, 1985b; Evans, 1990].

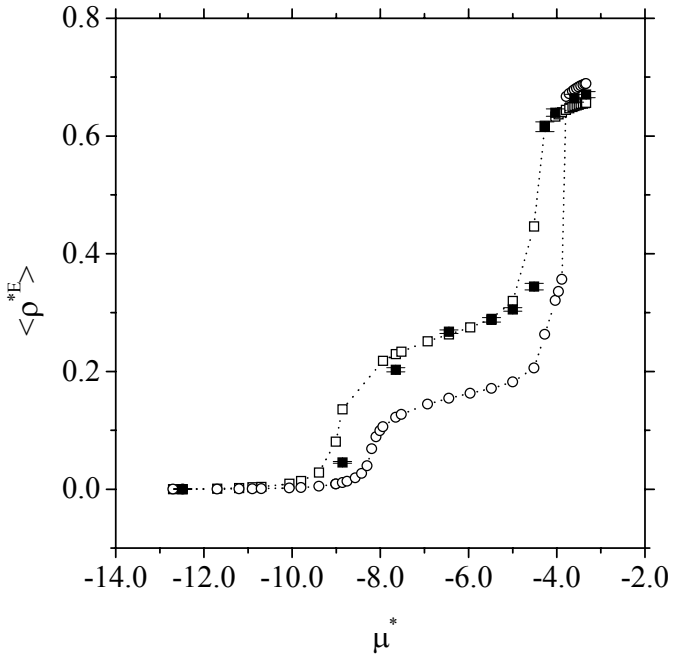

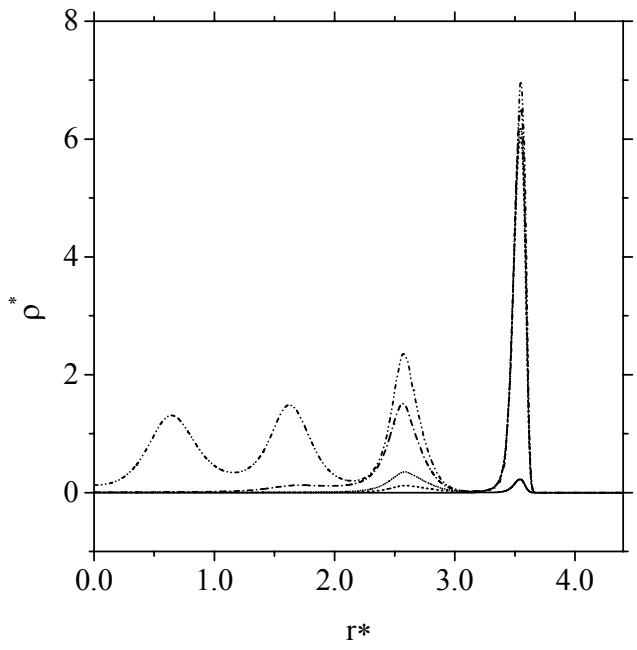

b)

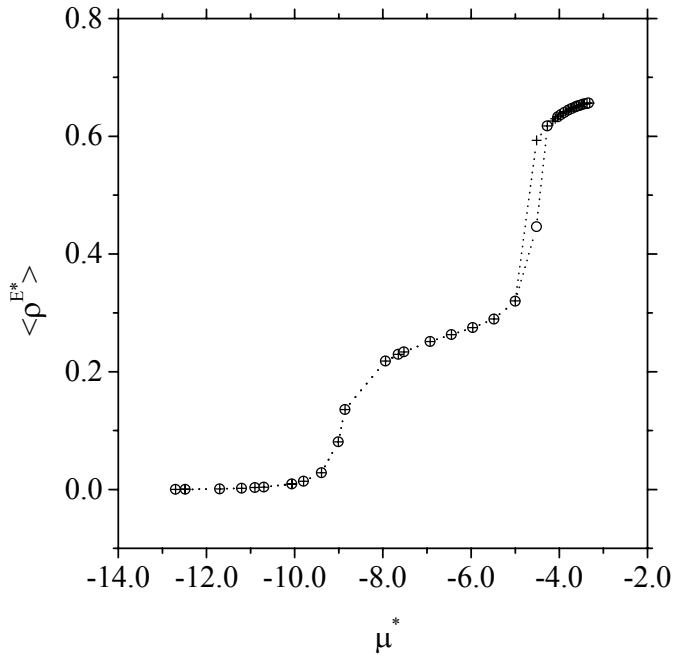

c)

Fig. 3.6. (a) Adsorption isotherms in $H = 8.8\sigma$ cylindrical and slit-like pores; the notation is the same as in Fig. 3.4(a). (b) Density profiles from FMT calculations in the cylindrical pore at five different μ^*, from bottom to top: -10.065, -5.478, -4.995, -4.513, -3.338. (c) Adsorption isotherms in the cylindrical pore by FMT, (circles) adsorption and (crosses) desorption branches.

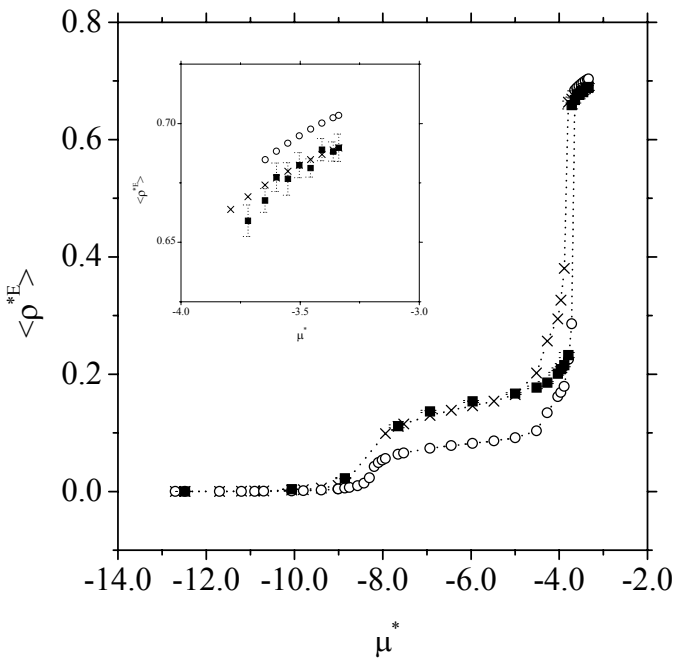
0.8
0.6
0.4
0.2
0.0
-14.0
-12.0
-10.0
-8.0
-6.0
-4.0
-2.0
μ*
<ρ*Γ>
0.70
0.65
-4.0
-3.5
-3.0

a)

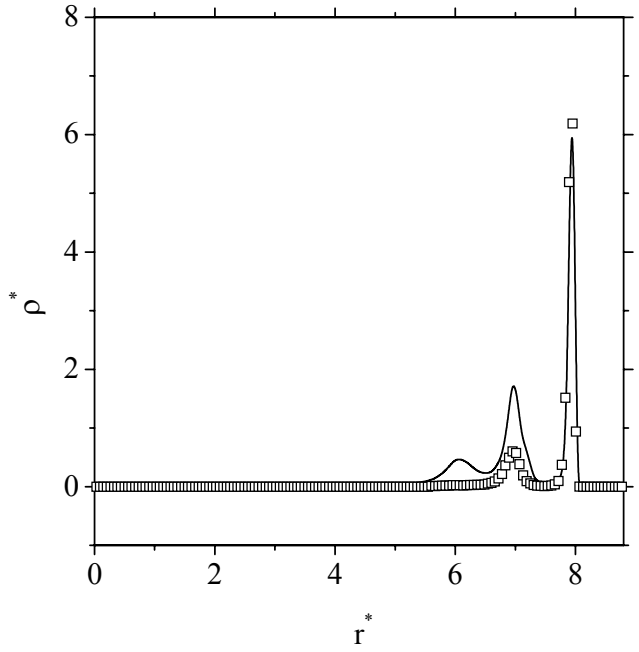
8
6
4
2
0
0
2
4
6
8
ρ*
r*

b)

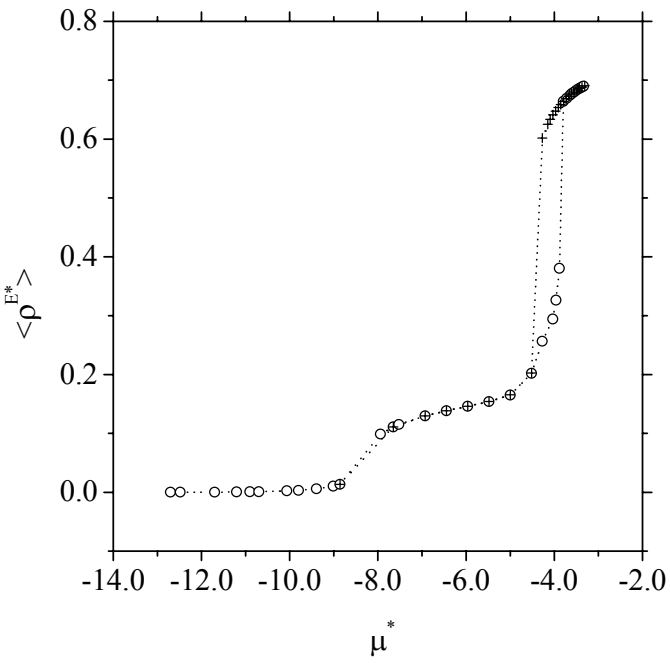

c)

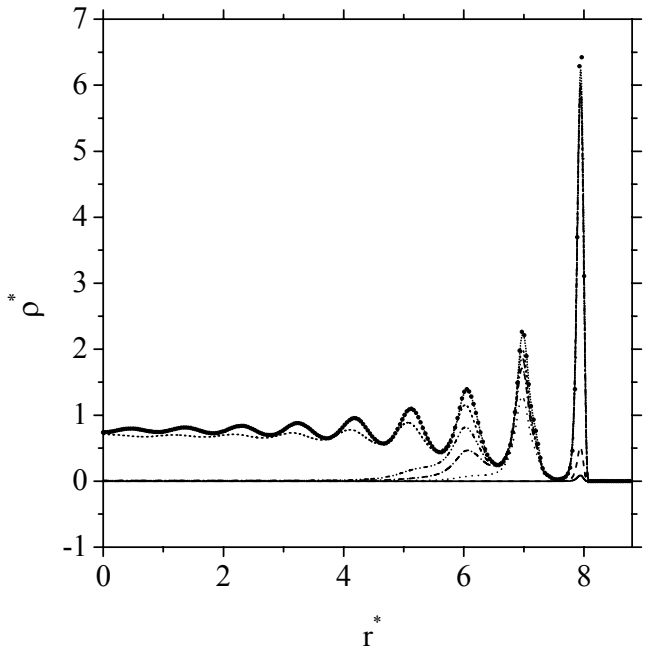

d)

Fig. 3.7. (a) Adsorption isotherms in $H = 17.6\sigma$ cylindrical and slit-like pores; the notation is the same as in Fig. 3.4(a), except that FMT adsorption in cylindrical pore shown as crosses for clarity. Inset shows the details in the high chemical potential region. (b) Density profiles from FMT calculations (lines) and GCMC simulations (symbols) at $\mu^* = -3.959$ for cylindrical pore. (c) Adsorption isotherms in the cylindrical pore by FMT calculations, (circles) adsorption and (crosses) desorption branches. (d) Density profiles from FMT in the cylindrical pore at seven different μ^*, from bottom to top -10.065, -8.858, -4.272, -3.959, -3.887, -3.791, -2.898.

Notice that, while in cylindrical geometry the agreement between calculated and simulated GCMC results at low chemical potential is excellent above capillary condensation, the values of the predicted excess density from Monte Carlo simulations are higher than those corresponding to the theory for both pore sizes (see Figs. 3.6(a) and 3.7(a)). The choice of the same molecular model leads in fact to a slightly different thermodynamic behavior in the bulk fluid properties. Hence, these differences are expected in a region of the isotherm dominated by the bulk fluid. For these two sizes and below the capillary condensation chemical potential, the excess density predicted for slit-like pores is lower than that corresponding to cylinders. The difference is less noticeable as the pore diameter increases, due to the loss of confinement. As in the previous cases, we have also considered the density profile behavior along the adsorption isotherms. Fig. 3.6(b) shows density profiles corresponding to a cylindrical pore of diameter $H = 8.8\sigma$ at different chemical potentials. When capillary condensation occurs, an increase of the density in the central part of the pore takes place. However, due to the higher degree of confinement, the fluid still displays a higher order than in planar geometries under the same conditions. As it can be seen in Fig. 3.6(c), the adsorption isotherm in the cylinder exhibits hysteresis, clearly indicating that the discontinuous jump observed in Fig. 3.6(a) must be ascribed to a gas-liquid phase transition inside the pore.

The adsorption behavior of a second wider mesopore of diameter $H = 17.6\sigma$ is analyzed in Figs. 3.7(a)-(d). We have also included the adsorption isotherm corresponding to the slit-like pore of the same size (see Fig. 3.7(a)). The same qualitative analysis as that regarding the previous pore size can be performed, although the differences between geometries tend to reduce as the pore size increases. In Fig. 3.7(b) we compare the density profiles obtained from FMT and simulation for the pore $H = 17.6\sigma$ closely underneath capillary condensation ($\mu^* = -3.959$). For this value of the chemical potential, only three layers are distinguishable. The hysteresis cycle is shown separately in Fig. 3.7(c) for more details. Finally, Fig. 3.7(d) shows a set of different theoretical density profiles for a sequence of chemical potential values. As can be seen, capillary condensation can be detected when the density profiles change from a gas-like to a liquid-like behavior, giving rise to a finite value of the local density in the central region of the pore.

Figs. 3.8(a) and (b) summarize the adsorption isotherms for the four pore sizes analyzed, corresponding, respectively, to cylindrical and planar geometries. In the cylindrical geometry, the smallest pore size, $H = 3.2\sigma$, exhibits a behavior completely determined by wall effects, including the first order 0 to 1 layering transition already mentioned. Due to the narrowness of this pore, only a single complete layer of molecules can be accommodated inside the pore. As the pore size is increased, $H= 4.8\sigma$, the formation of the first adsorbed layer is located at higher chemical potential than in the $H = 3.2\sigma$ and, moreover, seems to be thermodynamically of second order. An additional layer is continuously adsorbed as the chemical potential increases. This effect can be explained as a liquid-liquid enhanced interaction due to the proximity of opposite parts of the cylindrical wall that induces the exclusion of particles in the axial region of the pore and its possible liquid-like behavior and, thus, capillary condensation. A further increase in the pore size, $H = 8.8\sigma$ and 17.8σ, leads to multilayer adsorption with capillary condensation phase transition at high chemical potential. The formation of the

first layer corresponds to a continuous behavior and its location is affected by the curvature of the wall, being displaced towards lower chemical potentials as the curvature increases.

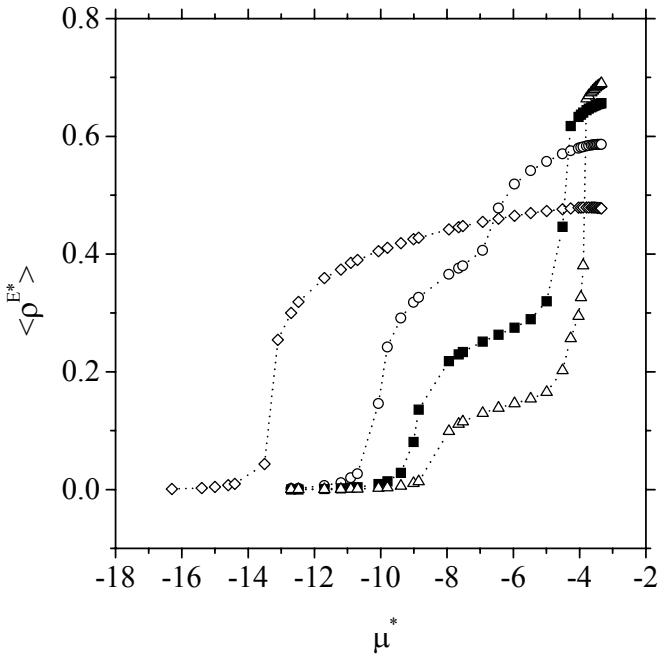

a)

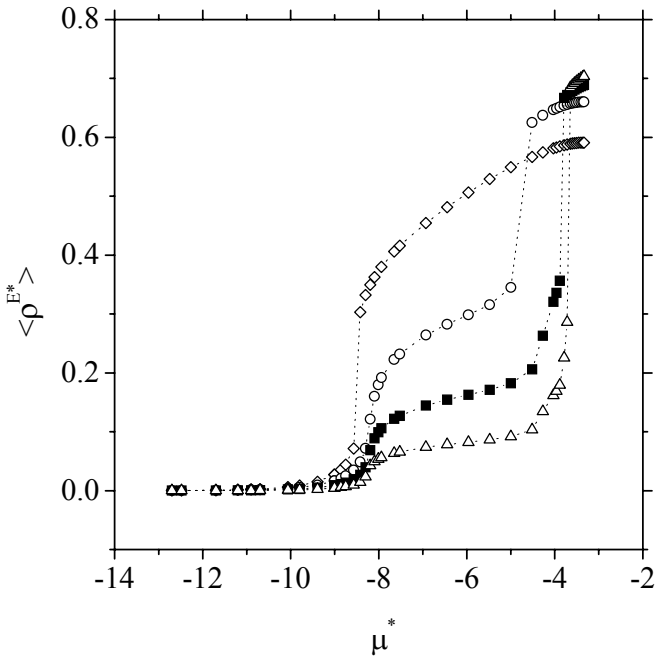

b)

Fig. 3.8. (a) Adsorption isotherms in cylindrical pores with different diameter: H = 3.2σ (open diamonds), 4.8σ (open circles), 8.8σ (closed squares), and 17.6σ (open triangles); from FMT calculations. (b) The same notation as in (a) but in slit-like pores.

In the analysis of the isotherms of pores with planar geometry, summarized in Fig. 3.8(b), we have observed that the pore of width $H = 3.2\sigma$, also exhibits a 0 to 1 first order layering transition, as in the case of cylindrical geometry. However, the formation of the first layer at larger pore widths is located around the same chemical potential, independently of the pore width, and corresponds to a continuum filling with no discontinuity in the first derivative of free energy, but with a large value of the second derivative that could correspond to a divergence. On the other hand, the capillary condensation is shifted by the confinement towards lower chemical potentials and it approaches the bulk liquid-vapor phase transition chemical potential as the pore width increases.

As an example of the effect of the strong geometrical constraint over the adsorption properties of cylindrical pores, we present the density profiles for different pore widths. In particular, Fig. 3.9 shows the density profiles corresponding to two cylindrical pores with $H = 4.0\sigma$ and 4.8σ. In the widest pore, geometrical constraints forbid the formation of a layer over the axis of the cylinder, while in the narrowest pore this layer is strongly favored, showing a peak much higher than the one close to the wall. In slit-like pores, although not represented here, the height of the observed peaks shows a progressive decrease as the molecules approach the center of the pore.

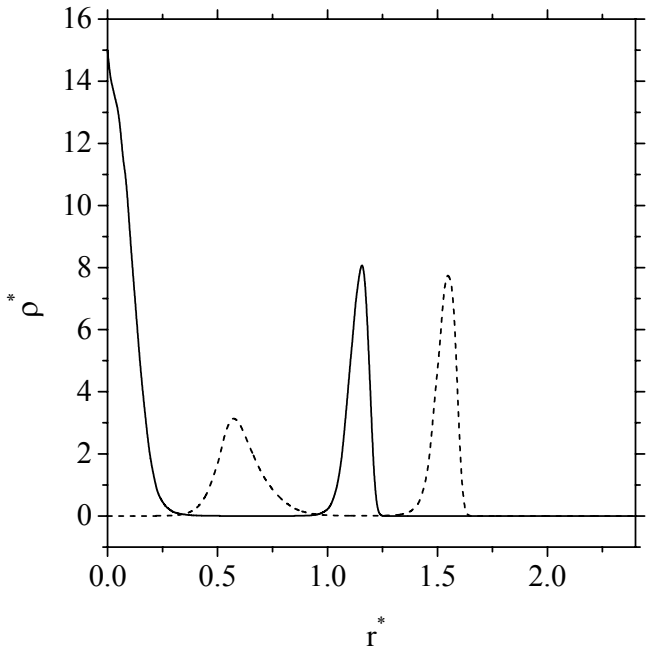

Fig. 3.9. Density profiles from FMT calculations in $H = 4.0\sigma$ (solid line), and in $H = 4.8\sigma$ (dashed line) cylindrical pores at the same chemical potential, $\mu^* = -3.338$.

Having described the phenomena observed for various pore sizes, it is worth to separately analyze the behavior of the free energy Eq. 2.5. We have identified three distinct features in the adsorption isotherms, namely, the first order 0 to 1 layering transition for the narrower pores, capillary condensation, and a sudden increase of the adsorbance due to the formation of dense thin layers at the solid surface. First, as seen

in Fig. 3.4(a), the isotherm for the pore size $H = 3.2\sigma$ show a weak discontinuity in both cases, indicating the first order nature of the transition [Evans, 1990]. Fig. 3.10(a) shows the behavior of the free energy in the vicinity of this transition for the planar pore, where the discontinuity of the first derivative can be observed, as well as the metastable lines of the free energy. Second, capillary condensation has been described as a shift of the bulk liquid-vapor phase transition, induced by the confinement [Evans and Tarazona, 1984; Evans and Marini Bettolo Marconi, 1985b]. In Fig. 3.10(b) we present the free energy of the isotherm corresponding to the cylindrical pore width H=17.6σ that shows a jump of its first derivative at the location of the capillary condensation transition, which serves to place the physical isotherm between the two metastable branches. Third, the sudden jump in the adsorption isotherm around μ^*=-8.0, in pores of planar geometry, could be reminiscent of a prewetting phenomenon existing for one wall in an infinite system [Evans, 1990; Rowlinson and Widom, 1984]. The detailed analysis of the free energy around this particular chemical potential, for H=17.6σ (see Fig. 3.10(c)) seems to indicate that this behavior cannot be attributed to a first order phase transition. The second derivative of the free energy (see Fig. 3.10(d)) shows a sharp peak that could suggest that the formation of the thin dense layer inside the pore corresponds to a second order phase transition. However, the numerical accuracy of our analysis does not permit us to distinguish whether the peak is a true divergence, corresponding to a second order phase transition, or it is finite, in which case we would identify a mere crossover between two regimes. Even more, the possibility of a very weak first order transition cannot completely be discarded, in view of the thermodynamic behavior associated to the formation of the first layer in the smaller pores analyzed. To be conclusive about the true nature of the transition and the effect of the wall curvature in its location, an exhaustive analysis beyond the scope of this work should be undertaken. Nevertheless, everything seems to indicate that the behavior related to the formation of the thin layer at the wall, in the cases analyzed in this chapter, could corresponds to phenomenology expected at the vicinity of a critical point, perhaps related to the critical end point of a prewetting line in semi-infinite system.

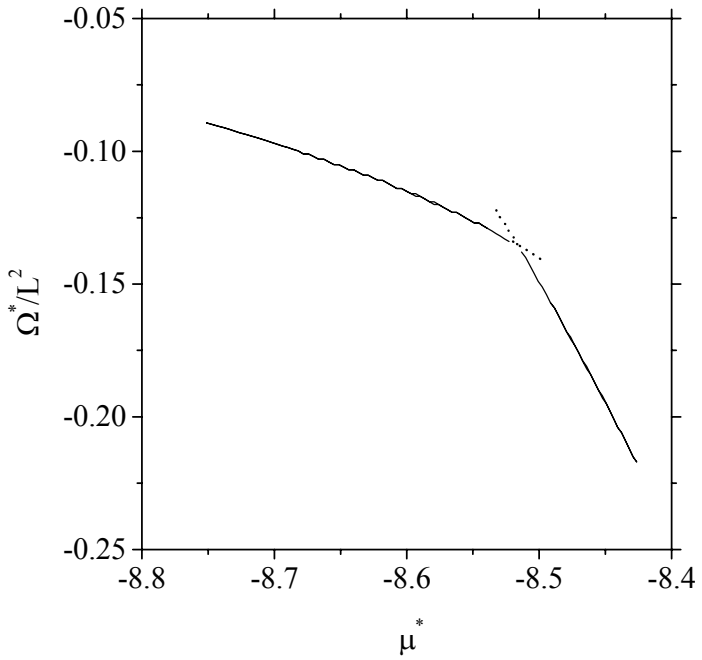
-0.05
-0.10
-0.15
-0.20
-0.25
-8.8
-8.7
-8.6
-8.5
-8.4
Ω^*/L^2
μ^*

a)

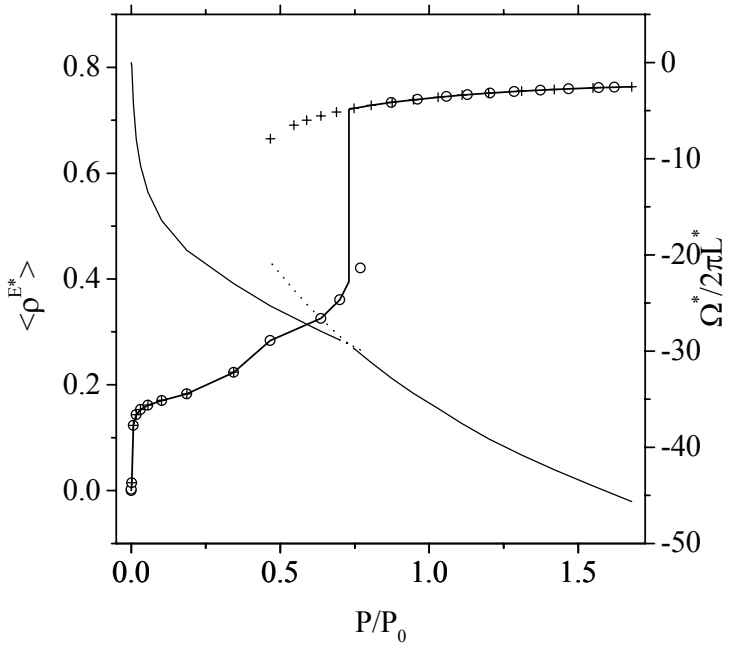
0.8
0.6
0.4
0.2
0.0
0
-10
-20
-30
-40
-50
0.0
0.5
1.0
1.5
$\langle\rho^{\Gamma*}\rangle$
$\Omega^*/2\pi L^*$
P/P_0

b)

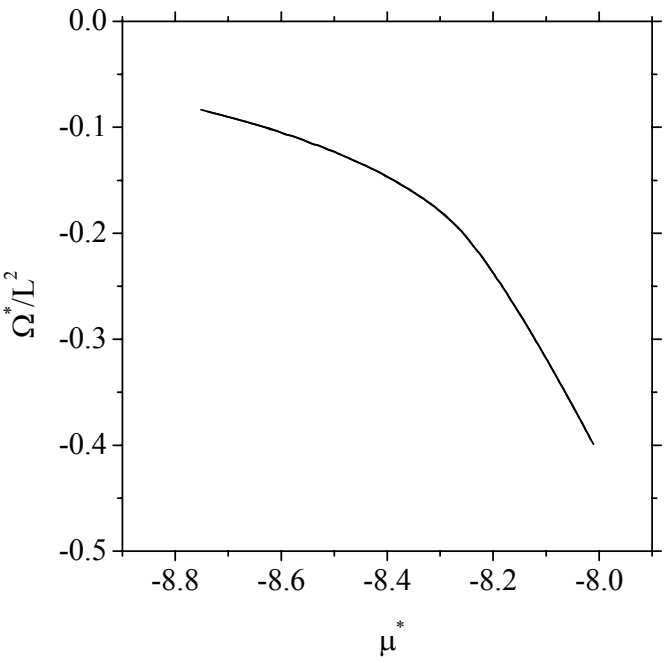

c

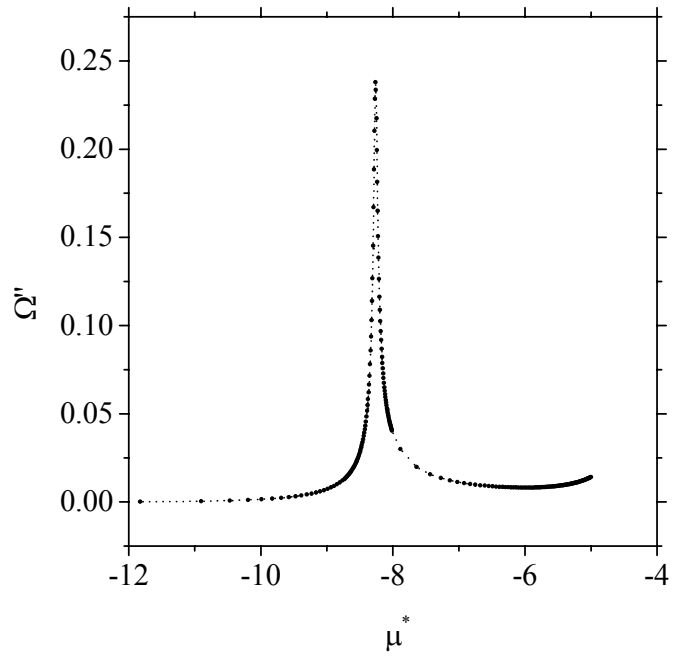

d)

Fig. 3.10. (a) Changes in the grand-potential energy of the system shown in the inset of Fig. 3.4(a), FMT calculations in the $H = 3.5\sigma$ planar pore. (b) Adsorption isotherm (open circles), desorption isotherm (crosses), and stable isotherm (solid line) in $H = 17.6\sigma$ cylindrical pore. The zigzag line shows the changes in the grand-potential energy of the system. (c) Changes in the grand-potential energy of the system $H = 17.6\sigma$ slit-like pore around $\mu^* = -8.0$. (d) Second derivative of the grand-potential energy of the same system in (c).

Finally, it is interesting to compare FMT results to those obtained using other formulations of DFT. Fig. 3.11 shows the adsorption isotherm obtained through our DFT formulation, with a cylindrical potential that takes the form [Tjatjopoulos *et al*., 1988]

$$\phi_{ext}(r,R)=\pi^2\rho_s\varepsilon_{sf}\sigma_{sf}^2\left[\frac{63}{32}\left[\frac{r}{\sigma_{sf}}\left(2-\frac{r}{R}\right)\right]^{-10}F\left[-\frac{9}{2},-\frac{9}{2};1;\left(1-\frac{r}{R}\right)^2\right]\right.$$
$$\left.-3\left[\frac{r}{\sigma_{sf}}\left(2-\frac{r}{R}\right)\right]^{-4}F\left[-\frac{3}{2},-\frac{3}{2};1;\left(1-\frac{r^2}{R}\right)\right]\right], \qquad (3.10)$$

where $F[\alpha,\beta;\gamma;\chi]$ are the hypergeometric functions [Press *et al*., 1992], and ρ_s is the density of oxygen atoms in the pore wall. Here, R is the radius of the pore of diameter H= 90Å (25.18σ) and σ_{sf} and ε_{sf} are the LJ solid-fluid interaction parameters. We have used here the same parameters as in the work by Ravikovitch *et al.* [2001] who, in Fig. 5 of their article, show experimental, GCMC and NLDFT [Tarazona, 1985] adsorption isotherm results. As seen in Fig. 3.11, it is remarkable that the behavior predicted by our calculations quantitatively agrees with the experimental and simulation results shown in this reference. However, the adsorption isotherm predicted by NLDFT shows steps indicating a layering pattern no present in the experimental data. Our FMT calculations are in good agreement with their GCMC results at low pressures and show a less pronounced layering than that of Ravikovitch *et al*. [2001].

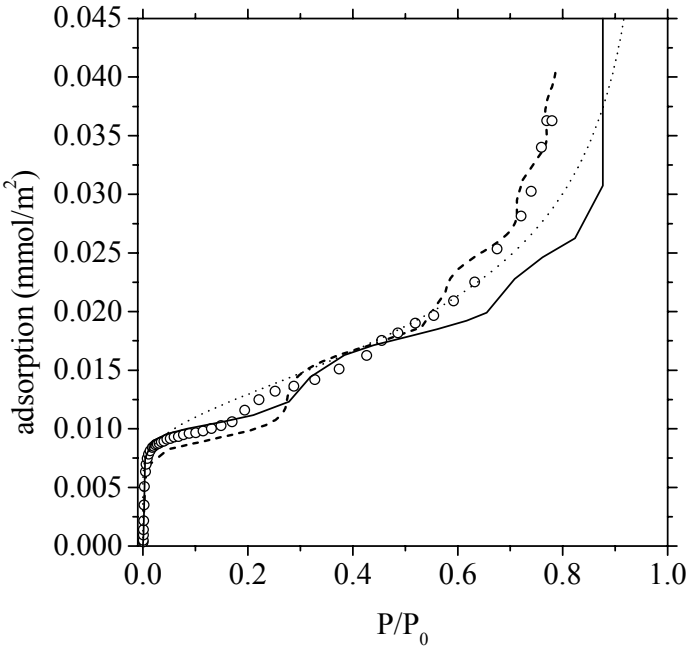

Fig. 3.11 Adsorption isotherms in H = 90Å (25.18σ) cylindrical pore; (solid line) FMT calculations of this work; (dashed line) NLDFT calculations [Ravikovitch, 2001]; (open circles) GCMC simulations [Ravikovitch, 2001]; (dotted line) experimental data on nonporous silica [Deboer *et al*., 1965].

3.4 Conclusions

In this work we have analyzed the ability of the FMT due to Kierlik and Rosinberg in predicting adsorption isotherms as well as density profiles in cylindrical pores, by comparison with data obtained from GCMC using the same molecular model. This work is of relevance in the context of the use of DFT calculations for the determination of pore-size distributions from experimentally obtained adsorption isotherms, as we will see in the next chapter.

A comparison of FMT for cylindrical pores with GCMC simulations has shown a very good agreement for the range of pore sizes studied, confirming the ability of the theory in the description of nearly one-dimensional confined systems. The exact limit of its validity for very narrow pores lies beyond the scope of this work.

Our results indicate that a layering behavior takes place in the smallest cylindrical pore considered, $H = 3.2\sigma$, while the adsorption in a planar pore of the same size needs a much higher chemical potential to achieve a significant adsorption. As the pore size increases, the influence of the geometry becomes less important, although a certain shift in the capillary condensation transition can still be observed. Additionally, for wider pores, such as $H = 8.8\sigma$ and 17.8σ, we obtain multilayer adsorption with capillary condensation at high chemical potentials, with the same qualitative behavior observed for both geometries. When the diameter size reaches the limit where the curvature effects are not of further relevance, the cylindrical pores reduce to the same quantitative behavior as the slit-like pores.

The formation of a thin adsorbed layer at intermediate and large pore sizes seems to correspond to a thermodynamic second order phase transition, for the range of parameters used and the thermodynamic conditions studied. However, the results found seem to indicate some relationship between this behavior and the prewetting transition observed in semi-infinite geometries, especially in the neighborhood of the critical end point of the prewetting line. The effect of the confinement is very important in this crossover behavior. In fact, the local curvature of the solid wall is the only responsible for the shift observed in cylindrical geometries in our study, although a deeper analysis is required to shed some light on this particular point.

From the comparison of FMT calculations *versus* NLDFT results, we conclude that the FMT is an excellent tool for the study of the behavior of fluids in confined cylindrical geometries.

3.5 References

Balbuena, P. B.; Gubbins, K. E., *Langmuir* **9**, 1801 (1993).

Ball, P. C.; Evans, R. *J. Chem. Phys*. **89**, 4412 (1988).

Brodka, A.; Zerda, T. W. *J. Chem. Phys*. **85**, 3710 (1991).

Bryk, P.; Cyrankiewicz, W.; Borowko, M.; Sokolowski, S. *Mol. Phys*. **93**, 111 (1998).

Curtin, W. A.; Ashcroft, N. W. *Phys. Rev. A* **32**, 2909 (1985).

Deboer, J. H.; Linsen, B. G.; Osinga, T. J. *J. Catal*. **4**, 643 (1965).

Dietrich, S., in *"Phase transitions and critical phenomena"*, edited by Domb, C. and Lebowitz, J. L. (Academic Press, New York, 1988), Vol. 12, Chap. 1, p.1.

Evans, R. *J. Phys.: Condens. Matter* **2**, 8989 (1990).

Evans, R., in *"Fundamentals of inhomogeneous fluids"*, edited by Henderson, D. (Marcel Dekker, Inc., New York, 1992), Chap. 3, p.85.

Evans, R.; Marini Bettolo Marconi, U. *Chem. Phys. Lett*. **114**, 415 (1985a).

Evans, R.; Marini Bettolo Marconi, U. *Phys. Rev. A* **32**, 3817 (1985b).

Evans, R.; Marini Bettolo Marconi, U. *J. Chem. Phys*. **86**, 7138 (1987).

Evans, R.; Marini Bettolo Marconi, U.; Tarazona, P. *J. Chem. Phys*. **84**, 2376 (1986).

Evans, R.; Marini Bettolo Marconi, U.; Tarazona, P. *J. Chem. Soc., Faraday Trans. 2* **82**, 1763 (1986).

Evans, R.; Parry, A. O. *J. Phys.: Condens. Matter* **1**, 7207 (1989).

Evans, R.; Tarazona, P. *Phys. Rev. Lett*. **52**, 557 (1984).

Freasier, B. C.; Nordholm, S. *Mol. Phys*. **54**, 33 (1986).

Freasier, B. C.; Nordholm, S. *J. Chem. Phys.* **79**, 4431 (1983).

Gelb, L. D.; Gubbins, K. E. *Langmuir* **14**, 2097 (1998).

Gelb, L. D.; Gubbins, K. E. *Langmuir* **15**, 305 (1999).

Gelb, L. D.; Gubbins, K. E.; Radhakrishnan, R.; Sliwinska-Bartkowiak, M. *Rep. Prog. Phys*. 62, 1573 (1999).

González, A.; White, J. A.; Román, F. L.; Evans, R. *J. Chem. Phys*. **109**, 3637 (1998).

Gregg, S. J.; Sing, K. S. W. *"Adsorption, surface area and porosity"*, 2nd edition (Academic Press Inc., London, 1982), Chap. 3, p.132.

Helfand, E.; Frisch, H. L.; Lebowitz, J. L. *J. Chem. Phys*. **34**, 1037 (1961).

Jiang, S.; Gubbins, K. E.; Balbuena, P. B. *J. Phys. Chem*. 98, 2404 (1994).

Johnson, M.; Nordholm, S. *J. Chem. Phys*. **75**, 1953 (1981).

Kierlik, E.; Fan, Y.; Monson, P. A.; Rosinberg, M. L. *J. Chem. Phys*. **102**, 3712 (1995).

Kierlik, E.; Rosinberg, M. L. *Phys. Rev. A* **44**, 5025 (1991).

Kierlik, E.; Rosinberg, M. L.; Fan, Y.; Monson, P. A. *J. Chem. Phys*. **101**, 10947 (1994).

Kierlik, E.; Rosinberg, M. L.; Finn, J. E.; Monson, P. A. *Mol. Phys*. **75**, 1435 (1992).

Kierlik, E.; Rosinberg, M. L. *Phys. Rev. A* **42**, 3382 (1990).

Lastoskie, C.; Gubbins, K. E.; Quirke, N. *Langmuir* **9**, 2693 (1993a).

Lastoskie, C.; Gubbins, K. E.; Quirke, N. *J. Phys. Chem*. **97**, 4786 (1993b).

Lebowitz, J. L. *Phys. Rev.* **133**, A895 (1964).

Lu, B. Q.; Evans, R.; Telo da Gama, M. M. *Mol. Phys*. **55**, 1319 (1985).

MacElroy, J. M. D. *Langmuir* **9**, 2682 (1993).

Maddox, M. W.; Olivier, J. P.; Gubbins, K. E. *Langmuir* **13**, 1737 (1997).

Meister, T. F.; Kroll, D. M. *Phys. Rev. A* **31**, 4055 (1985).

Nordholm, S.; Johnson, M.; Freasier, B. C. *Aust. J. Chem*. **33**, 2139 (1980).

Percus, J. K. *J. Chem. Phys*. **75**, 1316 (1981).

Percus, J. K. *J. Stat. Phys*. 28, **67** (1982).

Percus, J. K. *J. Stat. Phys.* **52**, 1157 (1988).

Peterson, B. K.; Gubbins, K. E.; Heffelfinger, G. S.; Marini Bettolo Marconi, U.; van Swol, F. *J. Chem. Phys.* **88**, 6487 (1988).

Peterson, B. K.; Heffelfinger, G. S.; Gubbins, K. E.; van Swol, F. *J. Chem. Phys*. **93**, 679 (1990).

Peterson, B. K.; Walton, J. P. R. B.; Gubbins, K. E. *Int. J. Thermophys*. **6**, 585 (1985).

Peterson, B. K.; Walton, J. P. R. B.; Gubbins, K. E. *J. Chem. Soc., Faraday Trans. 2* **82**, 1789 (1986).

Phan, S.; Kierlik, E.; Rosinberg, M. L.; Bildstein, B.; Kahl, G. *Phys. Rev. E* **48**, 618 (1993).

Phan, S.; Kierlik, E.; Rosinberg, M. L.; Yethiraj, A.; Dickman, R. *J. Chem. Phys*. **102**, 2141 (1995).

Press, W. A.; Teukolsky, S. A.; Vetterling, W. T.; Flannery, B. P. *"Numerical recipes in Fortran"*, 2nd edition (Cambridge University Press, U.S.A., 1992), Chap. 6, p.263.

Ravikovitch, P. I.; Vishnyakov, A.; Neimark, A. V. *Phys. Rev. E* **64**, 011602 (2001).

Ravikovitch, P. I.; Vishnyakov, A.; Russo, R.; Neimark, A. V. *Langmuir* **16**, 2311 (2000).

Reiss, H.; Frisch, H. L.; Lebowitz, J. L. *J. Chem. Phys.* **31**, 369 (1959).

Robledo, A.; Varea, C. *J. Stat. Phys*. **26**, 513 (1981).

Rouquerol, F.; Rouquerol, J.; Sing, K. *"Adsorption by Powders & Porous Solids"*, (Academic Press, London, 1999).

Rosenfeld, Y. *Phys. Rev. Lett*. **63**, 980 (1989).

Rosenfeld, Y.; Schmidt, M.; Löwen, H.; Tarazona, P. *Phys. Rev. E* **55**, 4245 (1997).

Rowlinson, J. S.; Widom, B. *"Molecular theory of capillarity"* (Claredon Press, Oxford, 1984).

Sliwinska-Bartkowiak, M.; Sowers, S. L.; Gubbins, K. E. *Langmuir* **13**, 1182 (1997).

Sowers, S. L.; Gubbins, K. E. *Langmuir* **11**, 4758 (1995).

Sullivan; D. E.; Telo da Gama, M. M., in *"Fluid interfacial phenomena"*, edited by Croxton, C. A. (Wiley & Sons, New York, 1986), Chap. 2, p.45.

Tarazona, P. *Mol. Phys*. **81** (1984).

Tarazona, P. *Phys. Rev. A* **31**, 2672 (1985); *Ibid.* **32**, 3148 (1985) (*erratum*).

Tarazona, P. *Phys. Rev. Lett*. **84**, 694 (2000).

Tarazona, P.; Evans, R. *Mol. Phys*. **47**, 1033 (1982).

Tarazona, P.; Evans, R. *Mol. Phys*. **48**, 799 (1983).

Tarazona, P.; Marini Bettolo Marconi, U.; Evans, R. *Mol. Phys*. **60**, 573 (1987).

Tarazona, P.; Telo da Gama, M. M.; Evans, R. *Mol. Phys*. **49**, 283 (1983).

Thiele, E. *J. Chem. Phys*. **39**, 474 (1963).

Tjatjopoulos, G. J.; Feke, D. L.; Mann, J. A. Jr. *J. Phys. Chem.* **92**, 4006 (1988).

Verlet, L.; Weis, J. J. *Phys. Rev. A* **5**, 939 (1972).

Weeks, J. D.; Chandler, D.; Andersen, H. C. *J. Chem. Phys*. **54**, 5237 (1971).

Wertheim, M. S. *Phys. Rev. Lett.* **10**, 321 (1963).

4. PORE-SIZE DISTRIBUTION OF MODEL POROUS GLASSES

4.1 Introduction

Density functional theory, applied to calculate the amount of fluid adsorbed at different pressures and pore sizes, has proved to be a very useful tool for analyzing the adsorption behavior of porous materials, and in particular, to obtain the PSD's of them [Lastoskie *et al*., 1993a; Ravikovitch *et al*., 2000]. However, several important simplifications should be made when an amorphous material is modeled within this approach. Thus, to establish the accuracy of these methods is a difficult task, making impossible to discern what comes from the approximations made in modeling the individual pores with those coming from the model used for the material as a whole.

In a attempt to use molecular modeling techniques for materials in a more realistic way, Gelb and Gubbins [1998] proposed a new approach to model porous silica glasses, using quench molecular dynamic methods that mimic the experimental processes in which these materials are produced. The resulting model glasses have a pore topology, porosity, surface area and adsorption isotherm behavior similar to the real glasses. A major advantage of these model materials is that they are precisely characterized at the molecular level, and hence they provide the ideal framework to test different approaches used in practice to characterize amorphous systems, where some approximations and assumptions need to be made. In particular, Gelb and Gubbins [1998, 1999] have obtained the nitrogen adsorption isotherms in these materials using Monte Carlo simulations, and they were able to determine the "real" PSD's of the model porous glasses (the geometrical PSD) [Gelb and Gubbins, 1999].

Controlled-pore glasses (CPG's) are widely used as stationary phase in chromatography [Haller, 1983; Schnabel and Langer, 1991]. These materials have excellent mechanical properties and can be prepared with a wide range of porosities and pore sizes [Elmer, 1991]. They can be modified to include a variety of functional groups, and the adsorption strength of the glasses can be adjusted over a wide range of values [Schnabel and Langer, 1991]. Although controlled-pore glasses were developed for use in size-exclusion chromatography, derivatized glasses can show a high chemical affinity for certain biomolecules, and can even be used as catalytic agents and bioreactors [Haller, 1983].

Gelb and Gubbins, in their work of 1999 carried out a study of the validity of the BJH method to obtain the distribution of void volume in model porous glasses. They concluded that when the BJH method is used, the PSD's obtained differ in a systematic

way from those determined directly from the pore structure using spherical probes. The BJH method yields PSD's which are narrower, and have a maximum in pore diameters about 10 Å smaller than the exactly known geometric PSD's. In a different work, Kanda *et al.* [2000] developed a new condensation model for cylindrical pores substituting the Kelvin model to consider a meniscus curvature in a more realistic way. They had proved this model in nanopores with ideal geometry (cylindrical [Yoshioka *et al*., 1997] and slit-shaped [Miyahara *et al*., 2000]), obtaining good agreement with simulations of the same systems. With the idea to test their model *vs*. a realistic geometry, they used the "system A" from the work of Gelb and Gubbins [1999], and compared the geometrical PSD *vs*. the obtained with the Kanda *et al*. [2000] condensation model. The agreement obtained is very good, but their study is not systematic, they did the comparison just in one of the four materials from Gelb and Gubbins's work, and actually, it may be fortuitous. They used system A because this one has only a small hysteresis loop, while one of the other systems exhibits a quite large hysteresis loop. For the other two samples, desorption branches are not shown and the extent of the hysteresis cannot be known. There is still argument about which branch to take for pore-size determination, though adsorption branch is often recommended, and the analysis of an isotherm with large hysteresis confuses the purpose of this examination.

In the DFT approach to obtain PSD, it is necessary to do approximations of two different classes; on the one hand, relative to the modeling of the adsorption in each pore, and on the other hand, referent to modeling the material itself. Regarding the first point, in the previous chapter an exhaustive comparison between DFT and GCMC simulations are done, establishing the accuracy of the theory. In this context, the goal of this part of the work is to analyze these different factors, establishing the relevance of each one of them. In particular, to prove the hypothesis of the independent-pore model using simple geometries when the material is amorphous. Additionally, to determine the most appropriate geometry to model porous glasses.

In this chapter we present the molecular model details and procedures of the Gelb and Gubbins work [1999] used here as the "experimental" systems. Following, the details of the molecular models of the fluid, of the wall, and of the calculations concerned with PSD. After that, we expose the theoretical adsorption isotherms obtained for cylindrical and slit-like pores. In the next section, we reconstruct the adsorption isotherm using the set of theoretical isotherms of different sizes weighted with the geometrical PSD's [Gelb and Gubbins, 1999] using both geometries. The following part is devoted to present the PSD's obtained from the inversion of adsorption integral equations for four materials using cylindrical and slit-like geometries, along with a test that the methods works well. Finally, we discuss the variety of possible sources of discrepancies, *e. g.* the validity of the wall model studying the adsorption behavior with different ε_{sf} parameter, or such as the mean field approximations done when the DFT is solved.

4.2 Molecular models

4.2.1 Model materials

CPG's and the related Vycor glasses are highly interconnected mesoporous silica materials. Their preparation is based on the near-critical phase separation of a binary liquid mixture, which produces complex networked structures, and were originally done by Haller [1965], who partially phase-separated a mixture of SiO_2, Na_2O, and B_2O_3, and etched out the borosilicate phase, leaving a nearly pure silica matrix with a porosity between 50% and 75%, and an average pore size between 45 and 4000 Å. There is other kind of materials with very similar features known as Vycor glasses. Those materials are prepared with a similar procedure and have a porosity near 28% and an average internal pore diameter between 40 and 70 Å [Elmer, 1991; Levitz *et al*., 1991].

Preparation of model glasses

The procedure employed by Gelb and Gubbins can be found in the original references [1998; 1999], but for continuity of the presentation of this work, we explain briefly the way in which they worked.

They mimic the preparation of the real glasses on a computer by simulating a system that exhibits this kind of phase separation, quenching it, removing one phase, and relaxing or annealing the resulting structure. This method "naturally" produces a structure with the same general characteristics as the experimental glasses. By varying the length of the quench period and the starting mole fraction of the mixture, they could tune the surface area, porosity, and average pore size over a wide range of values.

The simulation cells that they used were all of 270 Å on each side; they contained initially 868,000 atoms of the quench mixture. These simulation cells were periodic in all three directions, so that surface effects are not present. The initial mole fraction was $x = 0.7$, and quench configurations were taken at 225τ (sample "A"), 300τ (sample "B"), 375τ (sample "C"), and 450τ (sample "D") to prepare the four samples used in this study. Here $\tau = (\varepsilon/m\sigma^2)^{1/2} t$ is the reduced time; 1τ corresponds to 0.781 ps, and m is the mass of one atom. These samples all had porosities very near 30% and average pore sizes of approximately 33, 39, 45, and 50 Å, respectively. These models are fully connected, in that the void space is a single volume of very complex geometry, rather than several disconnected volumes. In the next figure (4.1), taken from the literature [1999], three of four of these materials are illustrated with different τ. A very detailed explanation of the whole recipe can be consulted in the reference of Gelb and Gubbins from 1998.

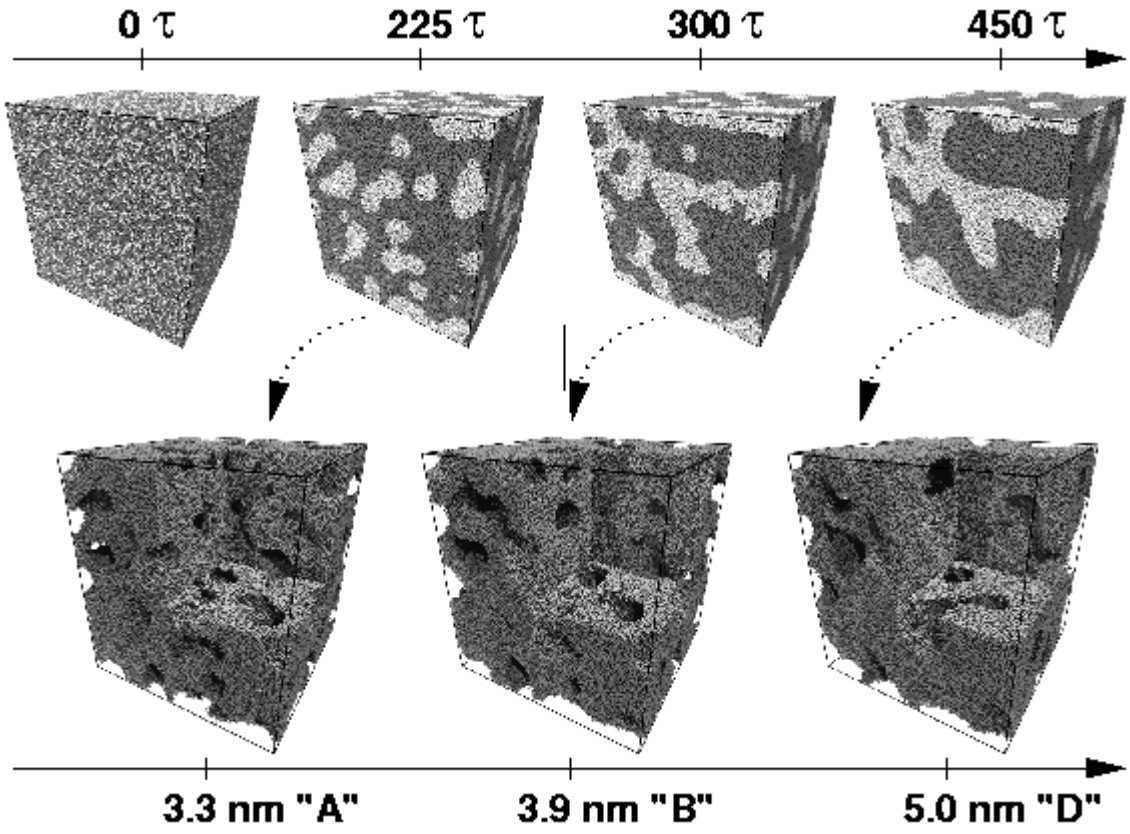

Figure 4.1. Generation of model materials. Samples "A", "B", and "D". Taken from Gelb and Gubbins [1999].

4.2.2 Theoretical adsorption isotherms

The model employed in this chapter to calculate the adsorption isotherms is the same as in the previous chapter. The adsorption isotherms on slit-like and cylindrical pores were obtained by FMT, as described in section 2.2, and with the molecular parameters used in section 3.2. The fluid employed, nitrogen at 77K, and the substrate are the same as in chapter 3. The only difference is the way to calculate the average density of nitrogen inside the pores. The reason to do it in this way is because in chapter 3 we were interested in a comparison *vs*. molecular simulation with the aim of establishing the validity of FMT to predict the adsorption on simple geometries. Instead of that, in this chapter, we are interested in the description of the best possible way to model materials, using the same definition of molecular surface than that used by Gelb and Gubbins. They used the definition known as "Connolly surface" [Connolly, 1983]. The difference between this and the one used in the previous chapter is shown in the figure 4.2, and in the equations 4.1 and 4.2. In the case of very long pores these differences are subtle, but when we are dealing with micro and mesopores these difference gain relevance.

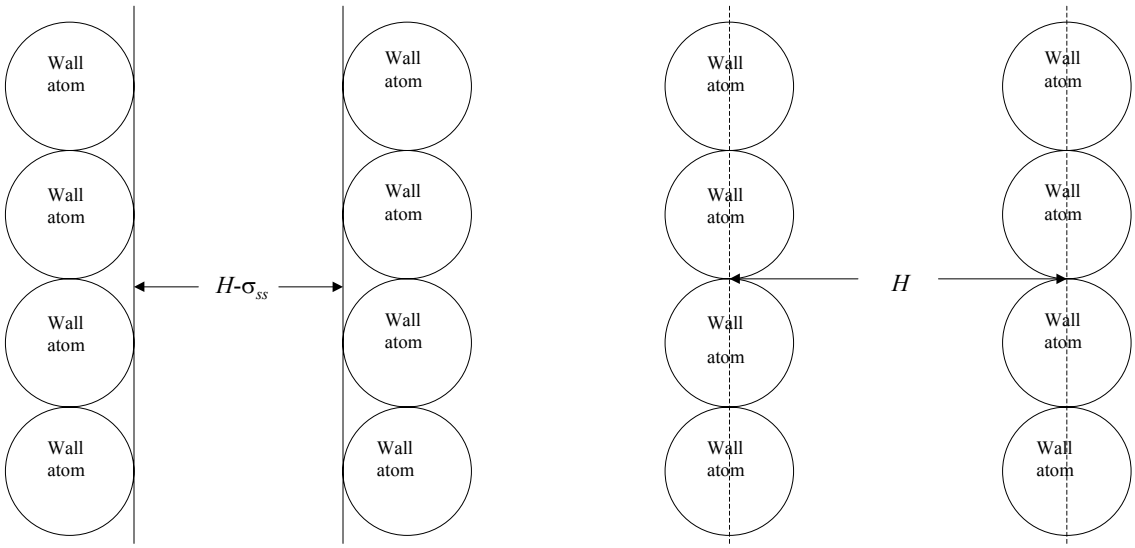

Figure 4.2. Two-dimensional representation of the different definitions for a molecular surface employed in this work: a)Connolly surface, and b)definition of the internal diameter or separation between two planes, H.

Cylindrical pores:
$$\langle \rho^{E} \rangle = \frac{8}{(H-\sigma_{ss})^{2}} \int_{0}^{H/2} r\rho(r)dr - \rho_{bulk} \tag{4.1}$$

Slit-like pores:
$$\langle \rho^{E} \rangle = \frac{1}{H-\sigma_{ss}} \int_{0}^{H} \rho(z)dz - \rho_{bulk} \tag{4.2}$$

There is another important point to take into account. The "experimental" adsorption isotherms represent the amount of fluid adsorbed per unit of volume of the solid material while the theoretical adsorption isotherms are fluid adsorbed per unit of void volume. Therefore, it is necessary to use the porosity of material to relate these different concepts of volume.

4.3 Pore-size distributions

We explain here the different approaches to obtain PSD's of materials. Although, we have just calculated the PSD inverting the adsorption integral equation with the regularization numerical method, for continuity of this thesis, we briefly expose the most relevant features of the other methods, as well.

4.3.1 Geometrical distribution

The method employed by Gelb and Gubbins [1999] to measure the PSD of their model materials is illustrated in Fig. 4.3, and it consists in the following. Consider the sub-volumes of the system accessible to spheres of different radii. Let $V_{pore}(r)$ be the volume of the void space "coverable" by spheres of radius r or smaller; a point X is in $V_{pore}(r)$

only if we can construct a sphere of radius r that overlaps X and does not overlap any substrate atoms (see Fig. 4.3). This volume is, in fact, equivalent to that enclosed by the pore's Connolly surface as it was mentioned before. $V_{pore}(r)$ is a monotonically decreasing function of r and is easily compared with the "cumulative pore volume" curves often calculated in isotherm-based PSD methods [Barret *et al.*, 1951]. The derivative $-dV_{pore}(r)/dr$ is the fraction of volume coverable by spheres of radius r but not by spheres of radius $r+dr$ and is a direct definition of the pore-size distribution [Pfeifer *et al.*, 1991]. The $V_{pore}(r)$ function can be calculated by a Monte Carlo volume integration [Allen and Tildesley, 1987].

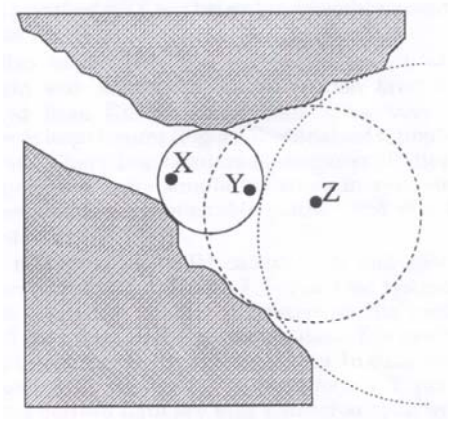

Fig. 4.3♣. Two-dimensional illustration of the geometric derivation of the PSD. Point "*X*" is only coverable by the smallest (solid) circle, while point "*Y*" is coverable by the smallest and midsize (dashed) circles, and point "*Z*" is coverable by all three circles. By determining the largest covering circle for every point in the void volume, a cumulative pore volume curve it is obtained.

For a material composed of spherical, cylindrical, or slit-shaped pores, this analysis would give the exact distribution of pore sizes. For an irregular material this geometric pore size definition is still fully applicable, while the assumptions that underlay many isotherm-based methods may not apply.

4.3.2 Inversion of integral adsorption equation

The integral isothermal adsorption equation for the case of PSD can be written as the convolution

$$\Gamma_V(\mu^*) = \mathcal{P} \int_{H_{min}}^{H_{max}} \rho^E(\mu^*, H) f(H) dH \tag{4.3}$$

♣ Taken from the work of Gelb and Gubbins, 1999.

where $\Gamma_V(\mu^*)$ represents the amount of adsorbate like particle number per unit of volume of adsorbent material (in Å), at reduced chemical potential μ^*; $\rho^E(\mu^*,H)$, the "kernel" function, describes the adsorption isotherm of an ideally homoporous material characterized by the pore width (or diameter) H in unit of particle number per volume of pore (void space in $Å^{-3}$), and $f(H)$ is the desired pore volume distribution function with respect to H. This size H is also in Å, while $f(H)$ is given in $Å^{-1}$. Finally, $\mathcal{P}$ is a measurement of the porosity (pore volume fraction per total volume), which is necessary to take in to account to compare both sides of Eq. 4.3. It is very important to remember this because it is a frequent source of confusions.

Eq. 4.3 represents an "inhomogeneous Fredholm equation of the first kind"

$$g(x) = \int_a^b k(x,s)u(s)ds \tag{4.4}$$

and its solution is well known to be an ill-posed problem [Press *et al*., 1986]. However, the integral equation of Fredholm of the second kind

$$g(x) = \int_a^b k(x,s)u(s)ds + \lambda_R u(x) \tag{4.5}$$

has a unique solution u which dependence on g is continuous, *i. e*., it is a well-conditioned problem. Therefore, it would be reasonable to take as an approximated solution of the equation 4.4, the solution of equation 4.5 with small values of λ_R. This is the base of the general theory of regularization [Press *et al*., 1986].

Since we are only interested in the numerical values of $f(H)$, we can rewrite equation 4.3 as a summation

$$\Gamma_V(\mu^*) = \mathcal{P}\sum_i \rho^E(\mu^*,H_i)f(H_i)\Delta H_i \tag{4.6}$$

where $\Gamma_V(\mu^*)$ is an experimental adsorption isotherm interpolated at the values of the chemical potential, μ^*, $\rho^E(\mu^*,H_i)$ is a matrix of values for theoretical isotherms, each row calculated at value of H_i at chemical potential μ^*, and $f(H_i)$ is the solution vector whose terms represent the volume in the sample characterized by each pore size H_i. The solution values desired are those that most closely, in a least squares sense, solve Eq. 4.6.

Since the data $\Gamma_V(\mu^*)$ contains some experimental error and the kernel models are not exact, we can expect the results, $f(H_i)$, to be only approximated. Indeed it is a characteristic of de-convolution processes to be unstable with respect to small errors in the data. This problem can be mitigated by choice of matrix dimensions. If we consider m members of the set of H and a vector μ^* of length n, it is clear that $n \times m$ must hold. If $n = m$, the solution of vector $f(H_i)$ is most sensitive to imperfections in the data. For $n > m$, the solution is stabilized because of the additional data constraints. In this work we use an over-determined matrix for which $n > m$.

There are additionally two other independent constraints on the solution that can be used to improve the stability of the process. One is that each f_i should be non-negative. The second regularization constraint is to require that for any real sample, the pore-size distribution must be smooth. As a measured of smoothness we use the size of the second derivative of $f(H_i)$. Then, the function to be minimized is

$$F = \sum_{j}^{n}\left(\Gamma_V\left(\mu_j^*\right) - \mathcal{P}\sum_{i}^{m}\rho^E\left(H_i,\mu_j^*\right)f\left(H_i\right)\Delta H_i\right)^2 + \lambda_R^2\sum_{i}^{m}\left(\frac{d^2 f\left(H_i\right)}{dH_i^2}\right)^2\Delta H_i^2 \qquad (4.7)$$

The problem is now reduced to finding the $f(H_i)$ such that the first term of the previous equation is small (a good fit to the data), and that the second one is small too (a smooth PSD), and $f(H_i) \geq 0$ (no negative pore volumen). The constant λ_R has been introduced to give an adjustment to the relative weight, or importance, of the two terms. If the model is good and the data very accurate, λ_R should be very small. Large values of λ_R are related to the smoothness of the resulting curve. Finding the vector $f(H_i)$ that minimizes F subject to the constraint that $f(H_i) \geq 0$ is a standard problem in pure linear algebra and can be solved exactly. In particular, here we have employed the Marquart-Levenberg method [Press *et al.*, 1986] to find the solution of our problem.

A tolerance of $1\text{x}10^{-14}$ has been used for all calculations done here. Since there are several solutions compatible with Eq. 4.7, we have devised a method to choose what we considered the most appropriate one. We have developed a Monte Carlo algorithm in which different initial guesses are given, generating random numbers between 0 and 1. When the program finds a solution of the minimum squared difference, the solution is kept, and the program runs again. The new solution is also kept, and compared to the previous one. The program will keep only the small between these two, for comparison with the next solution, in which the small one will be kept again. We follow this procedure 100 times, observing not further improvement after this.

4.4 Results and discussion

Since there are different factors that we would affect the estimation of the PSD of materials, and taking advantage of the fact that we are using molecular models, where we can systematically study the influence of different parameters in a particular property, we will proceed in the following way:

1. We first calculate the adsorption isotherms of individual pores (cylinder and slit-like pores) by FMT; the accuracy of the theory for these geometries and a wide range of pore sizes were proved in chapter 3.
2. We use the geometrical PSD measured in the work of Gelb and Gubbins [1999] to weight the individual isotherms, reconstructing the overall isotherm; in this way we check the accuracy of the independent pore model.
3. We estimate the PSD of the material by inversion of the adsorption integral equation using regularization methods, considering the two pore geometries.

4.4.1 Theoretical adsorption isotherms

In order to calculate the pore-size distribution of the material, a series of individual adsorption isotherms of nitrogen at 77K for both geometries were calculated. For slit-like pores the distance between walls ranged from 6 to 66 Å, with intervals of 3 Å. In the case of cylindrical pores, the pore diameter used in the calculations ranged from 12 to 66Å. Although desirable, there are two reasons that restraint us from calculating thinner cylindrical pores, one of them is that, as mentioned in chapter 3, the FMT does not accurately predict the one-dimensional limit, and hence it can not be reached in this approach; and we have also found convergence problems in the numerical solution of Euler-Lagrange equation (2.10).

We have observed different adsorption behaviors, depending on the pore size and geometry. Since this has been extensible discussed in the previous chapter, we will focus here only on using these isotherms to obtain the PSD of the porous glasses.

In figure 4.4(a) and (b) we present the collection of adsorption isotherms calculated for cylindrical and slit-like pores, respectively. For clarity we show some selected sizes, in the range of diameters mentioned above. It is interesting to note that in the cylindrical pores the adsorption occurs at lower pressures that the homologous slit-like pores, and the total capacity is higher in the slit-like case.

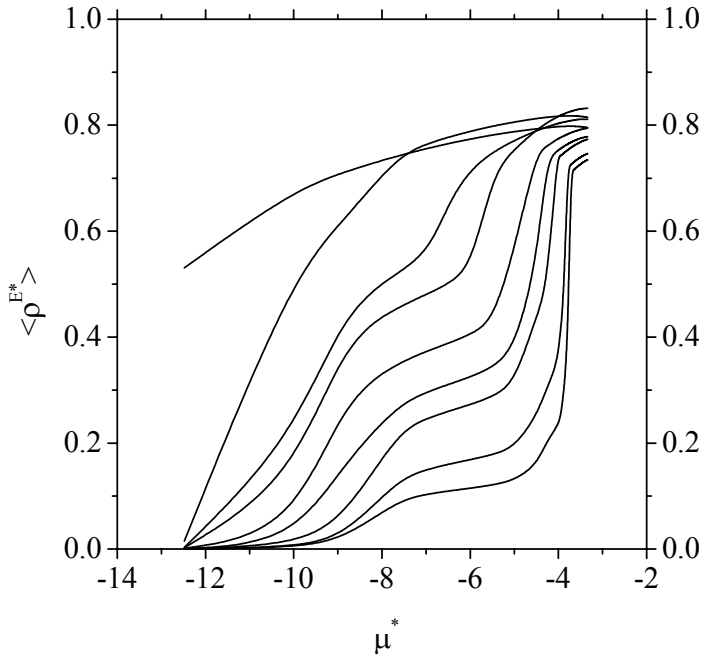

a)

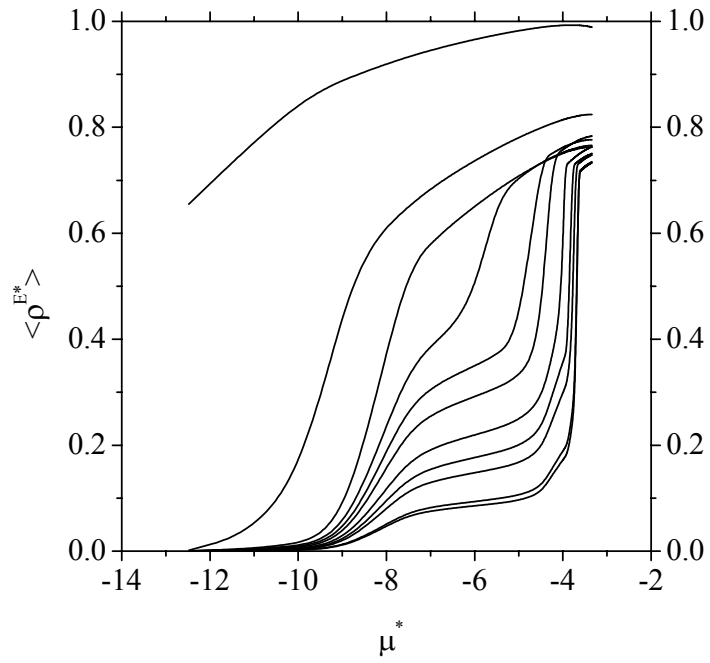

b)

Fig. 4.4. Adsorption isotherms of nitrogen at 77K on (a) cylindrical pores of the different diameters: H = 3.2, 4.0, 4.8, 5.6, 7.2, 8.8, 10.4, 16.0, and 17.6σ, (b) on slit-like pores of the different diameters: H = 1.6, 2.4, 3.2, 4.0, 4.8, 5.6, 7.2, 8.8, 10.4, 16.0, and 17.6σ, starting from left to right.

4.4.2 Adsorption isotherms reconstruction

As a first step on validating our method, we will use the individual adsorption isotherms obtained by FMT, weighted by the geometric PSD to predict the "experimental" adsorption isotherm of the four samples obtained by Gelb and Gubbins. A comparison between the predicted and the real isotherm will allow us to quantify the importance of considering the material made up of individual cylinders (or slit-like pores), assuming the same PSD, ignoring the interconnectivity of the real material.

Figure 4.5 shows these results for cylindrical pores. As it can be inferred from the figure, the reconstructed adsorption isotherm has the same shape as the "experimental" one, although the predicted adsorption is always higher, except for very low pressures, for the four materials considered. This discrepancy may have different causes:

- The model used to represent the individual isotherms and the method to obtain them may not be appropriate.
- The wall of the substrate may not be the same in both cases.
- We began the FMT calculations at pore diameters of 12Å, ignoring smaller pores.
- The material is not well represented by a collection of individual cylinders.

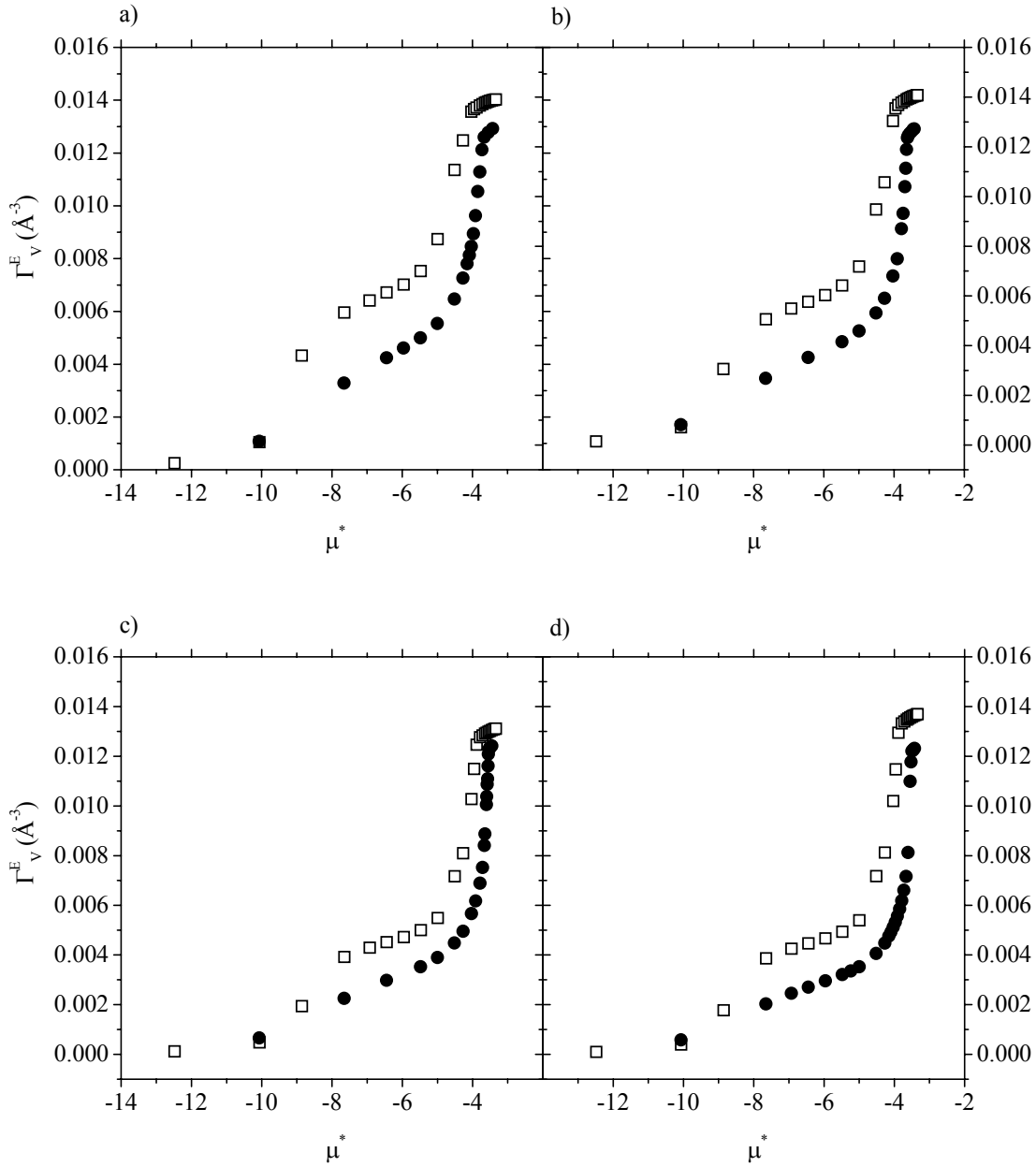

Fig. 4.5 Adsorption isotherms reconstructed using theoretical isotherms of cylindrical pores obtained with FMT calculations and weighted with the geometrical PSD's of Gelb and Gubbins [1999] (squares); compared with the "experimental" adsorption isotherms taken as well from the work of Gelb and Gubbins [1999] (circles) for the four different materials, A, B, C, and D (indicated by the correspondent label).

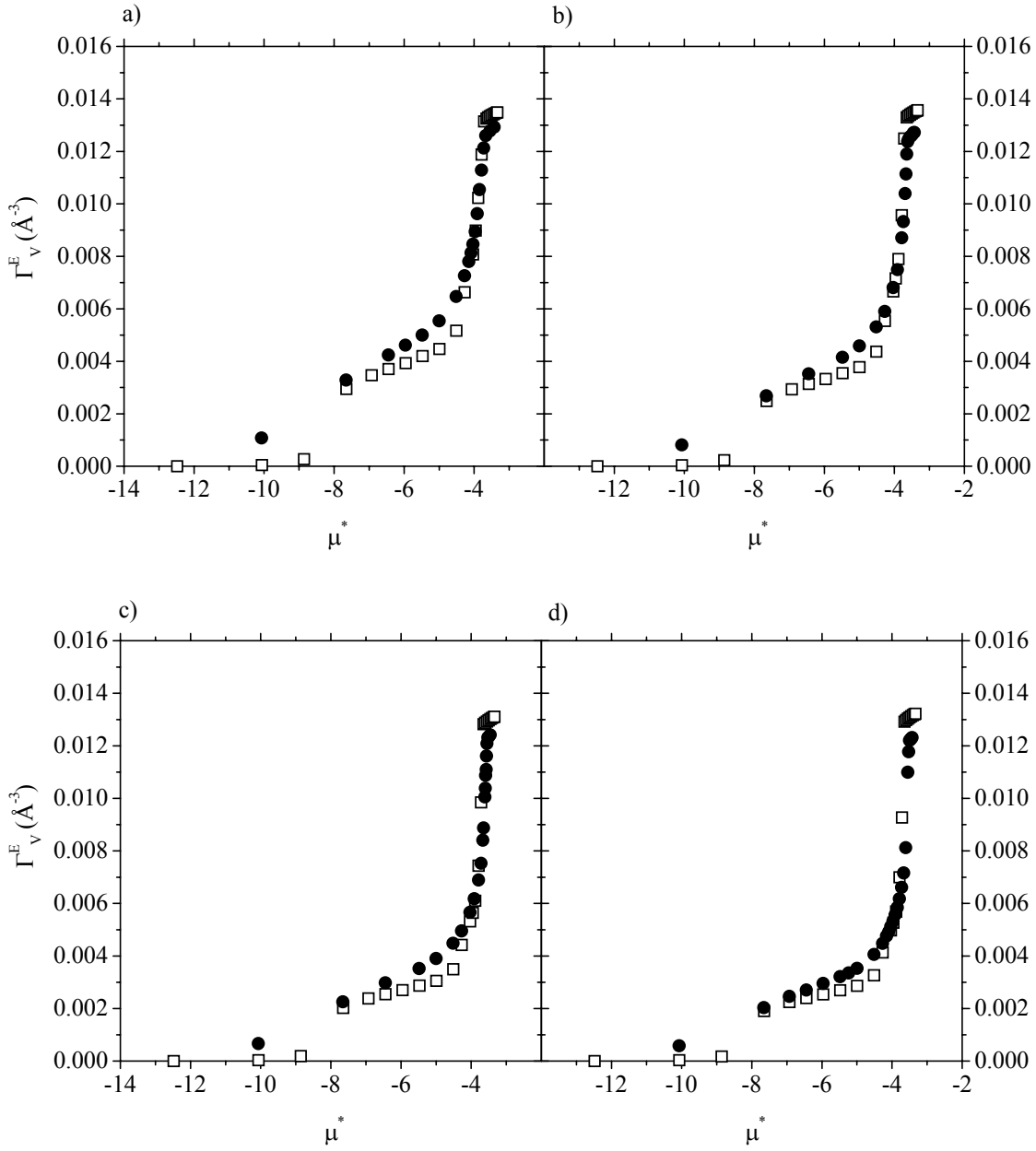

Fig. 4.6 Adsorption isotherms reconstructed using theoretical isotherms of slit-like pores obtained with FMT calculations and weighted with the geometrical PSD's of Gelb and Gubbins [1999] (squares); compared with the "experimental" adsorption isotherms taken as well from the work of Gelb and Gubbins [1999] (circles) for the four different materials, A, B, C, and D (indicated by the correspondent label).

Each of these points opens new possibilities, for instance, the last one may suggest that either the cylindrical geometry is not well chosen or that the interconnectivity among the pores is more important than what is usually assumed in this kind of modeling of adsorbent materials. A way to discern this point is to choose a different pore geometry and to proceed on the same manner, before further investigating the rest of the points presented here, trying to capture what are the essential facts that govern the PSD of these materials.

In figure 4.6 we show results equivalent to figure 4.5, but using a lineal combination of the individual isotherms of slit-like pores. It is clear that in this case the overall agreement between the reconstructed isotherms and the "experimental" ones improves in the four cases considered, showing that CPG are better represented by a collection of individual slit-like pores, rather than cylindrical pores. However, there are some discrepancies at low pressures (low chemical potentials), the adsorption predicted by the planar geometry is much lower than the experimental one, while this was the region well predicted for the cylindrical geometry (see figure 4.5). At intermediate pressures, the adsorption in planar pores is still lower, with the inflection of the curve more pronounced than the experimental one. This last point may be due to the fact that we did not include enough individual adsorption isotherms in this range of pore sizes, which would smooth this change. Finally, at high pressures, where the capillary condensation occurs in the wider pores, and the narrower ones are saturated, the material modeled as a collection of planar pores slightly over-predicts the adsorption. The behavior explained is common to the four materials used.

To further investigate what is the influence in the overall isotherm of including smaller pores in the analysis, we have reconstructed the isotherm as in figure 4.6, but using two smaller slit-like pores, H = 6 and 9 Å, and results are presented in figure 4.7. This can not be done in our case for the cylindrical pores, as explained before. A comparison of figures 4.6 and 4.7 shows a better agreement at intermediate pressures, but the agreement deteriorates at higher pressures. Since their relative weight in the PSD is very small, and considering that the predictions do not considerably improve, we decide that it is not essential to include these two small pores for characterization studies of these materials. However, since we had calculated them, they have been used in the calculations presented in the next section.

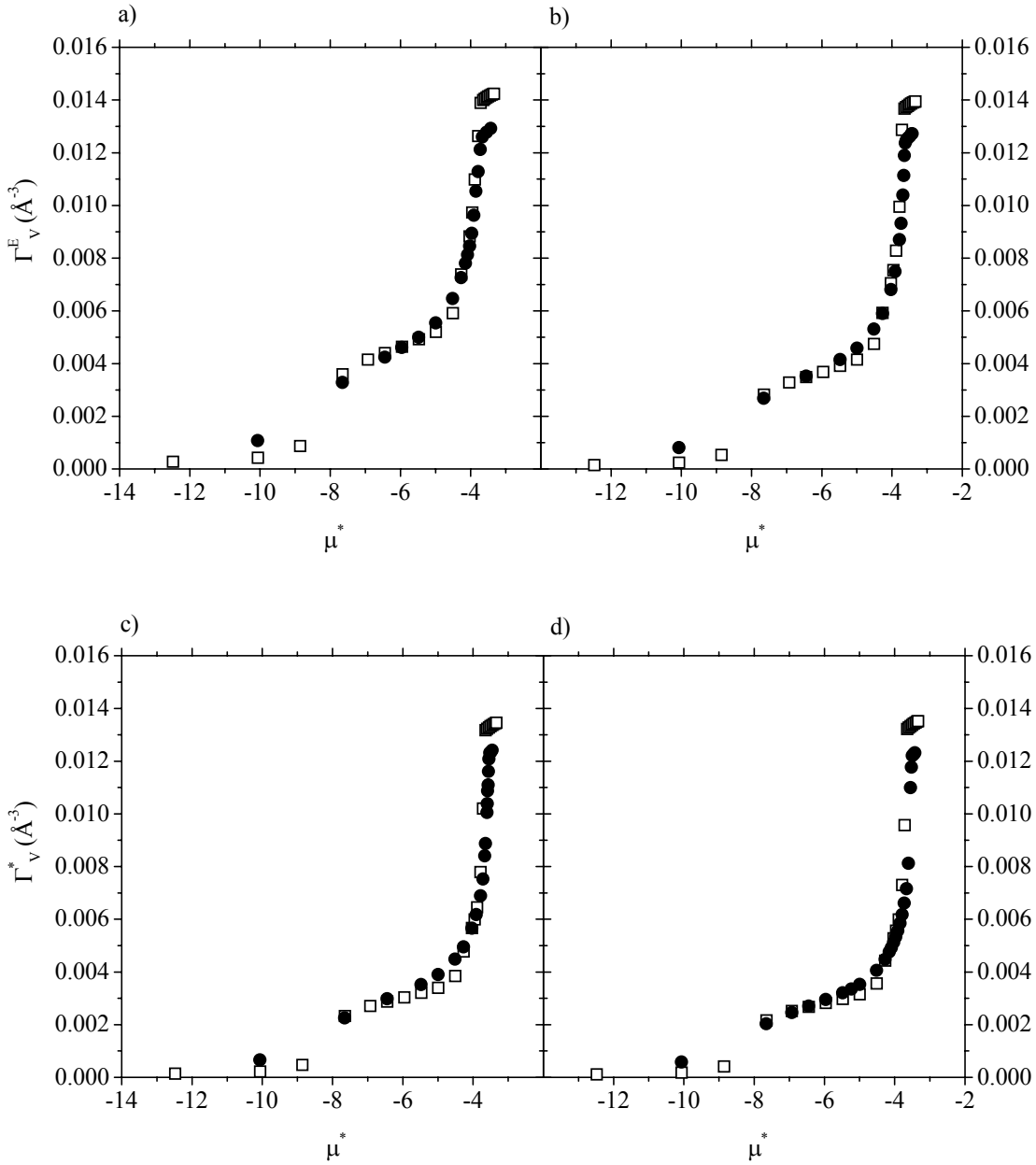

Fig. 4.7. Adsorption isotherms reconstructed using theoretical isotherms of slit-like pores obtained with FMT calculations and weighted with the geometrical PSD's of Gelb and Gubbins [1999] (squares) using 16 different pore sizes; compared with the "experimental" adsorption isotherms taken as well from the work of Gelb and Gubbins [1999] (circles) for the four different materials, A, B, C, and D (indicated by the correspondent label).

There are two more points that we have stressed and we would like to further investigate before proceeding to the inversion of the integral: the importance of the model used for the fluid, and for the substrate. To investigate the effect of the model fluid, we have chosen a vapor-liquid equilibrium point of the phase diagram of nitrogen, at 77K, and fitted σ and ε using the SPT equation of state, to reproduce the same vapor and liquid density, and the same vapor pressure as the fluid modeled by Gelb and Gubbins [1998, 1999]. The results are shown in table 4.1. In figure 4.8 we analyze the effect of choosing different fluid-fluid parameters for the bulk fluid for material A. As it can be expected, no significant changes are appreciated at low pressures, where the adsorption is dominated by the solid-fluid interactions, while changes are important at high pressures, where the fluid-fluid interaction is dominant, giving a higher adsorption than that obtained by Gelb and Gubbins for the "experimental" material. From the individual analysis of each pore (not shown here) we see that the use of different fluid-fluid parameters is more important for the case of the small pores, while it becomes less relevant as the pore size is increased. From this part we conclude that to choose a different set of molecular parameters to exactly reproduce the vapor-liquid equilibria of the bulk fluid at 77K is not particularly relevant.

Saturation pressure	0.01477	
Density of saturated liquid	0.726	
Parameter	**Fluid-fluid**	**Solid-fluid**
σ (Å)	3.64	3.17
ε/k_B (K)	88.90	142.99

Table 4.1. Values of the pressure and density of the saturated liquid nitrogen in reduced units, and the molecular interaction parameters fitted with the SPT equation of state.

Finally, in figure 4.9 we present the individual adsorption isotherm of a planar pore of H= 33Å for two different values of the solid-fluid interaction parameter, ε_{sf}, the one used in all the calculations presented here, and a second one corresponding to a more attractive wall. As expected, the adsorption is much stronger at low pressures for the second parameter, since the solid-fluid interactions are dominant in this region, and it is slightly higher in the rest of the isotherm. However, since the fluid-fluid interaction parameters are the same, the capillary condensation occurs at the same pressure. This may indicate that the model walls we are using here are slightly less adsorbent than the model of Gelb and Gubbins [1999].

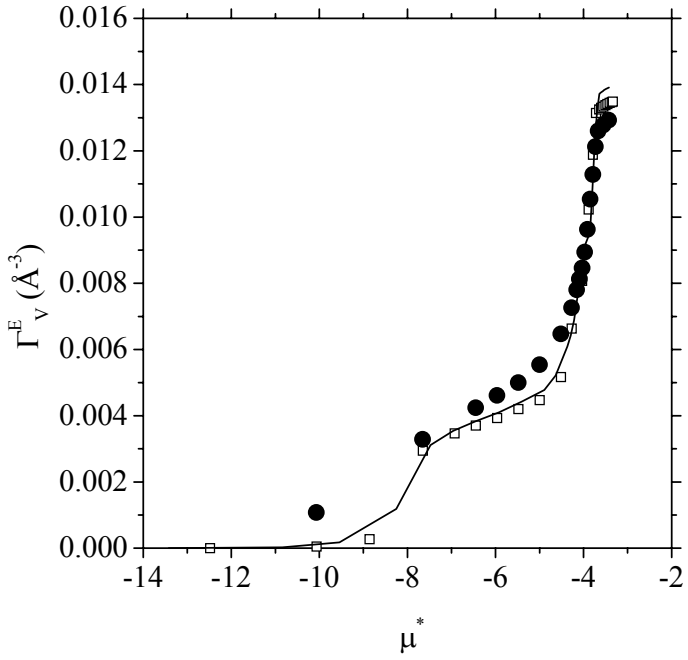

Fig. 4.8. Adsorption isotherms reconstructed using theoretical isotherms of slit-like pores obtained with FMT calculations for two different sets of molecular interaction parameters (squares and solid line), using 14 different pore sizes weighted with the geometrical PSD's of Gelb and Gubbins [1999]; compared with the "experimental" adsorption isotherm taken from Gelb and Gubbins [1999] (circles) for material A.

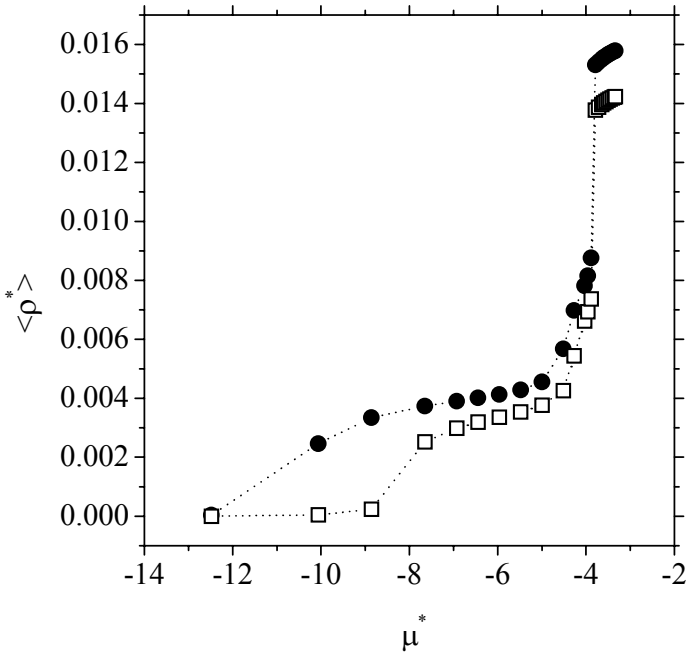

Fig. 4.9. Adsorption isotherms of nitrogen at 77K on a slit-like pore of H=33Å calculated with $\varepsilon_{sf}^* = 2.0$ (circles), and with $\varepsilon_{sf}^* = 1.55$ (squares).

To summarize this part: we can conclude that the individual pore model may be appropriate for CPG, if the appropriate pore geometry and molecular parameters are chosen. We have observed that the adsorption isotherms obtained by weighting individual isotherms with the geometrical PSD of the material are in better agreement with the overall isotherm of the material when using slit-like pores, instead of cylindrical pores, as a unique geometry. The particular choice of the fluid-fluid and solid-fluid interaction parameters is less important than the previous point. Once we have checked that the molecular parameters are accurate and that the individual pore model is adequate for these materials, we proceed to obtain the PSD's of these materials by inversion of the adsorption integral.

4.4.3 PSD by inversion of the adsorption integral equation

To validate our programs, we have fed in equation 4.7 the adsorption isotherms reconstructed in the previous section, instead of the "experimental" adsorption isotherm. The parameter values used in these calculations, the areas under the curves and the deviation between the fitted isotherms and the "experimental" ones are presented in table 4.2. Results for cylinders are shown in figure 4.10(a), while figure (b) shows the results for the case of slit-like pores. As observed in both figures, the PSD ($f(H)$ in equation 4.7) obtained is indistinguishable from the geometrical of Gelb and Gubbins. Since we recover the same results we can conclude that our mathematical procedure and computer codes to invert the integral are correct. The very small values of λ_R of table 4.2 are an indicative that in this case it is not necessary any smoothness parameter.

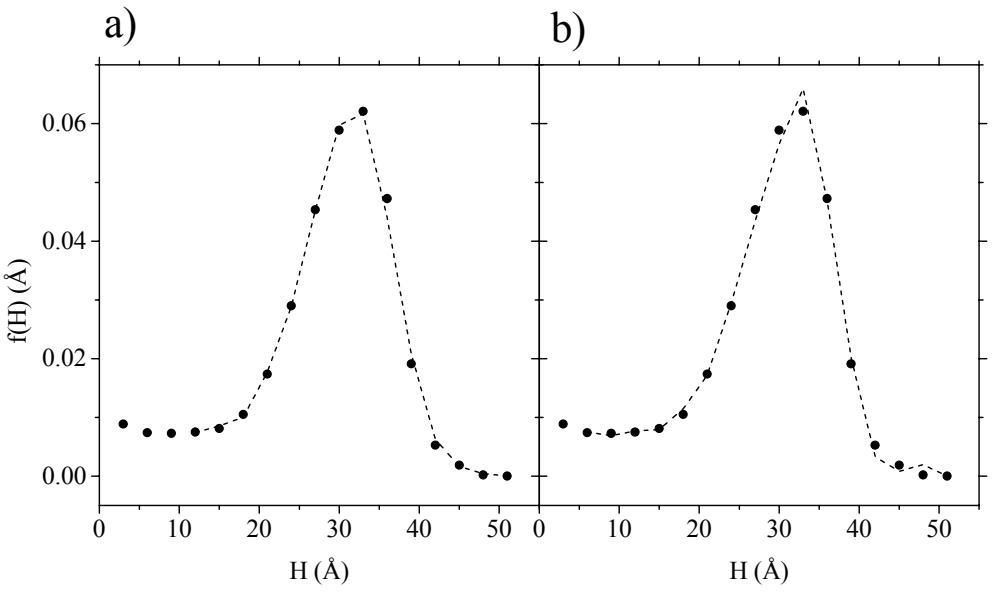

Fig. 4.10. PSD's (dashed lines) obtained from the inversion of equation 4.7 using the theoretical isotherms for the case a) the set of isotherms on cylinders from Fig. 4.4(a); and b) the set of isotherms on slit-like pores from Fig. 4.4(b). The symbols correspond to the geometrical distribution from the work of Gelb and Gubbins [1999] of sample A.

We have also checked the porosity value used in our calculations. The porosity value can be obtained by using $\mathcal{P} = 1$ when normalizing equation 4.7, *i.e.*, it is fulfilled that $\mathcal{P}\int f(H)dH = 1.0$. Following this procedure we have obtained a value very close to 30%, the same reported by Gelb and Gubbins [1999].

Once we have validated our method, we have inverted the adsorption integral equation considering both geometries, cylindrical and planar. The results obtained are compared to those obtained by Gelb and Gubbins with the BJH method, and with the geometrical one. It should be noticed that Gelb and Gubbins used just the adsorption branch of the isotherms, since the desorption branches obtained by simulation where very sharp, leading to PSD with non-physical sense.

Figure 4.11 shows the PSD's obtained by minimizing equation 4.7 for each of the four materials using adsorption isotherms for cylindrical pores. The parameters used and the area under the curve of each curve can see in table 4.3). The resulting isotherms from the fitting are compared to the "experimental" isotherms in figure 4.12. The percentages of deviations for each one of the fittings are also given in table 4.3. It is observed that the distributions obtained by inversion of the integral show, in general, a better agreement with the geometrical distributions that the ones calculated with the BJH method. The locus of the peak is at the same pore size, except for material B, and they all are unimodal. On the contrary, the BJH distributions show a maximum systematically located at smaller pores than the actual one, and there are not unimodal for materials A, B, C, showing more than one peak. The discrepancies between the BJH and the geometrical PSD were attributed to several factors [Gelb and Gubbins, 1999]. One of them is that the BJH method follows the Kelvin equation, which is known to underestimate the real values, especially for small pores [Gregg & Sing, 1982; Lastoskie *et al*., 1993a and b]. Besides, an additional source of error may comes from the use of the reference standard isotherm, it has been shown in a previous study [Gelb and Gubbins, 1998] that the surface adsorption in very narrow pores is systematically higher than for a planar surface of identical characteristics. Finally, since the pores of these materials have an irregular geometry, a quantitative agreement should not be expected.

System	Number of theoretical isotherms employed	Number of points of the experimental isotherm	Number of interpolated points of the experimental isotherm	γ_R	Area under the curve	% of deviation between the isotherms
A with cylinders	14	23	23	0.00001	0.94	0.023
A with slit-like pores	16	23	23	0.0000001	0.981	0.010

Table 4.2. Parameters and results from the fitted of Fig. 4.10. γ_R is the regularization parameter.

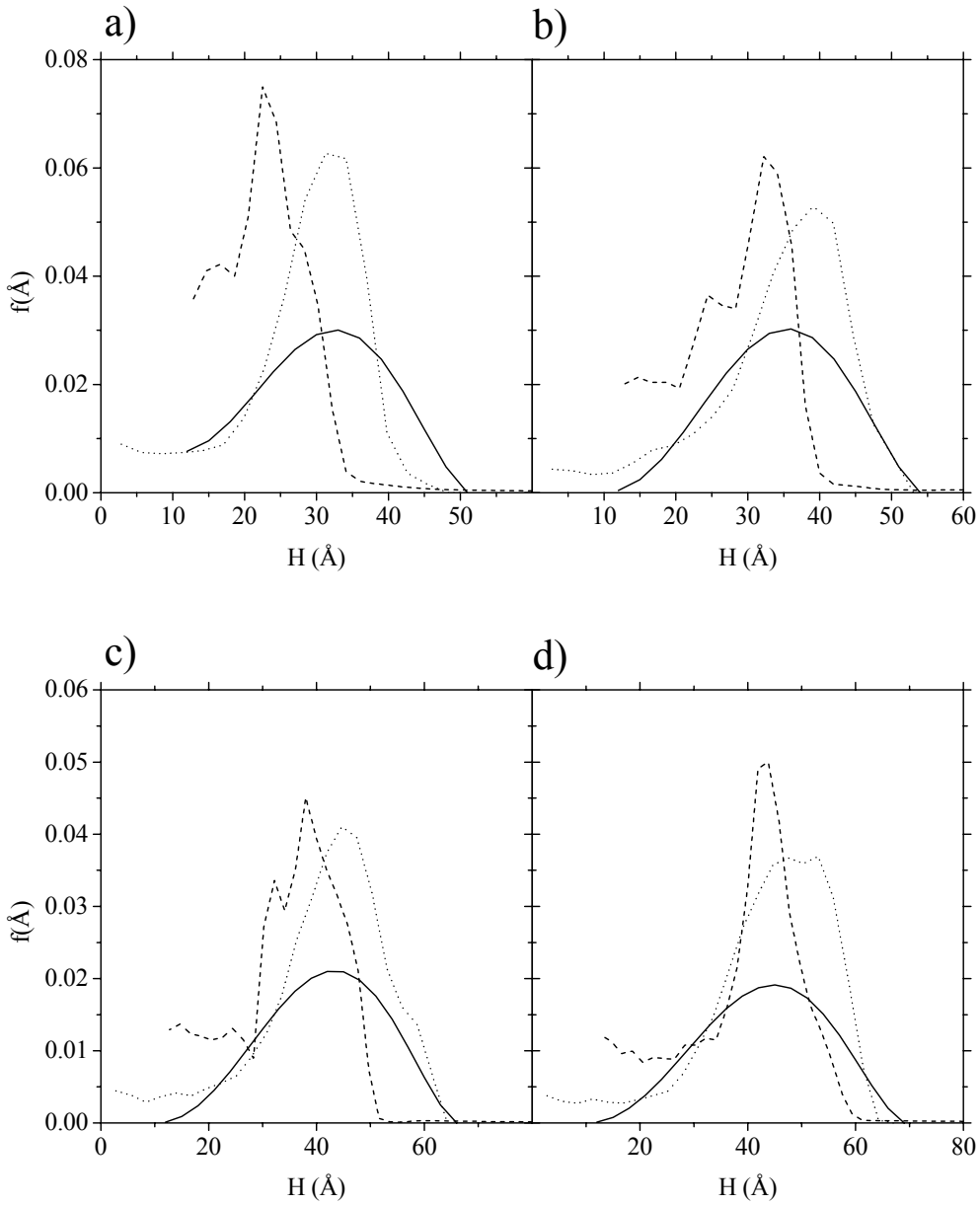

Fig. 4.11 PSD's obtained (solid line) in this work using cylindrical pores compared with geometrical PSD's (dotted line), and with BJH PSD's (dashed lines) from literature [Gelb and Gubbins, 1999] for each of the four systems A, B, C, and D (indicated with the corresponding label).

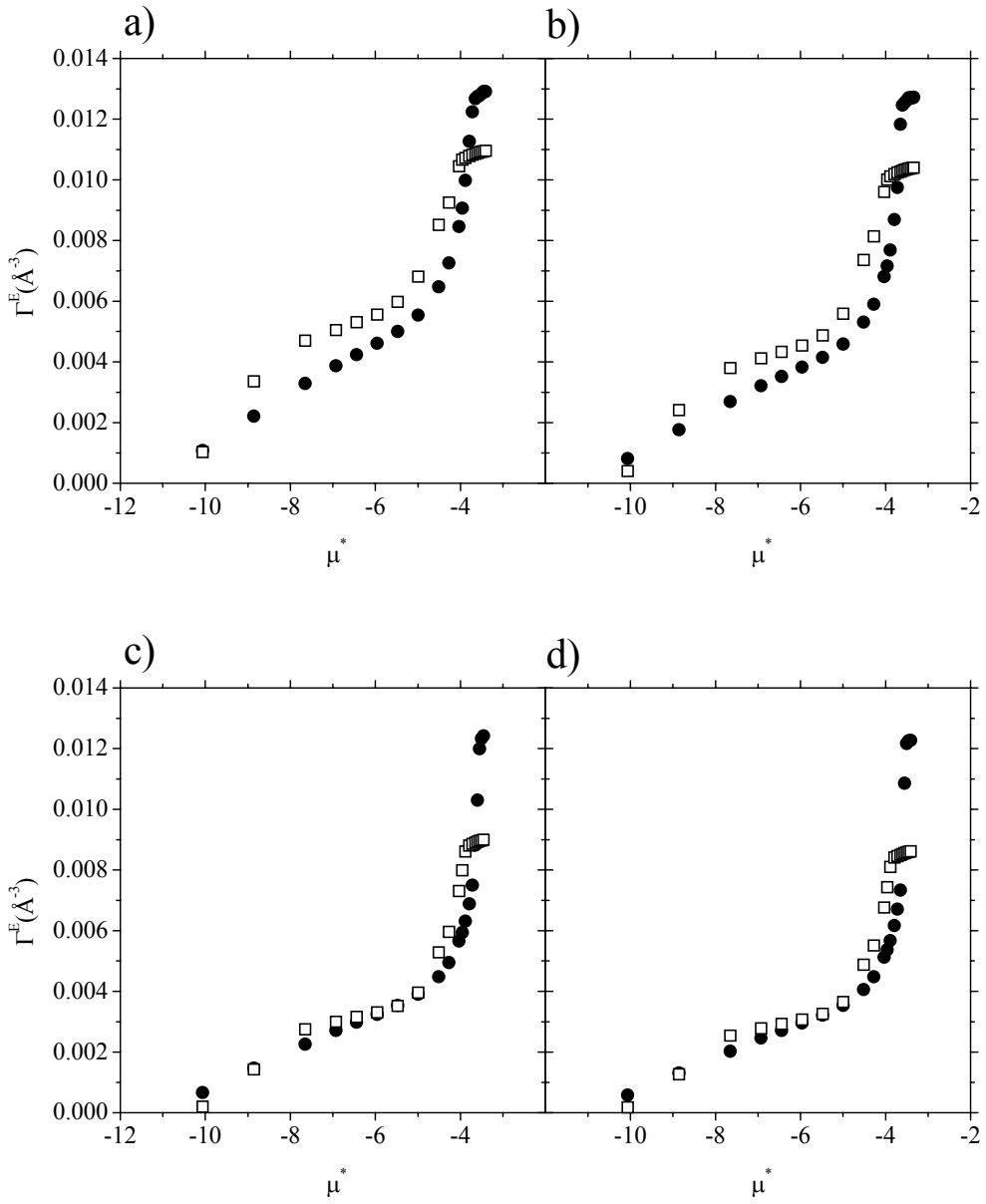

Fig. 4.12 Adsorption isotherms obtained (squares) in this work using cylindrical pores to resolve Eq. 4.7, compared with "experimental" isotherms (circles) from literature [Gelb and Gubbins, 1999] for each of the four systems A, B, C, and D (indicated with the corresponding label).

The values of λ_R in these cases (table 4.3) show that the sets of data are not very good and it is necessary to use the smoothness parameter. This fact could be probably solved, from the FMT part, by using a higher number of pore sizes and by refining the chemical potential values used in calculating the adsorption isotherms. We have also tried to interpolate each isotherm with a spline method, but at low chemical potentials the adsorption gives unphysical results, *i.e*. negative values.

We observe in figure 4.12 that the fitted adsorption isotherms of materials A and B are above the "experimental" adsorption isotherms of the material at low pressures, while there are under the experimental isotherm for the high pressure region, reaching a lower

saturation level. For materials C and D, we observe an excellent agreement between fitted and real isotherms, at low pressures, while the agreement clearly deteriorates at high pressures. Since we have already seen that the independent pore model applies for these materials, and we are doing a fitting, which effectively should screen the discrepancies between the real system and the collection of pores, in principle, the agreement should be better than what we obtain here. Hence, we can conclude that the discrepancies may come from the fact that the cylindrical geometry is not the most appropriate for these materials.

System	Number of theoretical isotherms employed	Number of points of the experimental isotherm	Number of interpolated points of the experimental isotherm	γ_R	Area under the curve	% of deviation between the isotherms
A	14	19	21	10	0.73	20.52
B	15	20	23	10	0.70	25.50
C	19	22	20	15	0.62	19.70
D	20	26	21	25	0.59	22.50

Table 4.3. Parameters and results from the fitted of Figs. 4.11 and 4.12 using cylindrical pores. γ_R is the regularization parameter.

The PSD obtained by inverting equation 4.7 using the adsorption in slit-like pores is shown in figure 4.13, for the four materials considered, and the parameters used, the area under the curve, and the percentages of deviation are given in table 4.4. It is observed a clear improvement in the location of the peaks, in all cases, and a better agreement with the extremes of the distributions. It should be noted that, as mentioned already, for the case of planar geometry, there are two additional narrow pores in this case, not included for cylinders. However, by looking at the results we can conclude that the addition of narrower pores into the analysis of the PSD with cylindrical pores would not improve the results, since the adsorption in narrow cylindrical pores is very high at low pressures, rapidly reaching saturation at higher pressures. To improve the agreement of the isotherms in figure 4.12 we would need more adsorption at high pressures, but a decrease of the adsorption at low pressures. For the case of planar geometry, the problem is that the obtained distributions are wider than the geometrical ones. This decreases the weight of the intermediate pores to the total isotherm, decreasing the adsorption in the high-pressure region, especially for materials C and D. As observed in figure 4.14, the overall agreement between the adsorption isotherms is excellent for the four materials studied, for the case of the slit-like pores. As a conclusion we can say that the planar pore model seems to be the appropriate model for materials A and B, describing almost quantitatively their behavior, and it seems to be very satisfactory for materials C and D. The small values of the regularization parameter show a better adequacy of the model in this case *versus* the cylindrical case. Moreover, in the first two systems (A and B), which fitted better than the two others (C and D) the value of λ_R gives the same importance to the smoothness term respect to the adsorption term (see Eq. 4.7).

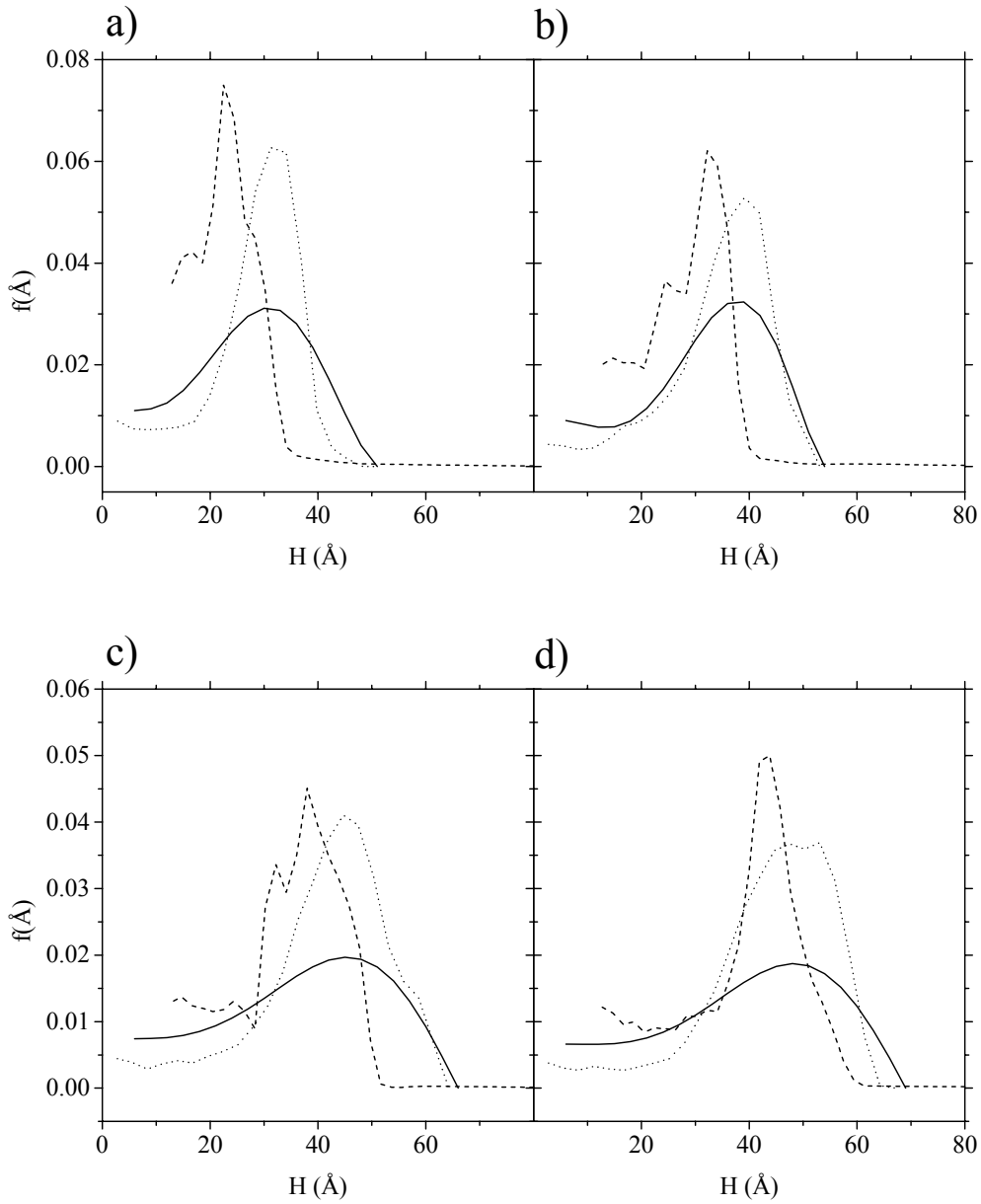

Fig. 4.13. PSD's obtained (solid line) in this work using slit-like pores compared with geometrical PSD's (dotted line), and with BJH PSD's (dashed lines) from literature [Gelb and Gubbins, 1999] for each of the four systems A, B, C, and D (indicated with the corresponding label).

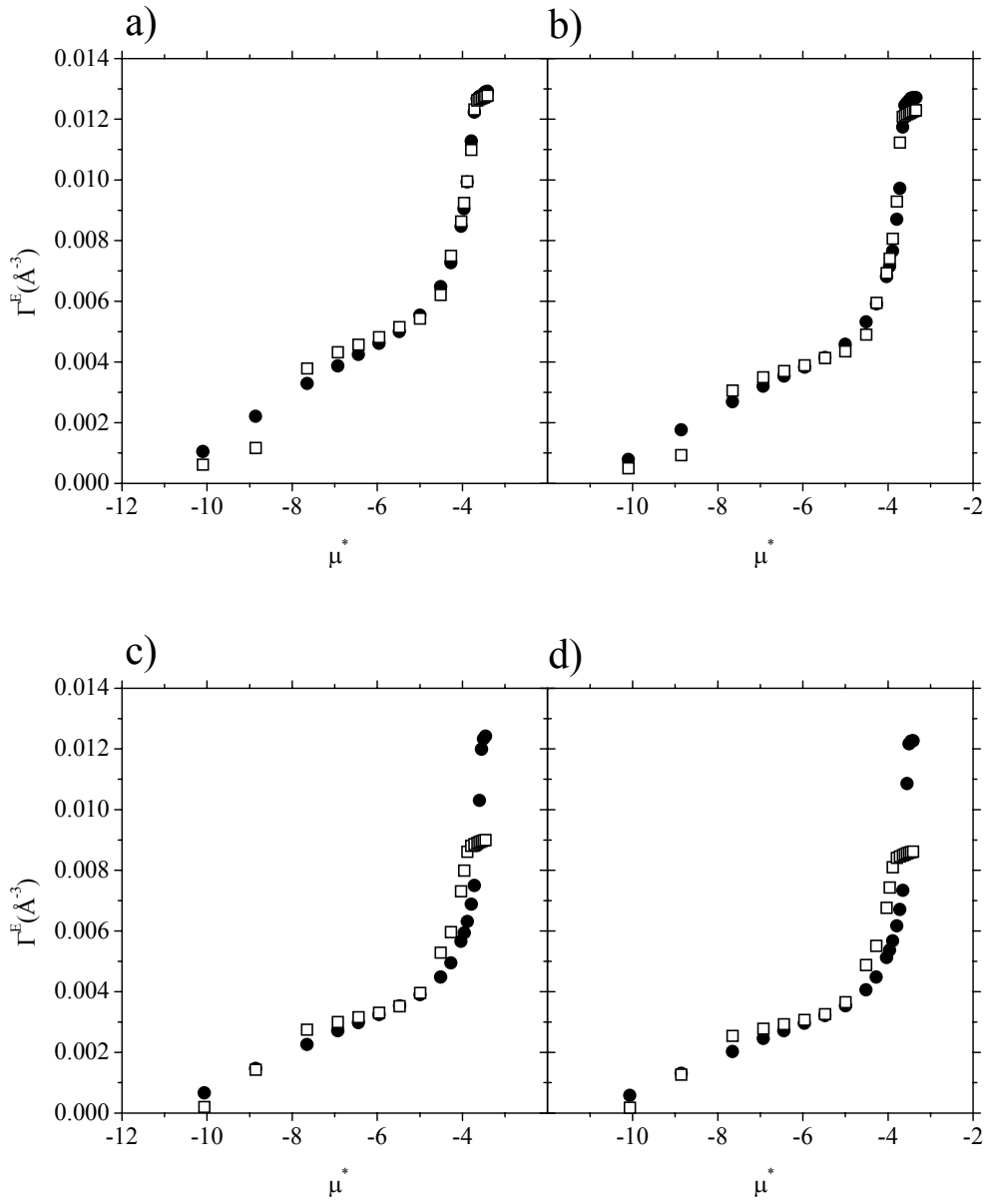

Fig. 4.14 Adsorption isotherms obtained (squares) in this work using slit-like pores to resolve Eq. 4.7, compared with "experimental" isotherms (circles) from literature [Gelb and Gubbins, 1999] for each of the four systems A, B, C, and D (indicated with the corresponding label).

Mean field and fluid-fluid interaction

Finally, as we have seen in chapter 3 of this memory, one of the main differences between the theoretical and the simulation approaches we have used is that there are some mean field approximations made in the theory when calculating adsorption isotherms. We have checked the importance of these approximations here and results are presented in figure 4.15, for a cylindrical pore of diameter H = 66 Å. As it is observed in the figure, the main difference comes from the inability of the theory to accurately predict the correct pore filling pressure (*c.a.* μ^* = -4.0), giving a smoother capillary condensation, and at lower chemical potentials. Another difference, less noticeable than the previous one, is the behavior at high pressures, once the capillary

condensation has taken place. In this case it is observed that the adsorption obtained in simulations is lower than that predicted by the theory. This can be explained by the fact that this is the region were the fluid-fluid interactions are dominant, and we are using the same set of parameters in both approaches (see table 3.1), when actually each model follows a different equation of state in the bulk.

System	Number of theoretical isotherms employed	Number of points of the experimental isotherm	Number of interpolated points of the experimental isotherm	γ_R	Area under the curve	% of deviation between the isotherms
A	16	19	21	1	0.88	7.24
B	17	20	23	1	0.85	8.09
C	21	22	20	10	0.77	10.75
D	22	26	21	10	0.73	12.74

Table 4.4. Parameters and results from the fitted of Figs. 4.13 and 4.14 using slit-like pores. γ_R is the regularization parameter.

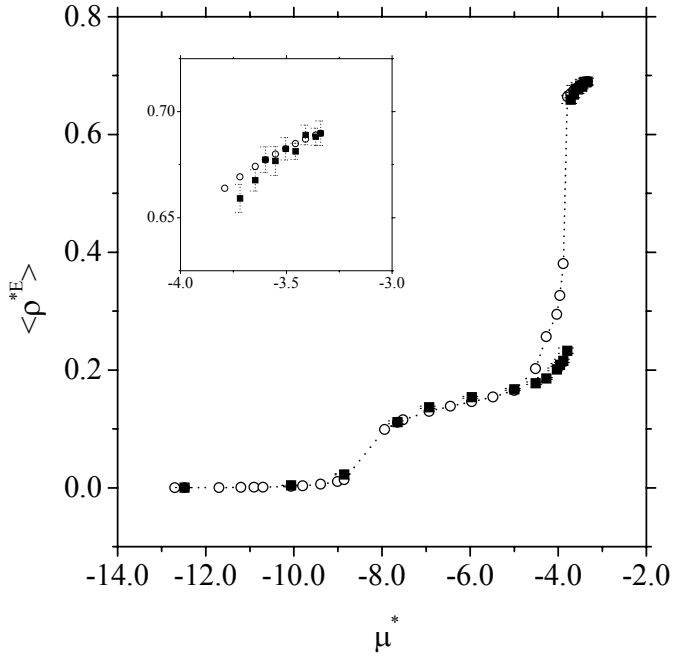

Fig. 4.15 Adsorption isotherms (circles) obtained in this work using FMT calculations and (squares) by GCMC simulations for a cylindrical pore of diameter H = 66Å.

4.5 Conclusions

In this chapter we have applied the FMT approach in conjunction with a regularization method to estimate the PSD of model porous glasses. We have chosen this particular

material because it was developed with molecular modeling techniques, and a direct comparison can be made with the theory used here. An additional advantage of these model materials, *versus* experimental ones, is that in this case the size and shape of the pores is well known, as well as the position of the atoms in the surface, making it a perfect material to check the accuracy of the theoretical characterization methods available.

Since there are several solutions of the adsorption integral equation compatible with the experimental adsorption isotherm, and several factors can hide defects of the molecular model, we have done the characterization in a systematic manner: we have first checked the accuracy of the FMT and the independent pore model for predicting the "experimental" adsorption isotherms using the geometrical PSD already known for the materials. This has been done with individual cylindrical and slit-like pores. Secondly, once the adsorption isotherm was successfully reconstructed, we inverted the integral adsorption isotherm with a regularization procedure. The accuracy of the inversion method has also been checked before estimating the PSD's of the different materials. Finally, once the method was proved to be correct, we used it to estimate the PSD's of four materials, and to predict the experimental adsorption isotherms. We have also studied the influence of choosing some particular molecular parameters for the fluid-fluid and the solid-fluid interaction in the adsorption behavior of these systems.

We have obtained that the independent pore model is adequate for the four materials investigated here. The slit-like geometry seems to represent the overall adsorption behavior better than the cylindrical geometry.

As far as the PSD obtained with our procedure is concerned, it is observed that the distributions obtained by inversion of the integral are in better agreement with the geometrical distributions than the ones calculated with the BJH method. The locus of the peak is at the same pore size, and all of them are unimodal, while the BJH distributions show a maximum systematically located at smaller pores, underestimating the PSD's of the material, and there are not unimodal.

Regarding the geometry of the individual pores making up the material, we can say that, although the PSD are broader than the geometrical ones, the adsorption predicted by a collection of individual slit-like pores is in almost quantitative agreement with the "experimental" adsorption isotherm. Hence as a conclusion, the individual pore model, and the planar geometry are appropriate to characterize these materials using DFT techniques, and they can be used with confidence to predict their adsorption behavior, a matter of future work.

4.6 References

Allen, M. P.; Tildesley, D. J. *"Computer simulation of liquids"* (Clarendon Press, Oxford, 1987), Chap. 4, p.110.

Barrett, E. P.; Joyner, L. G.; Halenda, P. P. *J. Am. Chem. Soc*. **73**, 373 (1951).

Connolly, M. L. *J. Appl. Crystallogr*. **16**, 548 (1983).

Elmer, T. H. In *"ASM Engineered Materials Handbook"*, edited by Schnieder, S. J., Jr. (ASM: Materials Park, OH), **4**, 427 (1991).

Gelb, L: D.; Gubbins, K. E. *Langmuir* **14**, 2097 (1998).

Gelb, L. D.; Gubbins, K. E. *Langmuir* **15**, 305 (1999).

Gregg, S. J.; Sing, K. S. W. *"Adsorption, surface area and porosity"*, 2nd edition (Academic Press Inc., London, 1982).

Haller, W. *Nature* **206**, 693 (1965).

Haller, W. In *"Solid Phase Biochemistry; Scouten"*, edited by W. H. (John Wiley and Sons, New York, 1983), p.535.

Kanda, H.; Miyahara, M.; Higashitani, K. *Langmuir* **16**, 6064 (2000).

Lastoskie, C.; Gubbins, K. E.; Quirke, N. *Langmuir* **9**, 2693 (1993a).

Lastoskie, C.; Gubbins, K. E.; Quirke, N. *J. Phys. Chem.* **97**, 4786 (1993b).

Levitz, P; Ehret, G.; Sinha, S. K.; Drake, J. M. *J. Chem. Phys*. **95**, 6151 (1991).

Miyahara, M.; Kanda, H.; Yoshioka, T.; Okazaki, M. *Langmuir* **16**, 4293 (2000).

Pfeifer, P.; Johnston, G. P.; Deshpande, R.; Smith, D. M.; Hurd, A. J. *Langmuir* **7**, 2833 (1991).

Press, W. H.; Teukolsky, S. A.; Vetterling, W. T.; Flannery, B. P. *"Numerical recipes in Fortran"*, 2nd edition (Cambridge University Press, U.S.A., 1992), Chap. 6, p.263.

Ravikovitch, P. I.; Vishnyakov, A.; Russo, R.; Neimark, A. V. *Langmuir* **16**, 2311 (2000).

Schnabel, R.; Langer, P. *J. Chromatogr*. **544**, 137 (1991).

Yoshioka, T.; Miyahara, M.; Okazaki, M. *J. Chem. Eng. Jpn.* **30**, 274 (1997).

5. PORE-SIZE DISTRIBUTION OF γ-ALUMINA

5.1 Introduction

Density functional theory has been applied with remarkable success to model well-crystalline materials such as zeolites [Cracknell and Gubbins, 1993; Cracknell *et al*., 1995], or such as porous glasses as we have done in chapter 4. This technique has also been applied to amorphous materials such as carbons, with good results for sorbents where the PSD is not very disperse [Lastoskie *et al*., 1993]. However, there is not a systematic study available at present to characterize alumina from a molecular perspective. This may be due to the fact that alumina is a quite amorphous material, with a wide distribution of pore sizes and shapes, and some surface heterogeneities. The material obtained in the laboratory strongly depends on the conditions present in the process of fabrication, and in some cases it is hard to reproduce exactly the same material [Cesteros *et al.*, 1999]. Additionally, this material is very attractive for practical applications, since it is abundant in nature, it has a relative low cost, and it can be used as an adsorbent for separation processes, as a catalyst and for the fabrication of membranes.

A way to check the accuracy of our approach in estimating PSD is to apply it to the same material modified in a systematic way. In this sense, it is interesting to analyze the effect in pore sizes when the γ-alumina is calcined. In general, when some adsorbent materials are heated, *i.e*. for a period of a few hours, at elevated temperature, they undergo sintering. Their specific surface diminishes, at lower temperatures probably by more complete adhesion between the particles, at higher temperatures by actual growth of the large particles at the expense of the smaller; the PSD changes concomitantly, though in some systems the total pore volume may change but little over a wide range of temperature [Gregg and Sing, 1978].

γ-alumina, one of the transition aluminas (Al_2O_3), is widely used as a catalyst and as an adsorbent [Gates, 1992; Tanabe *et al*., 1989]. Transition aluminas are metastable solids formed from $Al(OH)_3$ when it is heated through temperatures of some hundreds of Celsius degrees. As the solid is heated in air, it is decomposed into an oxide with a micropore structure and a high surface area of some hundreds of square meters per gram. Raising the temperature to about 1,100K leads to further transformation of the solid, with changes in structure of the primary particles and collapse of the pore structure, leading to the loss of almost all of the internal surface area, and ultimately giving the stable, extremely hard, crystalline γ-Al_2O_3 (corundum). The dimensions of the micropores are determined by the packing of the primary particles (crystallites); the micropores and some mesopores are the void spaces between those particles and have

dimensions of the order of 10-100 Å. The dimensions of the macropores are related to the dimension of agglomerates of crystallites [Ruthven, 1984; Suzuki, 1990; Gates, 1992; Tanabe *et al.*, 1989].

Despite the widespread interest in adsorption and catalytic applications of aluminas, and the great influence of their surface structure on these properties, there is still only a limited understanding about the real nature of the material. The alumina surface is certainly extremely complicated. There are several experimental, theoretical and molecular simulation studies attempting to explain the structure of alumina [Lippens, 1961; Peri, 1965; Knozinger and Ratnasamy, 1978; Alvarez *et al*., 1992; 1993; 1994; Vijay *et al*, 2002; Ionescu *et al*., 2002]. Most of these studies concentrate on finding the most stable structure, as well as the face shown, and they conclude that the preferentially exposed faces are (100) and (110). Vijay *et al*. [2002] have studied the occurrence of (001) surface of γ-alumina. The structure of the surface may affect the catalytic properties of alumina and its properties as a support. Lippens [1961] did extensive studies in crystallographic structures of several aluminas. His main conclusions are that Al_2O_3 occurs in various crystallographic forms, of which the η- and γ-phases are the most important ones. The oxygen ions are built up by layers of cubic close-packed stacking, with the aluminum ions arranged in octahedral and tetrahedral sites between oxygen ions.

Recently, Blas *et al*. [1998] have proposed a molecular model from simplified intermolecular potentials, that successfully describes the adsorption properties of pure ethane and ethylene on γ-alumina and CuCl-γ-alumina found experimentally by Yang *et al*. [1995; 1996]. The porous solid is described as a single cylindrical pore, with a diameter of the pore and the solid-fluid energy interaction parameter fitted to experimental available data, while the fluids are modeled using optimized potentials for liquid simulations (OPLS) parameters [Jorgensen *et al*., 1984]. This model gives good agreement with the experimental data, except at extreme conditions. For the case of bare alumina, the adsorption of ethane is underestimated at low pressures, and for alumina activated with CuCl the adsorption of ethylene is underestimated at the higher pressures studied, showing a plateau while the experimental adsorption of this substance continuously grows with pressure. The discrepancies between the model and the experiments are mainly attributed to the fact that this material is polydisperse. Additionally, it is important to note that, although, the results were very good in the case of a very simple model, the pore diameter size and the solid-fluid interaction energy were fitted and their physical values are not realistic.

In this chapter we present a PSD analysis for the interpretation of nitrogen adsorption isotherms on γ-alumina, as well as the experimental results needed for the analysis. The study is done with the independent pore model previously used for porous glasses (chapter 4). This model is based on the idea that the real alumina can be treated as an "effective porous material", in which all of the heterogeneity of the real material is approximated by a distribution of pore sizes. Hence, the interconnectivities among the pores, the different possible pore geometries and the heterogeneity of the real surfaces are not explicitly considered. With the PSD's obtained we investigate the sintering effect when alumina is calcined. The independent pore model analysis requires the

determination of a large amount of adsorption isotherms at different pressures and pore sizes, in order to evaluate the PSD's of the studied material. We have used FMT to fit the experimental adsorption isotherm of nitrogen on γ-alumina at temperature T = 77.35K. With the aim to test the predictive capability of the PSD, we present GCMC simulation results in the same material (untreated alumina) of ethane at 333.15K compared with experimental results from literature [Yang *et al*., 1995; 1996].

The remainder of this chapter is organized as follows. In the next section we present the experimental details and the isotherms measured, followed by the presentation of molecular model used to describe the nitrogen, the ethane molecules, and the γ-alumina. In section 5.4, we present the results and discussion of the PSD's and sintering effect in the same. In section 5.5 the application of PSD to adsorption of ethane on alumina is exposed, and finally, a summary of results and main conclusions obtained from this work are given in section 5.6.

5.2 Experimental adsorption isotherms

The γ-alumina used in this study was PSD-350 activated alumina from ALCOA Separations Technology, Inc. Two samples of aluminas were calcined in a furnace at 823.15K and 1,023.15K during several hours. The adsorption isotherms of nitrogen in the different samples were measured at 77.35K using a Micromeritics ASAP 2000 surface analyzer and the BET surface areas were calculated assuming a nitrogen molecule cross section of 0.164 nm^2. The same apparatus automatically calculates the pore-size distribution of the solids for pore diameters between 10 and 3,000 Å using the BJH method [Barrett *et al*., 1951]. These PSD's are used to compare with the PSD's obtained by FMT calculations and regularization method.

5.2.1 BET analysis of adsorption data

The Brunauer-Emmett-Teller (BET) isotherm [Brunauer *et al*., 1938] is a widely-used, well-behaved method for extracting effective surface areas and adsorption energies from isotherm data. The method is based on a model of multilayer adsorption, which satisfies several conditions:

- Adsorption occurs on adsorbing sites and on top of adsorbed molecules.
- The number of adsorbing sites per layer is constant.
- The energy of the first-layer adsorbing sites is uniform
- Molecules in all layers above the first behave as if in a bulk liquid.

Given these conditions, the statistical mechanical problem may be solved by a variety of methods to yield the fundamental equation

$$\frac{P/P_0}{n(1-P/P_0)} = \frac{1}{n_m c} + \frac{c-1}{n_m c}(P/P_0) \tag{5.1}$$

P/P_0 is the relative pressure, n is the amount adsorbed (per unit mass of adsorbent), n_m is the BET "monolayer capacity", and c is usually related to the net heat of adsorption by $c = \exp(q^{st}-q_L)/RT$, where q^{st} is the isosteric heat adsorption in the monolayer and q_L is the heat of condensation. Conventionally, adsorption data are plotted as $(P/P_0)Ln(1-P/P_0)$ *vs.* P/P_0, and the n_m and c parameters are determined from the slope and intercept of the resulting line. The monolayer capacity n_m is often divided by some predetermined "monolayer" density to obtain the "BET surface area" of the system. This quantity is often quoted in literature describing porous adsorbents and substrates. The monolayer density is usually taken from adsorption studies of nonporous material, where the surface are assumes that the average density of the monolayer is transferable between the two materials. If they area chemically similar, this is a reasonable assumption.

5.2.2 Adsorption isotherms

In the following figures we show the experimental isotherms of nitrogen at 77.35K measured in γ-alumina for this work. In the first one, Fig. 5.1, we can see the adsorption on the alumina without treatment in furnace. This isotherm corresponds to type IV in the classification of Brunauer, Deming and Teller (BDDT) [Brunauer *et al*., 1940]. This means that this alumina has an important proportion of mesopores but with a non-negligible proportion of micropores (or strong interaction of the substrate) and that it presents capillary condensation. The BET surface area obtained was of 315.1354 ± 2.2654 m^2/g.

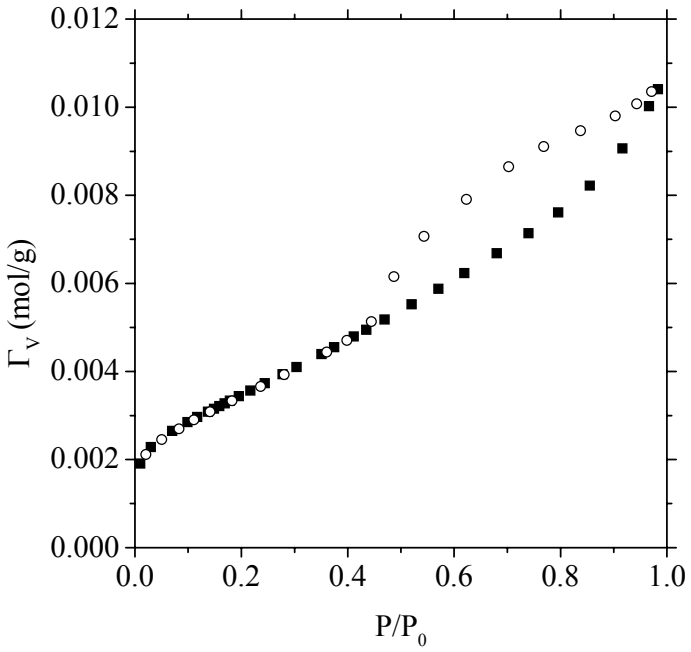

Fig. 5.1. Experimental adsorption isotherm of nitrogen at 77.35K on γ-alumina. The squares represent adsorption branch, and the circles desorption one.

Fig. 5.2 shows an experimental isotherm of nitrogen at 77.35K measured in the γ-alumina treated in a furnace during several hours at 823.15K. It can be appreciated that although the isotherm can still be classified as type IV, the presence of micropores

diminishes (the convex curvature in the region of low pressures is less notorious) in favor of the increase of the larger pores (the total adsorption in the region of high pressures is enlarge). The capillary condensation occurs at a higher pressure and the hysteresis loops lightly decreases. The BET surface area in this case was of 227.4075 ± 1.8002 m^2/g.

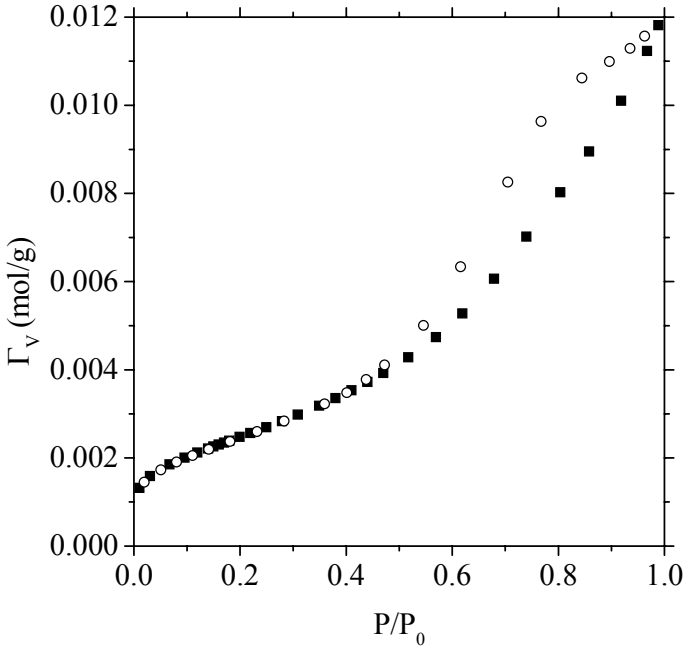

Fig. 5.2. Experimental adsorption isotherm of nitrogen at 77.35K on γ-alumina calcined at 823.15K. The squares represent adsorption branch, and the circles desorption one.

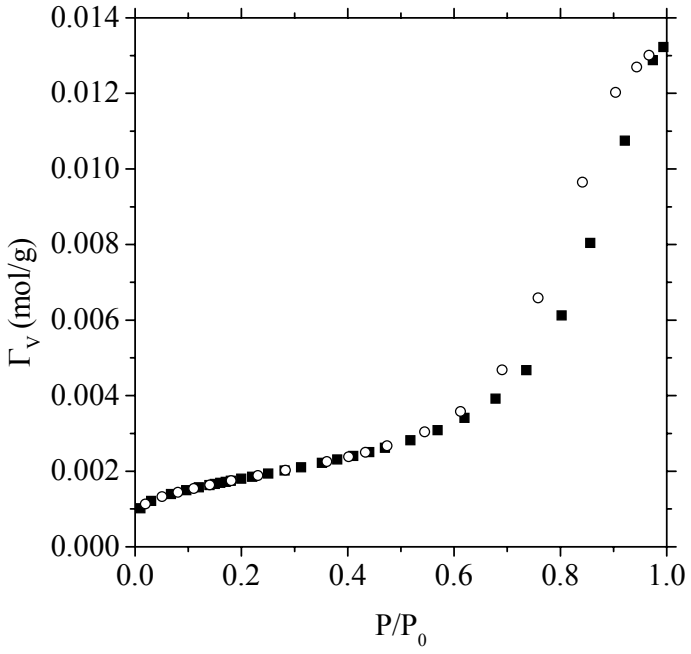

Fig. 5.3. Experimental adsorption isotherm of nitrogen at 77.35K on γ-alumina calcined at 1,023.15K. The squares represent adsorption branch, and the circles desorption one.

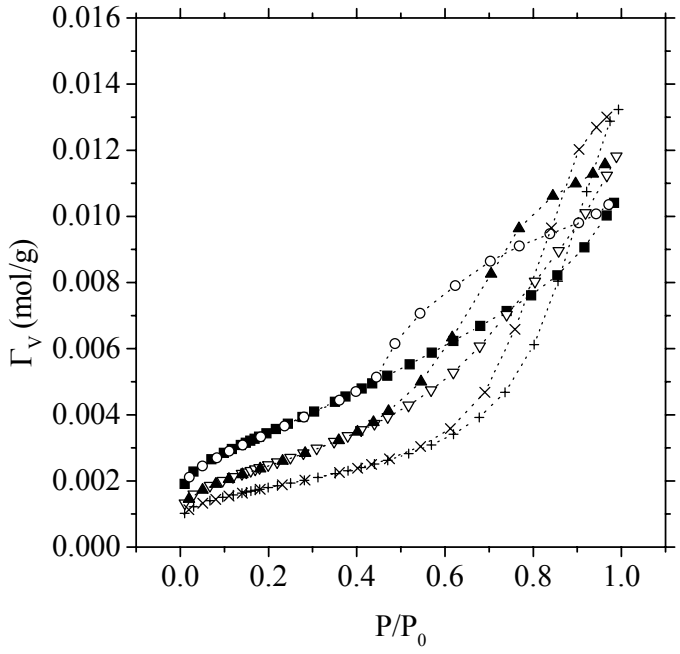

Fig. 5.4. Experimental adsorption isotherms of nitrogen at 77.35K on untreated γ-alumina, (circles and squares); on γ-alumina calcined at 823.15K, (triangles); and on γ-alumina heated at 1,023.15K, (crosses).

In Fig. 5.3 we represent the adsorption of nitrogen at 77.35K on alumina calcined during several hours at 1,023.15K. The evidence of the presence of macropores in detriment of micro and mesopores is furthermore evident. In this case, the classification

of isotherm is more suitable in type II that correspond at the adsorption isotherm in a non-porous material. The BET surface area of this isotherm had a value of 159.0018 ± 0.7351 m^2/g.

The differences on the features of this three adsorption isotherm are more clearly showed if we plot the curves in the same figure, as it is done in Fig. 5.4. Once we have seen that the operating conditions were appropriate for our purpose we can now check the accuracy of the DFT approach in conjunction with the regularization method for the PSD in capturing these experimental facts.

5.3 Molecular models

In this section, we present the details of molecular models used in this part. The model of the adsorbent material was very similar in both cases, when the adsorbate was nitrogen and when it was ethane. In the first part (nitrogen) we calculated the adsorption isotherms using FMT approach and in the second one (ethane), we used GCMC simulations procedure.

5.3.1 Nitrogen on γ-alumina

Fluid-fluid interactions

To model the fluid-fluid interactions of nitrogen molecules we have used the spherical LJ intermolecular potential. This potential was cut at 5σ and it was not shifted. We have used the SPT equation of state outlined in chapter 2 to fit the parameters in order to reproduce the bulk nitrogen saturated liquid density (0.02887 mol/cm^3 [CRC, 1981]), and saturation pressure (1 atm) at the normal boiling point of 77.35K. The potential parameters obtained in this work are shown in table 5.1. Here, we use the same FMT model that in chapter 3 in the sense of that the separation of LJ potential in the WCA fashion was done at $r_{min} = \sigma^{1/6}$, and the hard-sphere diameter was calculated with Eq. 3.3.

Solid-fluid interactions

We represent each individual pore as a cylinder where oxygen ions are modeled as spherical Lennard-Jones sites. The LJ potential was cut at 5σ and it was not shifted. These LJ spheres are arranged in 6 cylindrical layers, in such a way that the density of oxygen ions in γ-alumina, "true density" = 60.25 O_2 $ions/nm^3$ [Greenwood and Earnshaw, 1986], is approximately mimicked. The distance between two oxygen atoms in angular and axial directions is d. The rest of the consecutive layers forming the cylinders are separated by a distance Δ, in the same arranged that it used in chapters 3 and 4 as shown in figure 5.5. To reproduce the experimental density of oxygen ions inside the material, appropriate values of the geometrical parameters d and Δ are chosen (d = 2.364 Å and Δ = 3.0 Å). The pore diameter is measured from the center of the oxygen ions on opposite sides of the innermost layer, as indicated in figure 5.5. Each pore contains, in the radial direction (6) and along the cylinder axis (20), a sufficient

number of LJ spheres so that the interactions between the adsorbed molecules and the outer oxygen ions of the pore are negligible. The solid-fluid interaction molecular parameters, ε_{sf}, and σ_{sf}, the segment size and the dispersive energy, shown in table 5.1, are taken from Cascarini de Torre *et al*. [1995]. They quantified the parameters of the interaction between the fluid (N_2) and the atoms of the wall (Al_2O_3), and we use the Lorenz-Berthelot mixed rules to calculate the solid-solid parameters of the alumina. The total potential energy between a fluid molecule and the wall is given by the sum of all the oxygen contributions. It was calculated prior to the adsorption calculations, and was determined at the same points of the mesh of the DFT calculations. Due to the only radial dependence of the density profiles of the DFT model, the angular and axial dependence was integrated in the same way as in chapters 3 and 4.

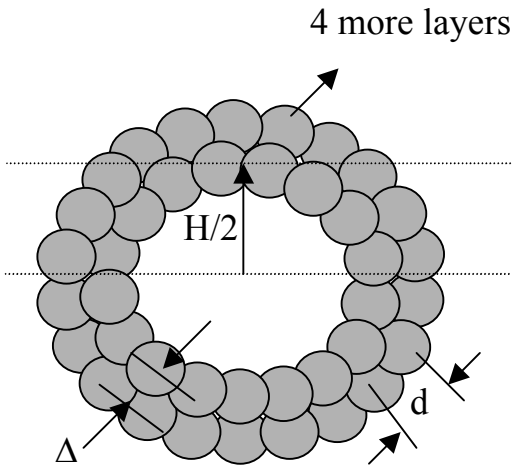

Fig. 5.5. Structure of one cylindrical pore and the definitions of geometrical parameters.

	σ (Å)	ε/k_B (K)	σ_{sf} (Å)	ε_{sf}/k_B (K)	σ_{ss} (Å)	ε_{ss}/k_B (K)
Nitrogen	3.54[a]	96.20[a]	3.16[b]	104.2[b]	2.78[c]	112.87[c]

Table 5.1. Nitrogen and Al_2O_3 LJ parameters. [a] Fitted to experimental values with SPT equation of state; [b] from the work of Cascarini de Torre *et al*. [1995]; [c] obtained by Lorenz-Berthelot combining rules.

Pore properties

The volume of the pore in this work is defined as a function of the effective diameter, w_{eff}, in the following way

$$w_{eff} = H - \sigma_{sf} \tag{5.2}$$

where H is defined in the way showed in Fig. 5.5.

5.3.2 Ethane on γ-alumina

In this part we used a simplified molecular model of adsorption of ethane on γ-Al_2O_3. In general, the PSD function of a polydisperse material can be approximated in the following way

$$f(H) \approx \sum_{k=1}^{m} c_k \delta\left(H - H_k\right) \tag{5.3}$$

where $\delta(H-H_k)$ are the δ-Dirac distribution functions centered at pore sizes H_k, with k = 1, ..., m, and m is given by the number of peaks of the distribution. c_k are weight constants associated to each mode. It is straightforward to demonstrate that the distribution has the same surface pore volume as that obtained from the DFT analysis if c_k is given by the area below each mode of the distribution. We will check the validity of this approximation for γ-Al_2O_3.

Fluid-fluid interactions

Fluid molecules are modeled in the same way that the nitrogen such as spherical LJ units. The parameters can be found in table 5.2 and were taken from the work of Cracknell *et al*. [1993].

	σ (Å)	ε/k_B (K)	σ_{sf} (Å)	ε_{sf}/k_B (K)
Ethane	3.95[a]	243.00[a]	3.37	165.60

Table 5.2. Ethane LJ parameters. [a] From the work of Cracknell *et al*. [1993].

Solid-fluid interactions

The molecular parameters of LJ interactions between the atoms in the wall and each ethane molecule were obtained following the Lorenz-Berthelot combining rules from the parameters of the solid in the nitrogen-alumina model (table 5.1), and the fluid-fluid parameters of ethane [Cracknell *et al.*, 1993].

In the ethane isotherms, the model of the alumina was the same that of nitrogen case but with one important difference. In this case we perform GCMC simulations, which are done in a continuous space. Therefore, the potential due to the alumina wall was also calculated prior to the simulations at a large number of grid points inside the pore, the grid was stored in a file, and the potential in a specific position during the simulation was calculated by linear interpolation.

Pore properties

The volume of the pore considered is the same as the one we used for the case of nitrogen in the previous section.

5.4 Pore-size distributions

In this section we present the theoretical adsorption isotherms calculated using the FMT approach in cylindrical pores, with the parameters mentioned previously. Additionally, we show the PSD's obtained by regularization method using this set of isotherms together with the experimental isotherms. Finally, we compare the PSD's extracted with the respective ones using a BJH analysis obtained directly from the experiments and the software of the Micromeritics apparatus.

5.4.1 Theoretical adsorption isotherms

The individual pore isotherms of nitrogen on γ-alumina have been obtained for an extensive range of pore sizes from 18 Å to 600 Å (20 isotherms in total) at 77.35K. Since not excess adsorption is observed for larger pores, there are not included in the analysis. The pore sizes values at which the adsorption isotherms were calculated are in table 5.3 and a representation of these isotherms can be seen in Fig. 5.6. Due to the high computational cost needed to obtain the FMT isotherms, we have only calculated 19 different points in each isotherm (a suitable grid was chosen). This should not be a problem, since we could interpolate with a spline numerical method to obtain additional data.

As expected, different adsorption behaviors have been observed depending on the pore size range studied. These differences were extensible discussed in chapter 3. We have just calculated the isotherm branch in each isotherm because this is the branch used from the experimental isotherms to obtain the PSD's.

H (Å)	H^*	H (Å)	H^*
18	5.1	90	25.4
20	5.6	100	28.2
25	7.1	150	42.4
30	8.5	200	56.5
35	9.9	250	70.6º
40	11.3	300	84.7
50	14.1	350	98.9
60	16.9	400	113.0
70	19.8	500	141.2
80	22.6	600	169.5

Table 5.3. Pore diameter sizes of the different isotherms calculated in this work.

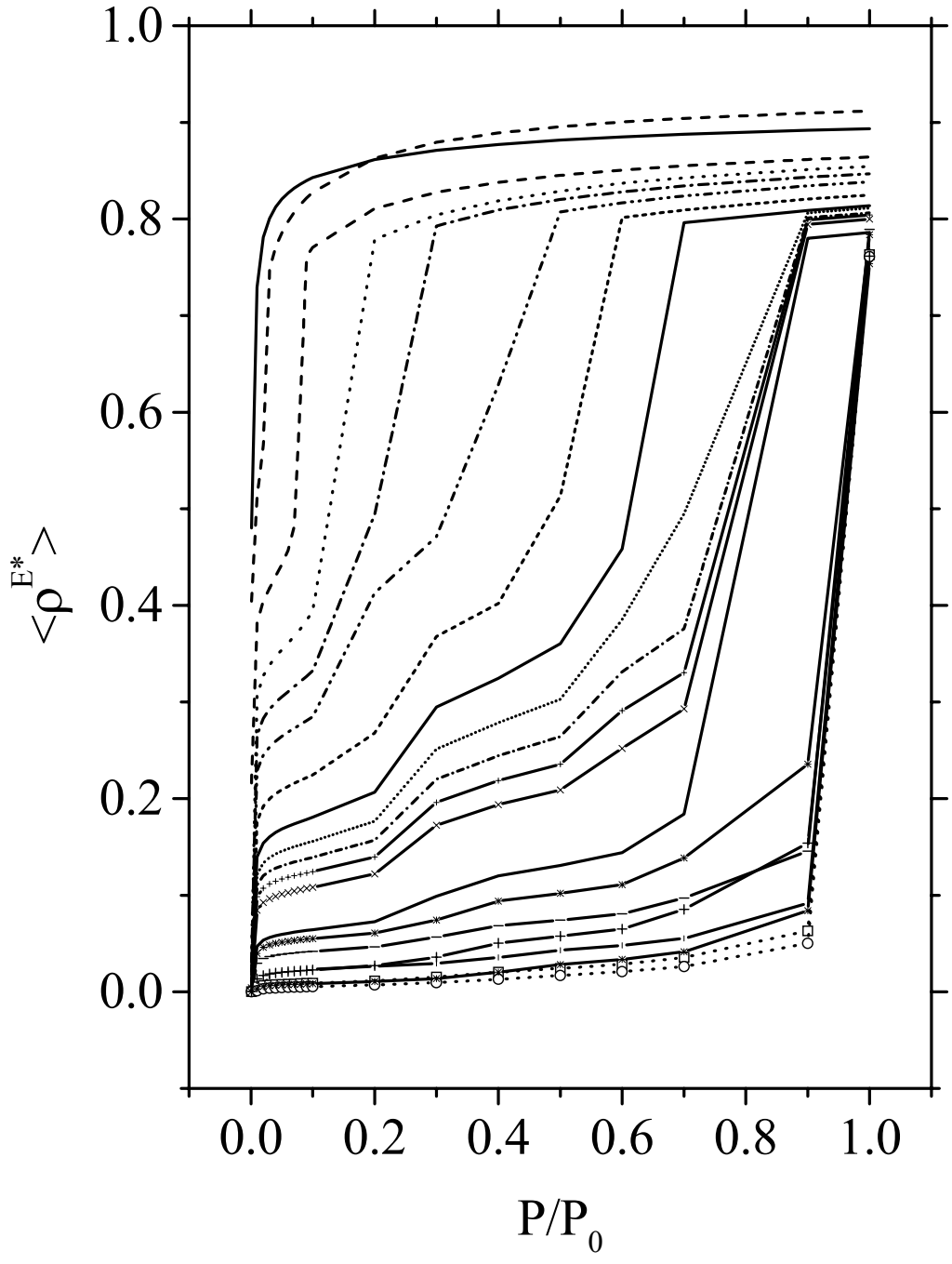

Fig. 5.6. Theoretical adsorption isotherms of nitrogen at 77.35K on cylindrical pores of γ-alumina of different diameters. The pore sizes increase from the left side to right side, and the values of them are presented in table 5.3.

5.4.2 Pore-size distribution calculations

The procedure followed to estimate the PSD from the inversion of the adsorption integral equation of the three samples treated is the same as the one used in chapter 4. The PSD obtained with FMT for the untreated alumina is shown in figure 5.7, where, for comparison, we also show the BJH PSD obtained from the software of the experimental apparatus. As expected for a material with a significant amount of micro and mesopores, as the alumina we are analyzing here, the BJH method underestimates the size of the pores present in the material. A comparison of the experimental and the isotherm obtained from the fitted PSD is shown in figure 5.8, with the percentage of deviation from the fitting presented in table 5.4. As we have mentioned already, only the adsorption branch is shown in both cases. An excellent agreement between experimental and theoretical results is observed, showing, not only the goodness of the method for estimating the PSD, but also the adequacy of the cylindrical geometry for this material.

System	Number of theoretical isotherms employed	Number of points of the experimental isotherm	Number of interpolated points of the experimental isotherm	γ_R	Area under the curve	% of deviation between the isotherms
Untreated alumina	17	30	19	100	1.20	6.05
Alumina calcined at 823.15K	18	30	19	1,000	1.38	10.80
Alumina calcined at 1,023.15K	18	30	19	10,000	1.56	8.82

Table 5.4 Parameters and results from the fitting of Figs. 5.7-5.13. γ_R is the regularization parameter.

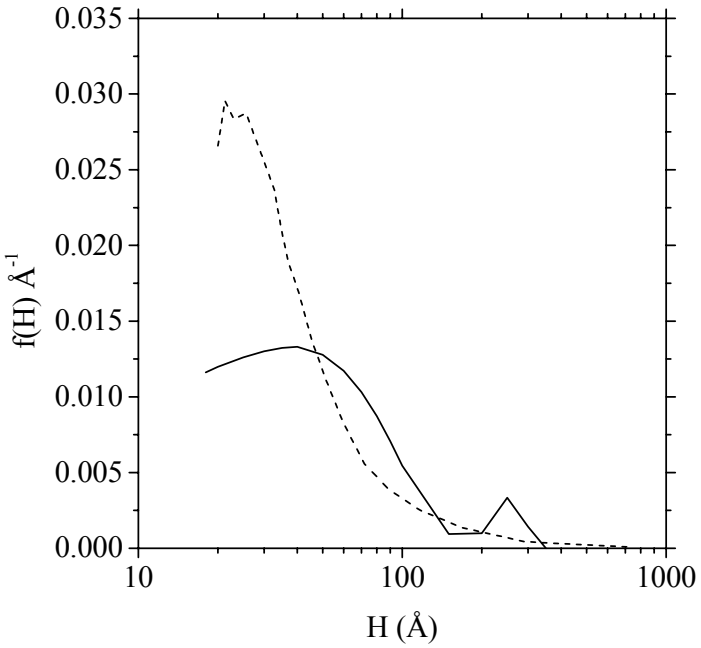

Fig. 5.7. PSD's of untreated γ-alumina, obtained by FMT calculations (solid line), and by BJH method (dashed line).

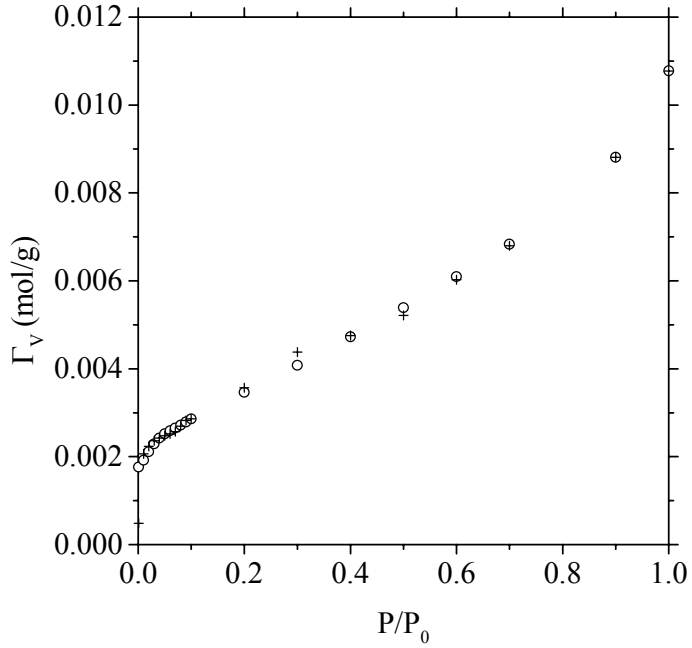

Fig. 5.8. Adsorption isotherm of nitrogen at 77.35K on γ-alumina. The circles represent the experimental data and the crosses the fitted curve obtained by FMT isotherms weighted for the PSD from Fig. 5.7.

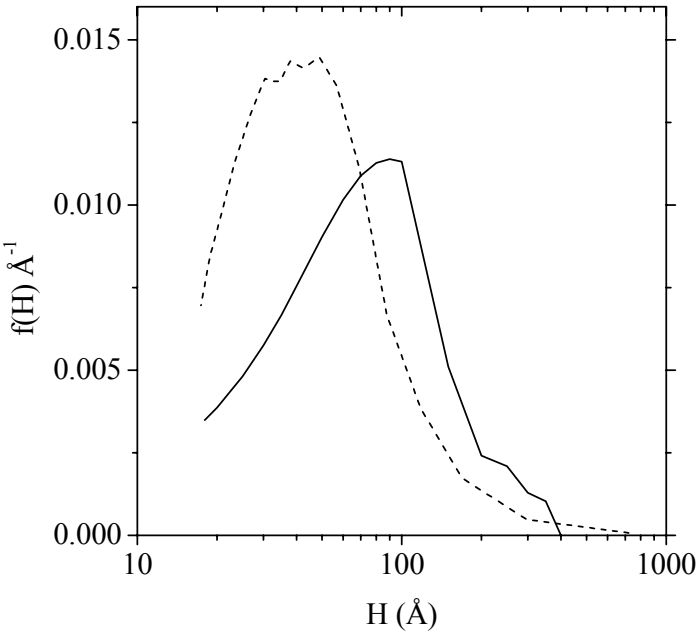

Fig. 5.9. PSD's of calcined γ-alumina at 823.15K, obtained by FMT calculations (solid line), and by BJH method (dashed line).

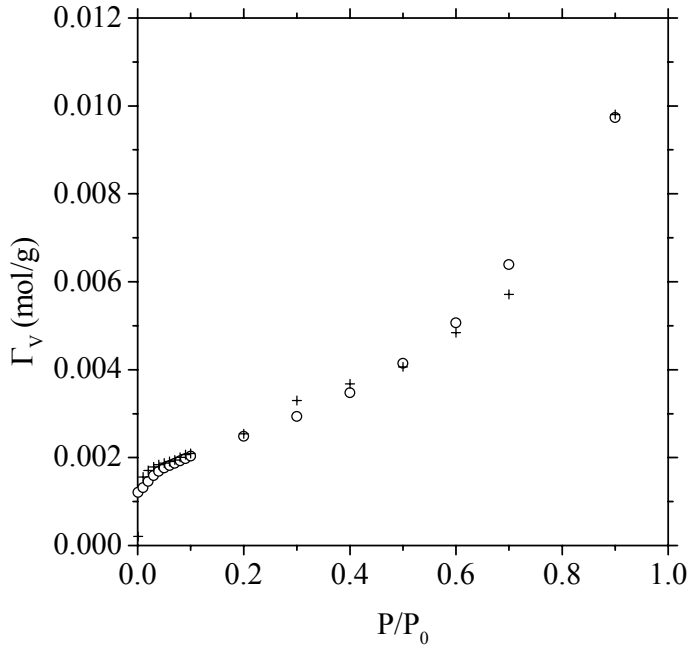

Fig. 5.10. Adsorption isotherm of nitrogen at 77.35K on γ-alumina calcined at 823.15K. The circles represent the experimental data and the crosses the fitted curve obtained by FMT isotherms weighted for the PSD from Fig. 5.9.

The PSD obtained for the calcined alumina at 823.15K is shown in figure 5.10, where we also show the BJH distribution obtained as before. There is still a significant difference between these two distributions. The maximum in the BJH case is located at 45 Å, while the maximum obtained from inversion of the integral equation is located at 100Å. The experimental and adsorption isotherms for this calcined material are presented in figure 5.11. As in the untreated material, the good agreement between both

of them proves the accuracy of the method, and of the model used in the theoretical approach.

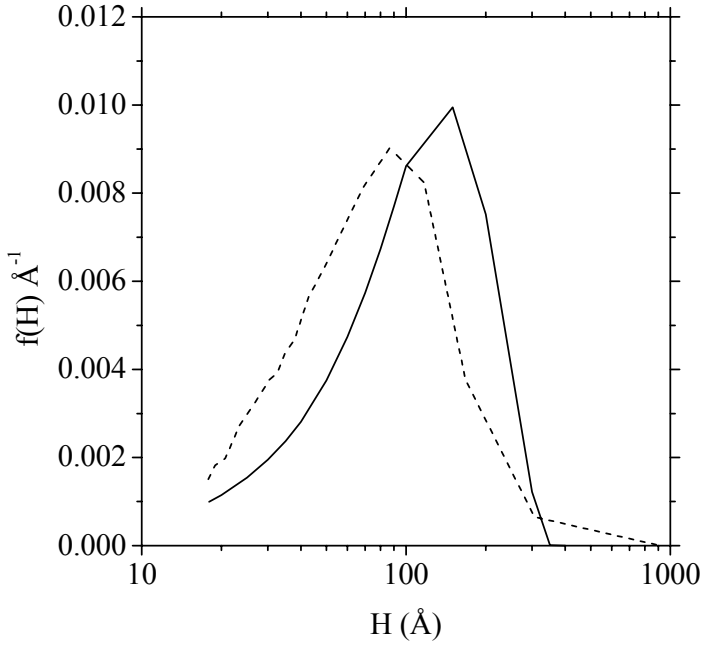

Fig. 5.11. PSD's of calcined γ-alumina at 1,023.15K, obtained by FMT calculations (solid line), and by BJH method (dashed line).

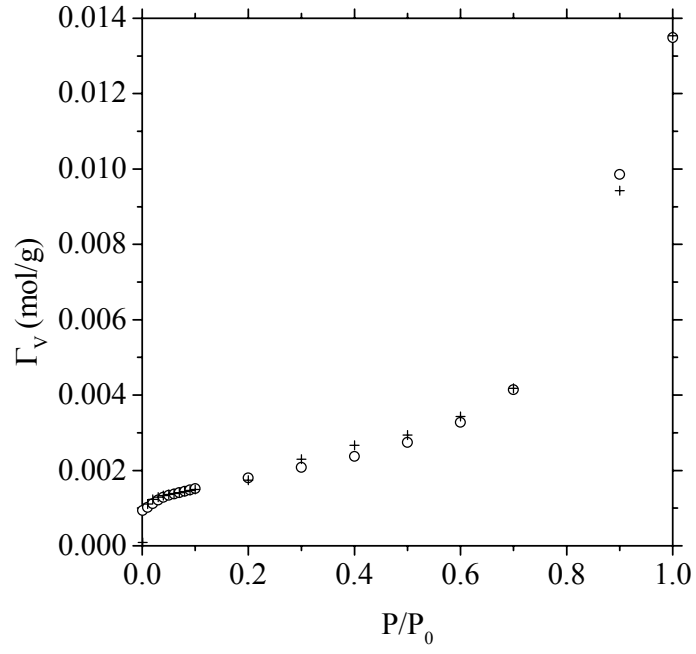

Fig. 5.12. Adsorption isotherm of nitrogen at 77.35K on γ-alumina calcined at 1,023.15K. The circles represent the experimental data and the crosses the fitted curve obtained by FMT isotherms weighted for the PSD from Fig. 5.11.

Finally, figures 5.11 and 5.12 show the corresponding results obtained for calcined alumina at 1,023.15K. It is observed than in this case the sintering process has destroyed the narrowest pores, and the agreement between the PSD obtained from both methods are in better agreement. This is an expected result, since it is known that the BJH method is accurate in the meso and macroporous region. In figure 5.12 we observe that the agreement between the experimental and the theoretical isotherm is excellent.

As we expected, when we calcined the alumina the material suffered a sintering process, in which the narrow pores progressively disappear, displacing the PSD to wider pore sizes. This phenomenon can be appreciated in figure 5.13, were the three PSD's are shown in the same plot. The distribution associated to the untreated alumina shows a maximum located at 40 Å, and a high proportion of pores located between 20 and 100 Å. The maximum is displaced in alumina calcined at 823.15K, and it is located at 100 Å, with the distribution centered on this value. Finally, the PSD corresponding to the alumina calcined at 1,023.15K shows a peak located around 200 Å. For this last material it is observed that there are very few narrow pores. The resulting curves of Figs. 5.9 and 5.11 should be improved when additional individual isotherms are used in the region of larger pores. The number of individual isotherms used to obtain the PSD is small in this pore range, giving sharp curves.

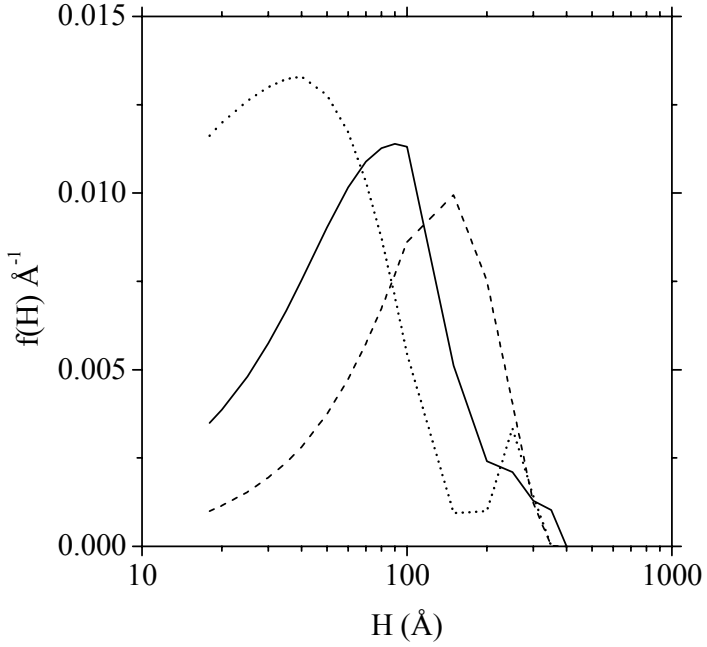

Fig. 5.13. PSD's of γ-alumina obtained by FMT calculations; dotted line represent untreated alumina, solid line is for alumina calcined at 823.15K, and dashed line represent alumina calcined at 1,023.15K.

5.5 Application of pore-size distributions to predict adsorption isotherms

With the aim of testing the accuracy of the PSD's obtained in previous section, we have calculated adsorption isotherms of ethane at 333.15K on untreated alumina. In particular, our objective is to test the robustness of the method by applying the PSD at some different thermodynamical conditions of those at which the material was characterized. It would be a way of establishing the predictive capability of the PSD obtained from our method.

As a first step, we have verified the validity of the equation 5.3, which establishes the possibility of to represent the whole adsorption in some material using only selected isotherms at certain pore size values. We have calculated two isotherms at H = 40 and 250 Å of nitrogen on alumina at the same thermodynamical conditions of the characterization. We have chosen these diameters because they are the maximum in the PSD of Fig. 5.7. These adsorption isotherms were calculated using GCMC simulations with the model presented in section 5.3.1. We have used the equation 5.3 to calculate the total adsorption with a weight factors c_k of 0.752 and 0.248 for the isotherm on H = 40 Å cylindrical pore and on H = 250 Å cylindrical pore, respectively.

The individual adsorption isotherms are presented in Fig. 5.14. It can be seen that the isotherm of the larger pore has a very small contribution, while the isotherm at 40 Å is the dominant contribution. As we expected, the use of only two individual isotherms does not reproduce all the richness of the experimental adsorption isotherm, but it gives approximate adsorption levels, which can be useful for applications on adsorption of different fluids. It is clear than the agreement could be improved if some additional individual isotherms are used. It would be interesting to investigate how many pore sizes would be necessary to include for obtaining quantitative agreement. The comparison between the average isotherm obtained with two GCMC isotherms and the experimental one is shown in Fig. 5.15.

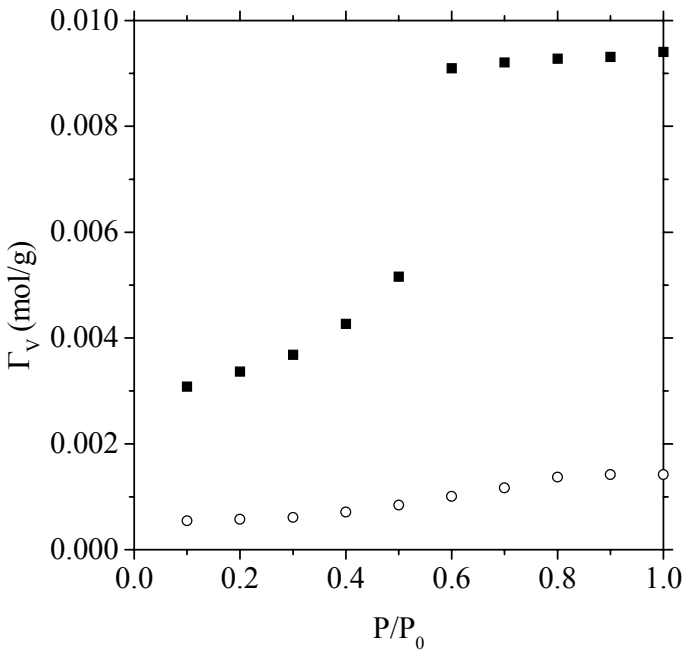

Fig. 5.14. Adsorption isotherms of nitrogen on untreated γ-alumina at 77.35K in two different cylindrical pores by GCMC simulations; (squares) H= 40 Å, and (circles) H = 250 Å.

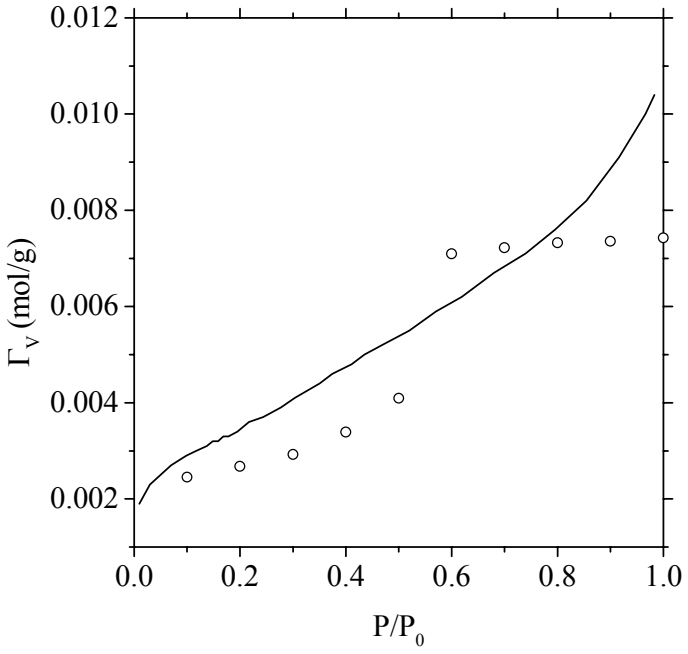

Fig. 5.15. Adsorption isotherms of nitrogen on untreated γ-alumina from (solid line) experimental results (the adsorption branch presented in Fig. 5.1), and obtained by a lineal combination of two isotherms by GCMC simulations at 77.35K.

We have given one step forward on applying molecular modeling techniques in a "predictive" manner: we have used a different fluid and we have calculated the adsorption isotherm at a different temperature, using the PSD obtained by FMT and the regularization method. In this case, we have used ethane at 333.15K. We have chosen

this system because we have experimental information from the literature [Yang *et al*., 1995; 1996]. We have calculated two isotherms at the same values of pore sizes (H = 40 and 250 Å) as for nitrogen. These adsorption isotherms were calculated using GCMC simulations with the model explained in section 5.3.2. The results are presented in Fig. 5.16, showing the comparison between the experimental adsorption isotherm and the GCMC weighted isotherm. Although, in principle this seems a not very good agreement, compared to what we have observed in the rests of the calculations presented here, some comments are in order. First of all, we are doing a first approximation using the Lorentz-Berthelot combining rules to calculate the fluid-wall interaction. It would be more appropriate to use very low pressure-adsorption measurements to determine the value of the energy interaction between the wall and the fluid. We have chosen this approach because we consider interesting to see the results in which we are studying a different fluid and the temperature is much higher than that used to obtain the PSD, without doing any fitting, to see the predictive capability of the method. In fact, this is the main difference between of this work and the previous one of Blas *et al.* [1998], in which they used a unique cylindrical pore and they fitted the diameter and the solid-fluid energy interaction parameter to the experimental adsorption isotherm. Here, we are doing a pure prediction.

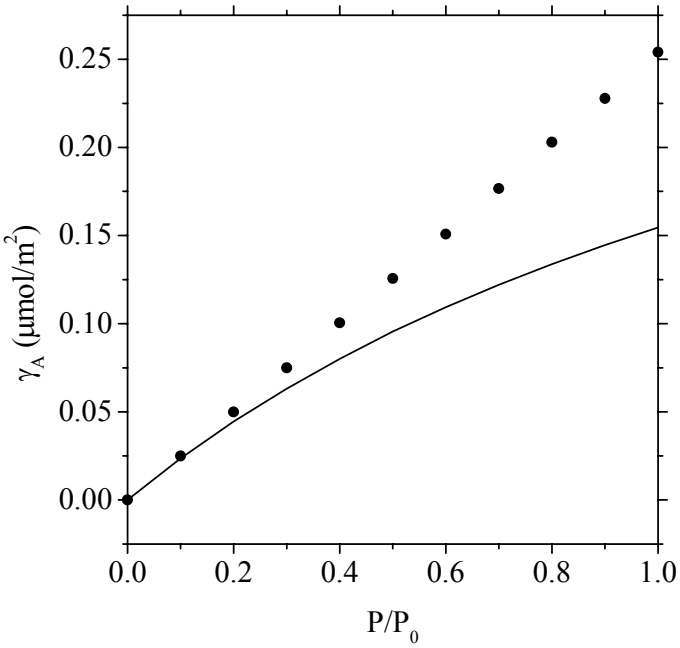

Fig. 5.16. Adsorption isotherms of ethane on untreated γ-alumina from (solid line) experimental results [Yang *et al*., 1995; 1996], and obtained by a lineal combination of two isotherms by GCMC simulations at 333.15K.

In Fig. 5.17 each individual isotherm at two different values of diameter size are presented for consistency. The dependence of the adsorption *versus* P/P_0 are lineal because the thermodynamical conditions are supercritical, and at these conditions capillary condensation is not present.

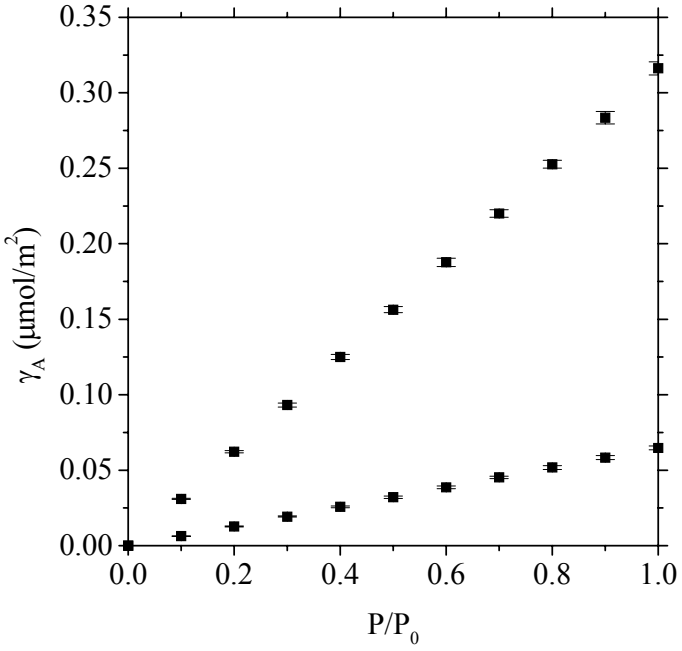

Fig. 5.17. Adsorption isotherms of ethane on untreated γ-alumina at 333.15K in two different cylindrical pores by GCMC simulations; (circles) H = 40 Å, and (squares) H = 250 Å.

Finally, an additional comment is that in the work of Blas and coworkers [1998] they modeled the ethane as a molecule of two sites, instead of the spherical LJ we have used here. Additional changes in the model can be done in a gradual way, improving the molecular model of the fluid.

5.6 Conclusions

In this chapter we have characterized three different samples of γ-alumina, one of them without treatment and the others two calcined in a furnace during several hours at 823.15 and 1,023.15K respectively. To do this we have measured adsorption isotherms of nitrogen at 77.35K in a Micromeritics ASAP 2000 apparatus. Additionally, we have obtained the PSD's provided by the software of the apparatus using the BJH method. We have calculated the theoretical isotherms using the model presented in section 5.3.1 by the FMT approach from section 2.2. We have inverted the adsorption integral equations with the regularization method presented in section 4.3, and finally, we have obtained the PSD's for our three samples of alumina, and the corresponding adsorption isotherms for the three materials. In this way we have observed the influence of the calcination of alumina in its PSD. Moreover, we have tested the accuracy of the FMT/Regularization method in a systematic way.

When we compared the PSD's obtained with the corresponding BJH distributions, we have verified that in the two first cases (untreated alumina and alumina calcined at

823.15K) the BJH method underestimated the size of the pores, giving PSD's shifted to the smaller sizes. In the case of alumina calcined at 1,023.15K, in which the sintering process has produced the disappearance of the smallest pores favoring the wider ones, the BJH PSD's and the FMT/regularization PSD's are very similar. With this, we corroborated the known fact that the BJH method is quite accurate in the macropores region.

Finally, we have checked the validity of representing the polydisperse material by the adsorption in the main sizes, weighted by the corresponding value in the distribution. For the case of nitrogen (same fluid and same conditions), the qualitative isotherms is obtained, although quantitative agreement can not be achieved. The same approximation has been used in a predictive manner, by studying the adsorption of a different fluid (ethane), and at other temperature (333.15K) in one of the characterized materials (untreated alumina). The results show that the method is simple and useful for obtaining the approximate adsorption levels, although additional pore sizes and better molecular models are necessary if quantitative agreement is searched.

5.7 References

Alvarez, L. J.; Sanz, J. F.; Capitán, M. J.; Odriozola, J. A. *Chem. Phys. Lett*. **192**, 463 (1992).

Alvarez, L. J.; Sanz, J. F.; Capitán, J. J.; Centeno, M. A.; Odriozola, J. A. *J. Chem. Soc. Faraday Trans.*, **89**, 3623 (1993).

Alvarez, L. J.; León, L. E.; Sanz, J. F.; Capitán, M. J.; Odriozola, J. A. *Phys. Rev. B*, **50**, 2561 (1994).

Barrett, E. P.; Joyner, L. G.; Halenda, P. P. *J. Am. Chem. Soc*. **73**, 373 (1951).

Blas, F. J.; Vega, L. F.; Gubbins, K. E. *Fluid Phase Equilib*. **117**, 150 (1998).

Brunauer, S.; Emmett, P. H.; Teller, E. *J. Am. Chem. Soc*. **60**, 309 (1938).

Brunauer, S.; Deming, L. S.; Deming, W. S.; Teller, E. *J. Amer. Chem. Soc.* **62**, 1723 (1940).

Cascarini de Torre, L. E.; Flores, E. S.; Llanos, J. L.; Bottani, E. J. *Langmuir*, **11**, 4742 (1995).

Cesteros, Y.; Salagre, P.; Medina, F.; Sueiras, J. E. *Chemistry of materials* **V11 N1**, 123 (1999).

Cracknell, R. F.; Gubbins, K. E. *Langmuir* **9**, 824 (1993).

Cracknell, R. F.; Gubbins, K. E.; Maddox, M.; Nicholson, D. *Accounts of Chem. Res.* **28**, 281 (1995).

Cracknell, R. F.; Nicholson, D.; Quirke, N. *Mol. Phys*. **80**, 885 (1993).

"*CRC Handbook of Chemistry and Physics*", 61st ed. (Weast, R., Ed.; CRC Press, West Palm Beach, FL, 1981).

Gates, B. C. "*Catalytic Chemistry*" (John Wiley & Sons Inc., New York, 1992).

Greenwood, N. N.; Earnshaw, A. "*Chemistry of the elements*" (Pergamon Press, Oxford, 1986).

Gregg, S. J.; Sing, K. S. W. "*Adsorption, surface area and porosity*" (Academic Press Inc., London, 1978).

Ionescu, A.; Allouche, A.; Aycard, J. P.; Rajzmann, M.; Hutschka, F. *J. Phys. Chem. B* 106, 9359 (2002).

Jorgensen, W. L.; Madura, J. D.; Swenson, C. J. *J. Am. Chem. Soc.* **106**, 6638 (1984).

Knozinger, H.; Ratnasamy, P. *Catal. Rev. Sci. E*ng. **17**, 31 (1978).

Lastoskie, C.; Gubbins, K. E.; Quirke, N.; *Phys. Chem*. **97**, 4796 (1993).

Lippens, D. B. *PhD Thesis*, Technische Hogeschol, Delft, Holanda, 1961.

Peri, J. B. *J. Phys. Chem*., 69, 211 (1965); *ibid.* 220; *ibid*. 231.

Ruthven, D. M. "*Principles of adsorption and adsorption processes*" (John Wiley & Sons, Inc., Nueva York, 1984**)**.

Suzuki, M. "*Adsorption engineering*" (Elsevier, Amsterdam, 1990).

Tanabe, K.; Nisono, M.; Ono, Y.; Hattoni, H. "*New solid, acids and bases*" (Elsevier, Amsterdam, 1989).

Vijay, A.; Mills Greg; Metiu H. *J. Chem. Phys*. **117**, 4509 (2002).

Yang, R. T.; Foldes, R. *Ind. Eng. Chem. Res.* 35, 1006 (1996).

Yang, R. T.; Kikkinides, E. S. *AIChE J.* **41**, 509 (1995).

6. SUMMARY AND FUTURE WORK

6.1 Summary

This work has been focused in the development and application of a methodology for the characterization of adsorbent materials using molecular modeling tools. In this context, the first step has been to use the FMT to model slit-like and cylindrical pores, testing the accuracy of the results obtained by comparison with molecular simulation results. It is been studied since from a theoretical perspective the adsorption behavior depends on the geometry of pores. This part of the work has been devoted to the modeling of the adsorption in each individual pore. After that, the second step has been focused on the establishment of the validity of a model used to represent the structure of the whole material. This model assumes the material as a set of independent pores, all of them with the same (simple) geometry but of different sizes, and without interconnection between them. To do that, a well-characterized model material was been used, and a technique to estimate the PSD, using experimental information and theoretical information, was implemented. Finally, to apply and to test the range of the applicability of the developed methodology, a real material was characterized, modifying its structure by calcination, with the aim of study the influence of these processes in the PSD. To do that, the material (alumina) was calcined, and the adsorption isotherms of nitrogen were measured, obtaining the corresponding PSD's using the combined technique of FMT/Regularization with cylindrical pores. After that, the prediction capability of the PSD obtained was estimated. For this, theoretical adsorption isotherms of ethane on alumina at 333.15K were calculated using GCMC simulations, and compared to experimental data from the literature. The diameter size of the pores chosen were the two peaks of the distribution, and the two isotherms obtained were lineally combined pondered with the ratio of the areas under the curves.

6.2 Future work

Fluids confined within narrow pores, with pore widths of a few molecular diameters, exhibit a very reach physical behavior. We have studied the nature of some phase transitions inside the pores in this work. We believe that the local curvature of the solid wall is the only responsible for the shift observed in cylindrical geometries in our study. But actually, we don't have enough time to deeper in this analysis and we think that it will be interesting to follow investigating about this particular point, and to shed some light on this topic.

We have presented preliminary results about the comparison of the isotherms obtained by two DFT versions in a cylindrical pore, but it would be necessary to do a systematic comparison and constitutes an interesting subject for future work.

We are interested in finding an appropriate material for olefin/paraffin separation by adsorption. With this objective, it would be necessary to deeper in the modeling of this kind of systems and to use the presented methodology here to do that.

Finally, it would be very interesting to apply this methodology to other porous materials.